EXPANDING THE POTENTIAL APPLICATIONS OF DECTIN-COATED LIPOSOMES

by

QUANITA JAHAN CHOUDHURY

(Under the Direction of Zachary Lewis)

ABSTRACT

Fungal infections account for approximately 2.5 million deaths globally each year and billions of dollars in healthcare costs annually in just the United States. However, only three primary classes of antifungal drugs exist to treat these infections. Issues with these classes of antifungal drugs include organ toxicity and rising levels of drug resistance. The polyene amphotericin B (AmB), which targets ergosterol in the fungal cell membrane, has been described as the "gold standard" of antifungal treatments due to its broad spectrum of activity. However, it also has an affinity for cholesterol, thus leading to severe side effects that limit its use. The liposomal formulation of AmB was designed to address these issues; although this was an improvement over the original formulation, the toxicity concerns are still a prevalent limiting factor. To address these issues, our research group created a targeted antifungal liposome (DectiSome), in which the liposome's surface is coated with Dectin immune receptors that specifically recognize fungal cells. Dectin-1 and Dectin-2 DectiSomes have improved targeting efficacy over untargeted liposomes in vitro against the clinically relevant fungal pathogens *Aspergillus fumigatus*, *Candida albicans*, and *Cryptococcus neoformans*. This work focuses on evaluating additional uses for this novel technology. The findings presented here demonstrate that (1) Dectin-1 DectiSomes have improved targeting efficacy in vitro against *Rhizopus*

delemar, a common causative agent of mucormycosis, (2) a novel Dectin-3 DectiSome has improved targeting efficacy in vitro against *R. delemar*, *C. albicans*, and *C. neoformans*, and (3) a biotinylated Dectin-1-coated liposome has potential as a fungal cell pull-down tool to facilitate additional analyses.

INDEX WORDS: Dectin; DectiSomes; amphotericin B; antifungals; liposomes; *Rhizopus delemar*; *Candida albicans*; *Cryptococcus neoformans*

EXPANDING THE POTENTIAL APPLICATIONS OF DECTIN-COATED LIPOSOMES

by

QUANITA JAHAN CHOUDHURY

B.S., University of Tennessee, 2018

A Dissertation Submitted to the Graduate Faculty of The University of Georgia in Partial Fulfillment of the Requirements for the Degree

DOCTOR OF PHILOSOPHY

ATHENS, GEORGIA

2024

EXPANDING THE POTENTIAL APPLICATIONS OF DECTIN-COATED LIPOSOMES

by

QUANITA JAHAN CHOUDHURY

Major Professor:	Zachary Lewis
Committee:	Richard Meagher
	Aaron Mitchell
	Michelle Momany

Electronic Version Approved:

Ron Walcott
Vice Provost for Graduate Education and Dean of the Graduate School
The University of Georgia
December 2024

DEDICATION

To:

Afsoruddin Choudhury and Khaleda K. Choudhury,

Golam Y. Choudhury and Dr. Sharikunnesa Choudhury,

Belwara K. Choudhury,

C.K. Zaman,

&

Wais Choudhury

I miss you all.

ACKNOWLEDGEMENTS

I am eternally grateful to my parents, Drs. Ruhul and Jannath Choudhury, and my brother, Mushrif Choudhury, for their constant support and confidence throughout my lifetime. I appreciate the encouragement of my extended family. In particular, my GA and SC families and my "khala-to-sisters" have been invaluable sources of support, especially over the last five years as I adjusted to a new environment; it would've been a much more difficult journey for me without them. I also want to acknowledge the support of Raeedah Choudhury, Samiha Ahsan, Emily Grimes, Jasmine Whitaker, and Drs. Shuhrat Choudhury, Samira Ibrahim, and Kamilya Schumacher.

This dissertation would not have been possible without the guidance and mentorship of Drs. Zack Lewis and Rich Meagher; I got to see what a positive long-term collaboration looks like, and I'm grateful to have had their support. I'm grateful to Dr. Suresh Ambati for his kindness and endless patience as I inundated him with questions. My committee members, (Zack, Rich, and) Drs. Aaron Mitchell and Michelle Momany, provided constructive feedback and were crucial to helping me develop as a scientist. My labmates, past and present, celebrated the high points and supported me through the low points. I want to specifically thank Felicia Ebot-Ojong and Yael Bar-Peled; I will always be grateful for our friendship. The UGA Department of Microbiology office staff (most notably Janice Stuart) and the UGA Office of Information Technology staff (most notably Boysey Callaway) have been very helpful throughout my time here. I also want to acknowledge my undergraduate research mentor Dr. Jesse Labbé; his lab introduced me to the world of scientific research, and the rest is history.

TABLE OF CONTENTS

Page

ACKNOWLEDGEMENTS v

CHAPTER

1 INTRODUCTION 1

Prevalence and Relevance of Fungal Infections 1

The Urgent Need for Effective Antifungals 5

From Liposomes to Targeted Liposomes 9

The Roles of Dectins 10

DectiSomes: Targeted Antifungal Liposomes 11

References 13

Figure 20

2 TARGETED DELIVERY OF ANTIFUNGAL LIPOSOMES TO *RHIZOPUS DELEMAR* 21

Abstract 22

Introduction 22

Materials and Methods 24

Results 28

Discussion 32

Supplementary Materials 36

Author Contributions 36

Funding 36
Data Availability Statement 37
Acknowledgements 37
Conflicts of Interest 37
References 37
Figures 42
3 DECTIN-3-TARGETED ANTIFUNGAL LIPOSOMES EFFICIENTLY BIND AND KILL DIVERSE FUNGAL PATHOGENS 52
Abstract 53
Introduction 53
Results 56
Discussion 66
Conclusions 72
Experimental Procedures 72
Author Contributions 79
Acknowledgements 80
Conflict of Interest Statement 81
Data Availability Statement 81
References 81
Figures 87
4 DECTISOMES AS POTENTIAL BIOLOGICAL PROBES 105
Introduction 105
Materials and Methods 107

Results 111

Discussion 114

References 118

Figures 121

5 DISCUSSION 129

Targeted Delivery of Antifungal Liposomes to *Rhizopus delemar* 129

Dectin-3-Targeted Antifungal Liposomes Efficiently Bind and Kill Diverse Fungal Pathogens 131

DectiSomes as Potential Biological Probes 133

References 135

CHAPTER 1

INTRODUCTION

Prevalence and Relevance of Fungal Infections

The fungal kingdom is estimated to contain several million species, although only approximately 150,000 have been characterized (Rokas, 2022). Approximately 200 species are capable of infecting humans (Fisher et al., 2020). However, their impact on public health cannot be overstated. Approximately 2.5 million deaths are directly linked to fungal infections globally each year (Denning, 2024). Fungal infections are predominantly associated with immunocompromised individuals, and these infections are expected to increase due to the rise of such conditions (such as diabetes, various cancers, and organ transplants). However, it is also worth noting that certain fungal infections, such as histoplasmosis and valley fever, can occur in immunocompetent individuals. The total economic burden of fungal infections on the U.S. healthcare system was estimated to be $11.5 billion in 2019, including $7.5 billion in direct costs (Benedict, Whitham, and Jackson, 2022).

Human fungal pathogens can be found in a variety of environments. Some pathogens, such as *Aspergillus fumigatus, Candida albicans,* and *Cryptococcus neoformans*, can be found worldwide (Rokas, 2022). *Coccidioides* spp. can be found in dry soil in the western U.S., while *Histoplasma* spp. can be found in bat guano in the Mississippi River Valley (One Health, 2019). *Candida albicans* can exist as a commensal species in the human microbiota but can cause invasive infections under certain circumstances (Kumamato, Gresnigt, and Hube, 2020).

Infections from *Candida auris*, a multidrug-resistant pathogen that was first characterized in 2009, are often acquired in hospitals (Forsberg et al., 2019).

Fungal infections are primarily acquired through spore inhalation or infection of open wounds. A healthy immune response includes pattern recognition receptors (PRRs) that identify unique characteristics of these fungi, such as cell wall components. Broadly speaking, these PRRs trigger signaling cascades that lead to, among other things, cytokine production and the recruitment of additional immune cells to target the pathogen.

The World Health Organization recently published a list of human fungal pathogens to prioritize for further research. Notable mentions include *Aspergillus fumigatus*, *Candida albicans* and *Cryptococcus neoformans* in the critical priority group, and *Rhizopus delemar* (Mucorales) in the high priority group (World Health Organization, 2022). The latter three pathogens, which are the focus of this dissertation, are further discussed in the following subsections.

Candida albicans

As mentioned previously, *C. albicans* can exist as a human commensal species or cause serious infections. Its dimorphic switching between the yeast form and the hyphal form (Mukaremera et al., 2017) and its ability to form dense biofilms on a variety of surfaces (such as dentures and implants) contribute to its ability to cause severe disease. It is the most common causative agent of candidiasis (Pappas et al., 2018). Approximately 1.5 million cases of invasive candidiasis occur each year, with an estimated mortality rate of 63% (Denning, 2024). The treatment regimen for invasive candidiasis is usually an echinocandin for the initial stage followed by a transition to an azole, although the polyene amphotericin B (AmB) is an available alternative (Pappas et al., 2016; Barantsevich and Barantsevich, 2022).

The *C. albicans* strain used in this dissertation is SC5314, a common reference strain originally isolated in 1984 from a disseminated candidiasis case (Gillum, Tsay, and Kirsch, 1984). The *C. albicans* cell wall contains two layers: (1) an inner layer containing chitin, short O-linked mannans, and (primarily) β-glucans, and (2) an outer layer containing long N-linked mannans (Gow and Lenardon, 2023). Although the presence of these particular carbohydrates enables the recognition of *C. albicans* by immune receptors such as the Dectins, the dynamic nature of the fungal cell wall helps *C. albicans* evade the immune response and survive despite the use of an antifungal treatment. For example, in response to the use of echinocandins, which target β-glucan synthase, *C. albicans* upregulates chitin synthesis pathways as a compensatory mechanism (Walker et al., 2008). β-glucan exposure is also regulated in response to various conditions, thus further minimizing the possibility of immune receptor recognition (Chen, Wagner, and Reynolds, 2022). However, it has also been reported that β-glucan exposure becomes more prevalent over the duration of a typical infection compared to the initial stages, thus explaining the involvement of β-glucan-recognizing immune receptors in candidiasis infections (Wheeler et al., 2008).

Cryptococcus neoformans

C. neoformans has a worldwide distribution but is primarily found in decaying matter and bird guano (May et al., 2016). Unique characteristics that enable its virulence include melanin production and a capsule with varying degrees of thickness depending on environmental circumstances (Ristow et al., 2023). It can cross the blood-brain barrier and lead to cryptococcal meningitis. Although cryptococcal meningitis can occur among different groups of immunocompromised patients, it is most notably associated with HIV/AIDS. Approximately

19% of AIDS-related mortality is linked to cryptococcal meningitis cases globally (Rajasingham et al., 2022). The overall mortality rate for cryptococcal meningitis is estimated at 75% (Denning, 2024). The treatment regimen usually involves some combination of an azole, AmB, and/or 5-flucytosine (Spadari et al., 2020). *Cryptococcus* spp. have intrinsic resistance against echinocandins despite the presence of the drug class's enzymatic target (Denning, 2003). The mechanism(s) that cause(s) this resistance are still unclear (Mukaremera, 2023).

The *C. neoformans* strain used in this study is H99, a common reference strain that was originally isolated in 1978 from a Hodgkin's disease patient (Janbon et al., 2014). The *C. neoformans* cell wall primarily contains a mix of β-glucans, chitosan, and chitin, while the surrounding capsule primarily contains glucuronoxylomannan and galactoxylomannan (Mukaremera, 2023). In addition to protecting the glucans from immune cell recognition, the capsule itself does not elicit a strong immune response (Zaragoza and Casadevall, 2004).

Rhizopus delemar

R. delemar (formerly *R. oryzae*) is a saprotroph that is part of the Mucorales order, which as a whole has a worldwide distribution; species-specific variation in distribution has been observed (Hoenigl et al., 2022). Virulence characteristics include the production of a unique toxin (mucoricin) and a set of spore coat proteins (cotH) that help facilitate invasion into a host (Soliman et al., 2021; Tahiri et al., 2023). It is the most common causative agent of mucormycosis. Despite varying incidence rates from country to country, 900,000 cases are estimated to occur globally each year (Prakash and Chakrabarti, 2019). In particular, India experienced a surge in COVID-19-associated mucormycosis cases; a potential link between the presence of Mucorales-rich cow dung in India and cultural practices that enable spore dispersion

has been discussed (Skaria et al., 2022). The treatment regimen usually involves a combination of AmB and either isavuconazole or posaconazole; surgery to remove infected tissue is also critical (Smith and Lee, 2022). Echinocandins are not effective against *Rhizopus* despite the presence of the enzymatic target (Reed et al., 2008).

The *R. delemar* strain used in this study is 99-880, a clinical strain originally isolated in 1999 from a rhinocerebral mucormycosis case (Broad Institute). The *Rhizopus* cell wall is not as thoroughly characterized as the cell walls of *Candida* and *Cryptococcus*. Miscellaneous studies have elucidated the presence of specific components rather than the precise structure. Enzymatic analyses indicate that chitosan, chitin, glucosamine, and N-acetylglucosamine are important components (Tominaga and Tsujisaka, 1981). Genome analyses indicate that *R. delemar* has 23 chitin synthases and 34 chitin deacetylases, further validating the importance of chitin and chitosan to its cell wall (Ma et al., 2009). Mucoran and mucoric acid, which contain glucuronic acid and mannose units, have also been reported (Lecointe et al., 2019). Specific links between the dynamic cell wall and immune response recognition/evasion are still being elucidated. However, it is known that β-glucan exposure during *Rhizopus* hyphal formation contributes to immune recognition via Dectin-1 (Chamilos et al., 2010).

The Urgent Need for Effective Antifungals

There are only three primary classes of antifungals - the polyenes, the echinocandins, and the azoles - that have been approved for treating serious infections since the 1950s. Briefly, the echinocandins and azoles have enzymatic targets (β-1,3-glucan synthase and lanosterol 14-α demethylase, respectively). Pros include the existence of oral formulations (azoles) and the minimal potential of drug-drug interactions (echinocandins). Cons include the rising likelihood

of drug resistance since these classes have enzymatic targets instead of structural targets. Polyenes target ergosterol, which is found in the fungal cell membrane. The first polyene, fungicidin (now known as nystatin), was reported in 1951 as a product of a *Streptomyces noursei* strain from a Virginian farm soil sample (Hazen and Brown, 1951; Hazen and Brown, 1952). The class has since expanded to include amphotericin B (AmB) and natamycin, among others. AmB, the focus of this dissertation, is further discussed below.

AmB was discovered in the 1950s as a product of a *Streptomyces nodosus* isolate that originated from a Venezuelan soil sample, and it was patented in 1954 (Dutcher et al., 1954). It consists of three main components: a polyol region, a polyene region, and a mycosamine unit (Volmer, Szpilman, and Carriera, 2010). The structural role and relevance of each region in relation to antifungal activity is still being elucidated. However, it is known that the mycosamine unit is required for AmB to interact with ergosterol, and the loss of this unit results in no antifungal activity (Palacios et al., 2011; Palacios, Anderson, and Burke, 2007).

The exact mechanism of action is still under debate. The original model indicated that polyenes create pores in the fungal cell membrane by forming complexes within the lipid bilayer, therefore causing ion leakage and cell death (Mesa-Arango et al., 2012). However, in one study, Gray et al. (2012) generated two derivatives of AmB: one that does not bind to ergosterol, form ion channels, or have antifungal activity (amphoteronolide B) and one that can bind to ergosterol but cannot form ion channels (C35deOAmB). By studying these derivatives in comparison to AmB in vitro, they showed that polyene-mediated fungal cell death requires binding to ergosterol but does not require the formation of ion channels. Anderson et al. (2014) proposed that AmB aggregates into an extramembranous sterol sponge that can extract ergosterol out of the fungal cell membrane; they showed that saturating AmB with ergosterol prior to treating fungal cells

significantly reduced AmB's ability to extract ergosterol from fungal cell membranes and, therefore, kill fungal cells. Mesa-Arango et al. (2014) showed that the production of reactive oxygen species (ROS) is also a critical component of AmB's effectiveness; ROS accumulation in fungal cells increased after AmB treatment, whereas the pretreatment of fungal cells with a respiratory chain inhibitor led to a significant reduction in AmB's ability to induce ROS accumulation. In summary, AmB's mechanism of action against ergosterol is a multifaceted process that is still being elucidated.

AmB is known to have a broad spectrum of fungicidal activity and, therefore, has been described as the "gold standard" of antifungal treatments (Saravolatz et al., 2003). However, it has several issues that have limited its clinical use. For example, AmB can also bind to cholesterol, albeit with a lower affinity compared to ergosterol (Kotler-Brajtburg et al., 1974; Readio and Bittman, 1982). A known side-effect is nephrotoxicity, which can ultimately lead to renal failure (Deray, 2002). Hepatotoxicity has also been reported, albeit rarely, since AmB can accumulate in the liver (Inselmann, Inselmann, and Heidemann, 2002).

Another issue is that AmB has poor solubility in water due to its amphipathic structure; it oligomerizes in aqueous solutions and forms insoluble aggregates (Torrado et al., 2008; Faustino and Pinheiro, 2020; Barratt and Bretagne, 2007). The oral bioavailability is reportedly as low as 0.2-0.9%, and this has severely hindered the development of oral formulations (Serrano and Lalatsa, 2017). The first AmB formulation to be licensed for mycoses treatment was AmB deoxycholate (Fungizone®), which is administered intravenously. In this formulation, AmB is complexed with sodium deoxycholate, a bile salt detergent that improves both the solubility of AmB in water and the stability of the subsequent aggregates that form in the solution (Cavassin et al., 2021). The particle size is less than 25 nm (Cavassin et al., 2021). However, the aggregates

dissociate almost immediately after the treatment is administered, causing the drug to be released into the bloodstream (Fanos and Cataldi, 2000). Additionally, the sodium deoxycholate itself could potentially contribute to the treatment's toxicity since bile salts can act on cell membranes (Zager, Bredl, and Schimpf, 1992).

Attempts at developing safer alternatives to Fungizone® led to the FDA approval of three lipid-based treatments in the mid-1990s: Abelcet®, Amphocil®, and AmBisome®. In Abelcet®, AmB is complexed with a ratio of certain lipids and suspended in 0.9% sodium chloride to form ribbon-like structures that range from 1,600 nm to 11,000 nm in size (Adedoyin et al., 1997; Cavassin et al., 2021). In Amphocil®, AmB is complexed with cholesteryl sulphate to form a colloidal dispersion of disc-like structures that range from 100 nm to 140 nm in size (Adler-Moore and Proffitt, 2008). Improvements with these treatments compared to Fungizone® include the ability to safely administer higher doses of AmB and higher concentrations of AmB being measured away from the kidneys. However, shortcomings of these treatments include infusion-related events and low lipid transition temperatures that can prevent the complexes from reaching their intended targets before disintegrating (Adedoyin et al., 1997; Hilery, 1997).

In AmBisome®, AmB is intercalated into the lipid bilayer of liposomes that are approximately 100 nm in size (Adler-Moore and Proffitt, 2008). Liposomes are spherical vesicles in which a lipid bilayer surrounds an aqueous core; therefore, they can package hydrophobic or hydrophilic compounds. Since the 1960s, liposomes have been used as drug delivery vehicles to treat diseases ranging from viral infections to different types of cancer. Pharmacological benefits of liposomes include an extended half-life for the drugs and a general reduction in drug toxicity (Hua and Wu, 2013). However, one limitation of conventional liposomes is that they are removed from circulation by the reticuloendothelial system (RES,

which contains the liver and spleen), thus limiting their overall effectiveness (Papahadjopoulos et al., 1991). Stealth, or pegylated, liposomes were generated to circumvent this; they contain polyethylene glycol, a polymer coating that improves the stability of the liposomes and interferes with RES recognition (Papahadjopoulos et al., 1991; Sercombe et al., 2015; Gregoriadis, 2016). AmBisome® exhibits similar improvements (such as higher standard drug dosages) over Fungizone® compared to the other formulations. Despite these improvements, infusion-related events and off-target effects (nephrotoxicity, hepatotoxicity, etc.) are still prevalent with the use of AmBisome® (Stone et al., 2016). Therefore, our research group wondered if the addition of a targeted specificity mechanism could help minimize these side effects and improve treatment efficacy.

From Liposomes to Targeted Liposomes

Targeted drug delivery can be classified into two categories: passive targeting involves the accumulation of the drug through the enhanced permeability and retention effect of tissues of interest, while active targeting involves the incorporation of a molecule that specifically recognizes the target of interest (Torchilin, 2010). Targeted drug delivery is a focus of cancer research, but targeted liposomes in medical mycology is a developing field of study. To our knowledge, our DectiSomes are the first published example of a targeted antifungal-loaded liposome (Ambati et al., 2019b). However, at least one other published example of a targeted antifungal liposome has emerged since then. An AmB-loaded liposome coated with a chitin-binding protein had increased antifungal activity against *C. neoformans* compared to the uncoated liposome (Taniguchi et al., 2022). Our targeting mechanism of choice is the Dectin immune receptors, which are further discussed below.

The Roles of Dectins

C-type Lectin Receptors (CLRs) are defined as proteins that contain at least one C-type lectin-like domain (CTLD); by this broad criterion, there are at least 1,000 proteins that can be further categorized into 17 subgroups with a variety of functions (Brown et al., 2018). Although commonly associated with the ability to bind carbohydrates, CLRs are also capable of binding a variety of substrates such as lipids, other proteins, and even ice (Brown et al., 2018). Mammalian CLRs contain three main components: the CTLD, a stalk domain, and a transmembrane domain. Our truncated versions of Dectins contain the CTLD (which we also refer to as the carbohydrate recognition domain or CRD) and a portion of the stalk domain.

Dectin-1 (CLEC7A), Dectin-2 (CLEC6A), and Dectin-3 (CLEC4D; also known as MCL or macrophage C-type lectin) are expressed on a variety of immune cell types, such as dendritic cells, neutrophils, and macrophages. Dectin-1 primarily recognizes β-glucans, which are present in a wide variety of pathogenic fungal genera. Dectin-2 and Dectin-3 primarily recognize alpha-mannans, although Dectin-3 also recognizes some unique components such as glucuroxylomannan in the *Cryptococcus* capsule and trehalose 6,6'-dimycolate in *Mycobacterium* spp. (Huang et al., 2018; Zhao et al., 2014). Dectin-2 reportedly recognizes more genera than Dectin-3, but this is potentially because Dectin-3 is not as thoroughly characterized. Dectin-2 and Dectin-3 are also capable of forming a heterodimer that has a greater affinity for mannans compared to their homodimers (Zhu et al., 2013). In addition to their broad recognition activity, Dectins are significantly smaller than antibodies that may recognize similar ligands (Meagher et al., 2023), making this an ideal choice for a targeting mechanism.

DectiSomes: Targeted Antifungal Liposomes

Given that one of the limitations of liposomal AmB is off-target effects and subsequent organ-associated toxicity, our research group wondered if a targeting mechanism could be incorporated onto liposomal AmB to minimize those effects. Since Dectins are known to specifically recognize various fungi as part of the human immune response, our research group generated DectiSomes - targeted antifungal-loaded liposomes - as a potential answer to this question. The four primary components of DectiSomes are (1) the liposome itself, (2) AmB intercalated into the lipid bilayer, (3) the respective Dectin receptor at the surface, and (4) rhodamine B at the surface for fluorescence microscopy purposes (**Figure 1**).

When constructing DectiSomes, the carbohydrate recognition domain and partial stalk domain sequences of Dectins are codon-optimized. A histidine tag, a flexible spacer region, and several lysine residues are added to the N-terminus of the final sequence. This construct is cloned into the pET-45b+ plasmid, which is subsequently used for *E. coli* transformations. The Dectin protein is purified and modified to add a DSPE-PEG lipid moiety to the lysine residues; this lipid moiety enables integration into the liposome bilayer. AmB is dissolved in dimethyl sulfoxide in excess and incubated with liposomes for a final drug concentration of approximately 11 mol%, which is comparable to the standard AmBisome® drug concentration. These drug-loaded liposomes are then incubated with the lipid-conjugated Dectin protein and rhodamine B-DHPE to generate the final DectiSome product. The DectiSome's Dectin coating, with its high affinity for fungal-specific glycans, is predicted to guide the DectiSomes toward their intended target - the fungal pathogen - and away from off-target sites such as host cells. This promotes a more concentrated diffusion of the drug around the fungal cell, therefore lowering the required effective drug dosage and the risk of off-target effects.

Prior to this dissertation project, our research group had shown that DectiSomes coated with either Dectin-1 or Dectin-2 bound to *A. fumigatus, C. albicans,* and *C. neoformans* more effectively in vitro than uncoated, drug-loaded liposomes (hereafter referred to as untargeted liposomes) or bovine serum albumin (BSA)-coated, drug-loaded liposomes, which were included as a non-specific binding control. Using a combination of germination measurements and metabolic activity assays, our research group showed that these DectiSomes also inhibited and/or killed these fungi more effectively than the respective controls in vitro (Ambati et al., 2019a; Ambati et al., 2019b). In parallel to this dissertation project, our research group has shown that these DectiSomes exhibit improved efficacy in vivo in murine models of pulmonary aspergillosis, disseminated candidiasis, and systemic cryptococcosis; they observed increased DectiSome binding to infection centers, higher survival rates with the DectiSome treatment, and lower levels of fungal burden in tissue samples (Ambati et al., 2021; Ambati et al., 2022; Pham et al., 2024). Our research group also published a recent in-depth review about the overall project (Meagher et al., 2023).

The goal of this dissertation is to expand upon the potential uses of DectiSomes as a novel technology. This was pursued in three primary directions: evaluating efficacy against different fungal pathogens, constructing additional types of DectiSomes, and repurposing DectiSomes outside of an antifungal treatment. Chapter 2 focuses on the in vitro efficacy of existing Dectin-1 DectiSomes on *R. delemar*. Chapter 3 focuses on the construction of Dectin-3 DectiSomes and their efficacy against several clinically relevant human fungal pathogens. Chapter 4 focuses on the potential applications of DectiSomes as biological probes. Chapter 5 summarizes the outcomes of the previous chapters and discusses future directions.

References

Adedoyin, A., Bernardo, J.F., Swenson, C.E., Bolsack, L.E., Horwith, G., DeWit, S., Kelly, E., Klasterksy, J., Sculier, J.P., DeValeriola, D., Anaissie, E., Lopez-Berestein, G., Llanos-Cuentas, A., Boyle, A., and Branch, R.A. (1997). Pharmacokinetic profile of ABELCET (amphotericin B lipid complex injection): combined experience from phase I and phase II studies. *Antimicrobial Agents and Chemotherapy*, 41 (10).

Adler-Moore, J.P., and Proffitt, R.T. (2008). Amphotericin B lipid preparations: what are the differences? *Clinical Microbiology and Infection*, 14.

Ambati, S., Ellis, E.C., Lin, J., Lin, X., Lewis, Z.A., and Meagher, R.B. (2019a). Dectin-2-Targeted Antifungal Liposomes Exhibit Enhanced Efficacy. *mSphere*, 4 (5).

Ambati, S., Ellis, E.C., Pham, T., Lewis, Z.A., Lin, X., and Meagher, R.B. (2021). Antifungal Liposomes Directed by Dectin-2 Offer a Promising Therapeutic Option for Pulmonary Aspergillosis. *mBio*, 12 (1).

Ambati, S., Ferraro, A.R., Kang, S.E., Lin, J., Lin, X., Momany, M., Lewis, Z.A., and Meagher, R.B. (2019b). Dectin-1-Targeted Antifungal Liposomes Exhibit Enhanced Efficacy. *mSphere*, 4 (2).

Ambati, S., Pham, T., Lewis, Z.A., Lin, X., and Meagher, R.B. (2022). DectiSomes: Glycan Targeting of Liposomal Drugs Improves the Treatment of Disseminated Candidiasis. *Antimicrobial Agents and Chemotherapy*, 66 (1).

Anderson, T.M., Clay, M.C., Cioffi, A.G., Diaz, K.A., Hisao, G.S., Tuttle, M.D., Nieuwkoop, A.J., Comellas, G., Maryum, N., Wang, S., Uno, B.E., Wildeman, E.L., Gonen, T., Rienstra, C.M., and Burke, M.D. (2014). Amphotericin forms an extramembranous and fungicidal sterol sponge. *Nature Chemical Biology*, 10.

Barantsevich, N., and Barantsevich, E. (2022). Diagnosis and Treatment of Invasive Candidiasis. *Antibiotics*, 11 (6).

Barratt, G., and Bretagne, S. (2007). Optimizing efficacy of Amphotericin B through nanomodification. *International Journal of Nanomedicine*, 2 (3).

Benedict, K., Whitham, H.K., and Jackson, B.R. (2022). Economic Burden of Fungal Diseases in the United States. *Open Forum Infectious Diseases*, 9 (4).

Broad Institute. Mucorales Genomes. Accessible at: https://www.broadinstitute.org/fungal-genome-initiative/mucorales-genomes

Brown, G.D., Willment, J.A., and Whitehead, L. (2018). C-type lectins in immunity and homeostasis. *Nature Reviews Immunology*, 18.

Cavassin, F.B., Baú-Carneiro, J.L., Vilas-Boas, R.R., and Queiroz-Telles, F. (2021). Sixty years of Amphotericin B: An Overview of the Main Antifungal Agents Used to Treat Invasive Fungal Infections. *Infectious Diseases and Therapy*, 10 (1).

Chamilos, G., Ganguly, D., Lande, R., Gregorio, J., Meller, S., Goldman, W.E., Gilliet, M., and Kontoyiannis, D.P. (2010). Generation of IL-23 Producing Dendritic Cells (DCs) by Airborne Fungi Regulates Fungal Pathogenicity via the Induction of T_H-17 Responses. *PLoS ONE*, 5 (9).

Chen, T., Wagner, A.S., and Reynolds, T.B. (2022). When Is It Appropriate to Take Off the Mask? Signaling Pathways That Regulate β(1,3)-Glucan Exposure in *Candida albicans*. *Frontiers in Fungal Biology*, 3.

Denning, D.W. (2003). Echinocandin antifungal drugs. *The Lancet*, 362 (9390).

Denning, D.W. (2024). Global incidence and mortality of severe fungal disease. *The Lancet Infectious Diseases*, 24 (7).

Deray, G. (2002). Amphotericin B nephrotoxicity. *Journal of Antimicrobial Chemotherapy*, 49.

Dutcher, J.D., Gold, W., Pagano, J.F., and Vandeputte, J. (1954). Amphotericin b, its production, and its salts. Patent # US2908611A. Accessible at: https://patents.google.com/patent/US2908611A/en.

Fanos, V., and Cataldi, L. (2000). Amphotericin B-Induced Nephrotoxicity: A Review. *Journal of Chemotherapy*, 12 (6).

Faustino, C., and Pinheiro, L. (2020). Lipid Systems for the Delivery of Amphotericin B in Antifungal Therapy. *Pharmaceutics*, 12 (1).

Fisher, M.C., Gurr, S.J., Cuomo, C.A., Blehert, D.S., Jin, H., Stukenbrock, E.H., Stajich, J.E., Kahmann, R., Boone, C., Denning, D.W., Gow, N.A.R., Klein, B.S., Kronstad, J.W., Sheppard, D.C., Taylor, J.W., Wright, G.D., Heitman, J., Casadevall, A., and Cowen, L.E. (2020). Threats Posed by the Fungal Kingdom to Humans, Wildlife, and Agriculture. *mBio*, 11 (3).

Forsberg, K., Woodworth, K., Walters, M., Berkow, E.L., Jackson, B., Chiller, T., and Vallabhaneni, S. (2019). *Candida auris*: The recent emergence of a multidrug-resistant fungal pathogen. *Medical Mycology*, 57 (1).

Gillum, A.M., Tsay, E.Y.H., and Kirsch, D.R. (1984). Isolation of the *Candida albicans* gene for orotidine-5'-phosphate decarboxylase by complementation of *S. cerevisiae ura3* and *E. coli pyrF* mutations. *Molecular and General Genetics*, 198.

Gow, N.A.R., and Lenardon, M.D. (2023). Architecture of the dynamic fungal cell wall. *Nature Reviews Microbiology*, 21.

Gray, K.C., Palacios, D.S., Dailey, I., Endo, M.M., Uno, B.E., Wilcock, B.C., and Burke, M.D. (2012). Amphotericin primarily kills yeast by simply binding ergosterol. *Proceedings of the National Academy of Sciences of the United States of America*, 109 (7).

Gregoriadis, G. (2016). Liposomes in Drug Delivery: How It All Happened. *Pharmaceutics*, 8 (2).

Hazen, E.L., and Brown, R. (1951). Fungicidin, an Antibiotic Produced by a Soil Actinomycete. *Experimental Biology and Medicine*, 76 (1).

Hazen, E.L., and Brown, R. (1952). Nystatin and method of producing it. Patent # US2797183A. Accessible at: https://patents.google.com/patent/US2797183A/en.

Hillery, A.M. (1997). Supramolecular lipidic drug delivery systems: From laboratory to clinic A review of the recently introduced commercial liposomal and lipid-based formulations of amphotericin B. *Advanced Drug Delivery Reviews*, 24 (2-3).

Hoenigl, M., Seidel, D., Carvalho, A., Rudramurthy, S.M., Arastehfar, A., Gangneux, J-P., Nasir, N., Bonifaz, A., Araiza, J., Klimko, N., Serris, A., Lagrou, K., Meis, J.F., Cornely, O.A., Perfect, J.R., White, P.L., and Chakrabarti, A. (2022). The emergence of COVID-19 associated mucormycosis: a review of cases from 18 countries. *The Lancet Microbe*, 3 (7).

Hua, S., and Wu, S.Y. (2013). The use of lipid-based nanocarriers for targeted pain therapies. *Frontiers in Pharmacology*, 4.

Huang, H-R., Li, F., Han, H., Xu, X., Li, N., Wang, S., Xu, J-F., and Jia, X-M. (2018). Dectin-3 Recognizes Glucuroxylomannan of *Cryptococcus neoformans* Serotype AD and *Cryptococcus gattii* Serotype B to Initiate Host Defense Against Cryptococcosis. *Frontiers in Immunology*, 9.

Inselmann, G., Inselmann, U., and Heidemann, H.T. (2002). Amphotericin B and liver function. *European Journal of Internal Medicine*, 13 (5).

Janbon G., Ormerod, K.L., Paulet, D., Byrnes III, E.J., Yadav, V., Chatterjee, G., Mullapudi, N., Hon, C-C., Billmyre, R.B., Brunel, F., Bahn, Y-S., Chen, W., Chen, Y., Chow, E.W.L., Coppée, J-Y., Flyod-Averette, A., Gaillardin, C., Gerik, K.J., Goldberg, J., Gonzalez-Hilarion, S., Gujja, S., Hamlin, J.L., Hzueh, Y-P., Ianiri, G., Jones, S., Kodira, C.D., Kozubowski, L., Lam, W., Marra, M., Mesner, L.D., Mieczkowski, P.A., Moyrand, F., Nielsen, K., Proux, C., Rossignol, T., Schein, J.E., Sun, S., Wollschlaeger, C., Wood, I.A., Zeng, Q., Neuvéglise, C., Newlon, C.S., Perfect, J.R., Lodge, J.K., Idnurm, A., Stajich, J.E., Kronstad, J.W., Sanyal, K., Heitman, J., Fraser, J.A., Cuomo, C.A., and Dietrich, F.S. (2014). Analysis of the Genome and Transcriptome of *Cryptococcus neoformans* var. *grubii* Reveals Complex RNA Expression and Microevolution Leading to Virulence Attenuation. *PLoS Genetics*, 10 (4).

Kotler-Brajtburg, J., Price, H.D., Medoff, G., Schlessinger, D., and Kobayashi, G.S. (1974). Molecular Basis for the Selective Toxicity of Amphotericin B for Yeast and Filipin for Animal Cells. *Antimicrobial Agents and Chemotherapy*, 5 (4).

Kumamato, C.A., Gresnigt, M.S., and Hube, B. (2020). The gut, the bad and the harmless: *Candida albicans* as a commensal and opportunistic pathogen in the intestine. *Current Opinion in Microbiology*, 56.

Lecointe, K., Cornu, M., Leroy, J., Coulon, P., and Sendid, B. (2019). Polysaccharides Cell Wall Architecture of Mucorales. *Frontiers in Microbiology*, 10.

Ma, L-J., Ibrahim, A.S., Skory, C., Grabherr, M.G., Burger, G., Butler, M., Elias, M., Idnurm, A., Lang, B.F., Sone, T., Abe, A., Calvo, S.E., Corrochano, L.M., Engels, R., Fu, J., Hansberg, W., Kim, J-M., Kodira, C.D., Koehrsen, M.J., Liu, B., Miranda-Saavedra, D., O'Leary, S., Ortiz-Castellanos, L., Poulter, R., Rodriguez-Romero, J., Ruiz-Herrera, J., Shen, Y-Q., Zeng, Q., Galagan, J., Birren, B.W., Cuomo, C.A., and Wickes, B.L. (2009). Genomic Analysis of the Basal Lineage Fungus *Rhizopus oryzae* Reveals a Whole-Genome Duplication. *PLoS Genetics*, 5 (7).

May, R.C., Stone, N.R.H., Wiesner, D.L., Bicanic, T., and Nielsen, K. (2016). *Cryptococcus*: from environmental saprophyte to global pathogen. *Nature Reviews Microbiology*, 14.

Meagher, R.B., Lewis, Z.A., Ambati, S., and Lin, X. (2023). DectiSomes: C-type lectin receptor-targeted liposomes as pan-antifungal drugs. *Advanced Drug Delivery Reviews*, 196.

Mesa-Arango, A.C., Scorzoni, L., and Zaragoza, O. (2012). It only takes one to do many jobs: Amphotericin B as antifungal and immunomodulatory drug. *Frontiers in Microbiology*, 3.

Mesa-Arango, A.C., Trevijano-Contador, N., Román, E., Sánchez-Fresneda, R., Casas, C., Herrero, E., Argüelles, J.C., Pla, J., Cuenca-Estrella, M., and Zaragoza, O. (2014). The Production of Reactive Oxygen Species Is a Universal Action Mechanism of Amphotericin B against Pathogenic Yeasts and Contributes to the Fungicidal Effect of This Drug. *Antimicrobial Agents and Chemotherapy*, 58 (11).

Mukaremera, L. (2023). The *Cryptococcus* wall: A different wall for a unique lifestyle. *PLoS Pathogens*, 19 (2).

Mukaremera, L., Lee, K.K., Mora-Montes, H.M., and Gow, N.A.R. (2017). *Candida albicans* Yeast, Pseudohyphal, and Hyphal Morphogenesis Differentially Affects Immune Recognition. *Frontiers in Immunology*, 8.

One Health: Fungal Pathogens of Humans, Animals, and Plants: Report on an American Academy of Microbiology Colloquium held on Oct. 18, 2017. Washington (DC): American

Society for Microbiology; 2019. Accessible at: https://asm.org/reports/one-health-fungal-pathogens-of-humans,-animals,-an.

Palacios, D.S., Anderson, T.M., and Burke, M.D. (2007). A Post-PKS Oxidation of the Amphotericin B Skeleton Predicted to be Critical for Channel Formation Is Not Required for Potential Antifungal Activity. *Journal of the American Chemical Society*, 129 (45).

Palacios, D.S., Dailey, I., Siebert, D.M., Wilcock, B.C., and Burke, M.D. (2011). Synthesis-enabled functional group deletions reveal key underpinnings of amphotericin B ion channel and antifungal activities. *Proceedings of the National Academy of Sciences of the United States of America*, 108 (17).

Papahadjopoulos, D., Allen, T.M., Gabizon, A., Mayhew, E., Matthay, K., Huang, S.K., Lee, K.D., Woodle, M.C., Lasic, D.D., and Redemann, C. (1991). Sterically stabilized liposomes: improvements in pharmacokinetics and antitumor therapeutic efficacy. *Proceedings of the National Academy of Sciences of the United States of America*, 88 (24).

Pappas, P.G., Kauffman, C.A., Andes, D.R., Clancy, C.J., Marr, K.A., Ostrosky-Zeichner, L., Reboli, A.C., Schuster, M.G., Vazquez, J.A., Walsh, T.J., Zaoutis, T.E., and Sobel, J.D. (2016). Clinical Practice Guideline for the Management of Candidiasis: 2016 Update by the Infectious Diseases Society of America. *Clinical Infectious Diseases*, 62 (4).

Pappas, P.G., Lionakis, M.S., Arendrup, M.C., Ostrosky-Zeichner, L., and Kullberg, B.J. (2018). Invasive candidiasis. *Nature Reviews Disease Primers*, 4.

Pham, T., Shi, R., Ambati, S., Meagher, R., and Lin, X. (2024). All hands on Dec: Treating cryptococcosis with dectin decorated liposomes loaded with antifungals. *iScience*, 27 (7).

Prakash, H., and Chakrabarti, A. (2019). Global Epidemiology of Mucormycosis. *Journal of Fungi*, 5 (1).

Rajasingham, R., Govender, N.P., Jordan, A., Loyse, A., Shroufi, A., Denning, D.W., Meya, D.B., Chiller, T.M., and Boulware, D.R. (2022). The global burden of HIV-associated cryptococcal infection in adults in 2020: a modelling analysis. *The Lancet Infectious Diseases*, 22 (12).

Readio, J.D., and Bittman, R. (1982). Equilibrium binding of amphotericin B and its methyl ester and borate complex sterols. *Biochimica et Biophysica Acta (BBA) – Biomembranes*, 685 (2).

Reed, C., Bryant, R., Ibrahim, A.S., Edwards Jr., J., Filler, S.G., Goldberg, R., and Spellberg, B. (2008). Combination Polyene-Caspofungin Treatment of Rhino-Orbital-Cerebral Mucormycosis. *Clinical Infectious Diseases*, 47 (3).

Ristow, L.C., Jezewski, A.J., Chadwick, B.J., Stamnes, M.A., Lin, X., and Krysan, D.J. (2023). *Cryptococcus neoformans* adapts to the host environment through TOR-mediated remodeling of phospholipid asymmetry. *Nature Communications*, 14.

Rokas, A. (2022). Evolution of the human pathogenic lifestyle in fungi. *Nature Microbiology*, 7.

Saravolatz, L.D., Ostrosky-Zeichner, L., Marr, K.A., Rex, J.H., and Cohen, S.H. (2003). Amphotericin B: Time for a New "Gold Standard". *Clinical Infectious Diseases*, 37 (3).

Sercombe, L., Veerati, T., Moheimani, F., Wu, S.Y., Sood, A.K., and Hua, S. (2015). Advances and Challenges of Liposome Assisted Drug Delivery. *Frontiers in Pharmacology*, 6.

Serrano, D.R., and Lalatsa, A. (2017). Oral amphotericin B: The journal from bench to market. *Journal of Drug Delivery Science and Technology*, 42.

Skaria, J., John, T.M., Varkey, S., and Kontoyiannis, D.P. (2022). Are Unique Regional Factors the Missing Link in India's COVID-19-Associated Mucormycosis Crisis? *mBio*, 13 (2).

Smith, C., and Lee, S.C. (2022). Current treatments against mucormycosis and future directions. *PLoS Pathogens*, 18 (10).

Soliman, S.S.M., Baldin, C., Gu, Y., Singh, S., Gebremariam, T., Swidergall, M., Alqarihi, A., Youssef, E.G., Alkhazraji, S., Pikoulas, A., Perske, C., Venkataramani, V., Rich, A., Bruno, V.M., Dunning Hotopp, J., Mantis, N.J., Edwards Jr., J.E., Filler, S.G., Chamilos, G., Vitetta, E.S., and Ibrahim, A.S. (2021). Mucoricin is a ricin-like toxin that is critical for the pathogenesis of mucormycosis. *Nature Microbiology*, 6.

Spadari, C.C., Wirth, F., Lopes, L.B., and Ishida, K. (2020). New Approaches for Cryptococcosis Treatment. *Microorganisms*, 8 (4).

Stone, N.R.H., Bicanic, T., Salim, R., and Hope, W. (2016). Liposomal Amphotericin B (AmBisome ®): A review of the pharmacokinetics, pharmacodynamics, clinical experience and future directions. *Drugs*, 76 (4).

Tahiri, G., Lax, C., Cánovas-Márquez, J.T., Carrillo-Marín, P., Sanchis, M., Navarro, E., Garre, V., and Nicolás, F.E. (2023). *Mucorales* and Mucormycosis: Recent Insights and Future Prospects. *Journal of Fungi*, 9 (3).

Taniguchi, H., Ishimime, Y., Minamihata, K., Santoso, P., Komada, T., Saputra, H., Uchida, K., Goto, M., Taira, T., and Kamiya, N. (2022). Liposomal Amphotericin B Formulation Displaying Lipid-Modified Chitin-Binding Domains with Enhanced Antifungal Activity. *Molecular Pharmaceutics*, 19 (11).

Tominaga, Y., and Tsujisaka, Y. (1981). Investigation of the Structure of *Rhizopus* Cell Wall with Lytic Enzymes. *Agricultural and Biological Chemistry*, 45 (7).

Torchilin, V.P. (2010). Passive and Active Drug Targeting: Drug Delivery to Tumors as an Example. In: Schäfer-Korting, M. (eds) *Drug Delivery. Handbook of Experimental Pharmacology*, vol 197. Springer, Berling, Heidelberg.

Torrado, J.J., Espada, R., Ballesteros, M.P., and Torrado-Santiago, S. (2008). Amphotericin B formulations and drug targeting. *Journal of Pharmaceutical Sciences*, 97 (7).

Volmer, A.A., Szpilman, A.M., and Carriera, E.M. (2010). Synthesis and biological evaluation of amphotericin B derivatives. *Natural Product Reports*, 9.

Walker, L.A., Munro, C.A., de Bruijn, I., Lenardon, M.D., McKinnon, A., and Gow, N.A.R. (2008). Stimulation of Chitin Synthesis Rescues *Candida albicans* from Echinocandins. *PLoS Pathogens* 4 (4).

Wheeler, R.T., Kombe, D., Agarwala, S.D., and Fink, G.R. (2008). Dynamic, Morphotype-Specific *Candida albicans* β-Glucan Exposure during Infection and Drug Treatment. *PLoS Pathogens* 4 (12).

World Health Organization. (2022). WHO fungal priority pathogens list to guide research, development and public health action. Accessible at: https://www.who.int/publications/i/item/9789240060241.

Zager, R.A., Bredl, C.R., and Schimpf, B.A. (1992). Direct amphotericin B-mediated tubular toxicity: Assessments of selected cytoprotective agents. *Kidney International*, 41 (6).

Zaragoza, O., and Casadevall, A. (2004). Antibodies Produced in Response to *Cryptococcus neoformans* Pulmonary Infection in Mice Have Characteristics of Nonprotective Antibodies. *Infection and Immunity*, 72 (7).

Zhao, X-Q., Zhu, L-L., Chang, Q., Jiang, C., You, Y,. Luo, T., Jia, X-M., and Lin, X. (2014). C-type Lectin Receptor Dectin-3 Mediates Trehalose 6,6'-Dimycolate (TDM)-induced Mincle Expression through CARD9/Bcl10/MALT1-dependent Nuclear Factor (NF)-κB Activation. *Journal of Biological Chemistry*, 289 (43).

Zhu, L-L., Zhao, X-Q., Jiang, C., You, Y., Chen, X-P., Jiang, Y-Y., Jia, X-M., and Lin, X. (2013). C-Type Lectin Receptors Dectin-3 and Dectin-3 Form a Heterodimeric Pattern-Recognition Receptor for Host Defense against Fungal Infection. *Immunity*, 39 (2).

Figure

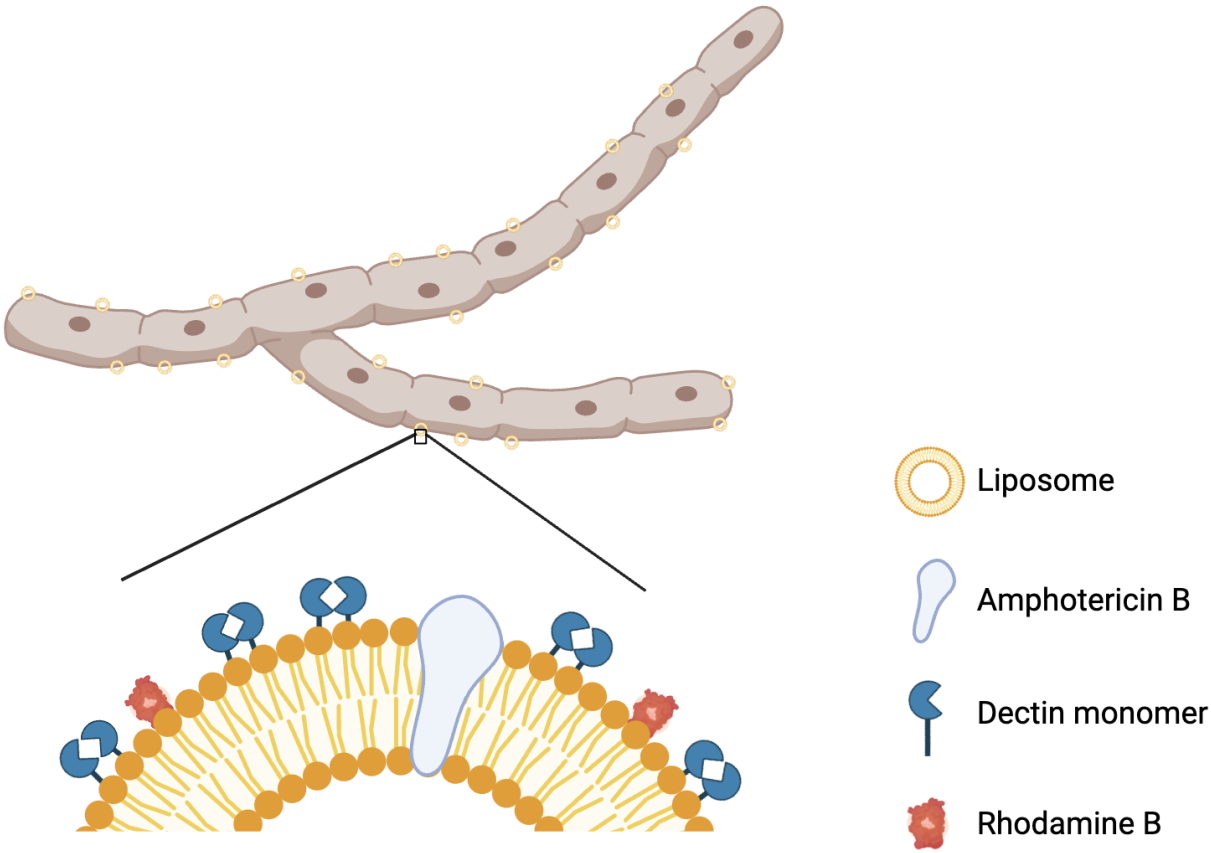

Figure 1: DectiSomes are targeted liposomes that are fungal-specific. Several DectiSomes are bound to a fungal hypha. (Inset) A DectiSome has four main components: (1) the liposome itself, (2) the antifungal amphotericin B in the liposomal membrane, (3) the fluorescent protein rhodamine B at the liposomal surface, and (4) the respective Dectin monomers at the liposomal surface. The Dectin monomers form dimers that facilitate binding to fungal-specific glycans, such as cell wall carbohydrates. Figure made in BioRender.

CHAPTER 2

TARGETED DELIVERY OF ANTIFUNGAL LIPOSOMES TO *RHIZOPUS DELEMAR*[1]

[1]Choudhury Q.J., Ambati S., Lewis Z.A., and Meagher R.B. (2022). Targeted delivery of antifungal liposomes to *Rhizopus delemar. Journal of Fungi* 8 (4), 352. Paper link: https://www.mdpi.com/2309-608X/8/4/352. Reprinted here with permission of publisher.

Abstract

Mucormycosis (a.k.a. zygomycosis) is an often-life-threatening disease caused by fungi from the ancient fungal division Mucoromycota. Globally, there are nearly a million people with the disease. *Rhizopus* spp., and *R. delemar* (*R. oryzae, R. arrhizus*) in particular, are responsible for most of the diagnosed cases. Pulmonary, rhino-orbito-cerebral, and invasive mucormycosis are most effectively treated with amphotericin B (AmB) and particularly with liposomal formulations (e.g., AmBisome®). However, even after antifungal therapy, there is still a 50% mortality rate. Hence, there is a critical need to improve therapeutics for mucormycosis. Targeting AmB-loaded liposomes (AmB-LLs) with the pathogen receptor Dectin-1 (DEC1-AmB-LLs) to the beta-glucans expressed on the surface of *Aspergillus fumigatus* and *Candida albicans* lowers the effective dose required to kill cells relative to untargeted AmB-LLs. Because Dectin-1 is an immune receptor for *R. delemar* infections and may bind it directly, we explored the Dectin-1-mediated delivery of liposomal AmB to *R. delemar*. DEC1-AmB-LLs bound 100- to 1000-fold more efficiently to the exopolysaccharide matrix of *R. delemar* germlings and mature hyphae relative to AmB-LLs. DEC1-AmB-LLs delivering sub-micromolar concentrations of AmB were an order of magnitude more efficient at inhibiting and/or killing *R. delemar* than AmB-LLs. Targeted antifungal drug-loaded liposomes have the potential to improve the treatment of mucormycosis.

Introduction

Globally there are approximately 900,000 individuals with mucormycosis, mostly in India[1,2]. Among those at particular risk are patients with lung diseases; neutropenic patients, such as those receiving prolonged immunosuppression for hematopoietic stem cell transplants;

patients receiving long-term treatment for inflammatory diseases; and patients with diabetic ketoacidosis, COVID-19, or AIDS[3-10]. The number of reported cases of mucormycosis has increased 6- to 7-fold in the last four decades[7], paralleling the increasing numbers of individuals on immunosuppressants and very recently COVID-19. Among the diverse Mucoromycota[11], the genus *Rhizopus* and one species in particular, *Rhizopus delemar* (*R. oryzae*, *R. arrhizus*), are responsible for 50% or more of all diagnosed cases[7,12,13]. *R. delemar* is an opportunistic pathogen living in soil on rotting vegetation. The primary infection route is via inhalation of its sporangiospores, which leads most commonly to pulmonary and rhino-orbito-cerebral infections[14]. Liposomal amphotericin B (AmB) followed by isavuconazole (ISZ) and/or posaconazole (POS) are the most commonly prescribed antifungals[15]. The surgical removal of infected tissue prior to antifungal therapy significantly improves the outcome[16,17]. However, even with antifungal therapy and surgery, there is still approximately a 50% to 99% mortality rate within several months of diagnosis depending upon the level of dissemination at the time of accurate diagnosis and treatment[7,14,16,18]. Clearly, there is a critical need for improved antifungal therapies for mucormycosis.

The immune response to infections caused by *Rhizopus* spp. is mediated by signaling from the C-type lectin pathogen receptor Dectin-1 (*CLEC7A*)[12]. Dectin-1 is expressed on the surface of some classes of leukocytes, including dendritic cells and neutrophils. Indirect evidence suggests Dectin-1 may bind directly to oligoglucans expressed by *Rhizopus*[19,20]. Two Dectin-1 monomers float together such that their extracellular carbohydrate recognition domains (CRDs) form homo-dimers that bind with high affinity to beta-glucans in the cell wall and/or the exopolysaccharide matrices of pathogens[21]. We have been developing DectiSomes as anti-infective agents, using C-type lectin pathogen receptors to target liposomes loaded with

antifungal drugs to pathogenic fungi[22-24]. We have shown that the CRD and stalk region of Dectin-1 may be tethered to liposomes loaded with antifungal drugs, targeting these liposomes specifically to beta-glucans on the surface of fungal pathogens[23,25]. As designed, Dectin-1 CRD monomers float in the liposomal membrane and form the functional homo-dimers necessary for beta-glucan binding. Dectin-1-coated, AmB-loaded liposomes (DEC1-AmB-LLs) bind to the cell walls and exopolysaccharides of *Aspergillus fumigatus* and *Candida albicans* orders of magnitude more strongly than untargeted AmBisome®-like AmB-LLs. DEC1-AmB-LLs also inhibit and/or kill in vitro-grown *A. fumigatus* 100-fold more efficiently than AmB-LLs, reducing the in vitro effective dose for 90% killing more than 10-fold. Considering that Dectin-1 might bind directly to *R. delemar*, we explored the binding of DEC1-AmB-LLs to *R. delemar* and their potential to enhance the efficacy of antifungal liposome treatment.

Materials and Methods

Fungal Strain and Culture Conditions

All studies were performed with *R. delemar* strain 99–880 (ATCC MYA-4621). Sporangiospore stocks were stored frozen at −80°C in 20% glycerol and were prepared fresh for the following experiments by harvesting sporangiospores from potato dextrose agar (PDA; ThermoFisher, Cat# 0013-01-4, Waltham, MA, USA) plates. PDA plates were inoculated with 2 x 10^6 *R. delemar* sporangiospores, which were evenly spread with sterile glass beads and incubated at 37°C. After three days, 1X phosphate-buffered saline (PBS) + 0.05% tween was added to the surface of the plates, and sporangiospores were scraped from the surface into a sterile 250 mL beaker. The sporangiospores were then filtered through a 40 μm cell strainer (Fisherbrand, Cat# 22363547, Rockingham County, NH, USA) into a 50 mL conical tube. The

tube was centrifuged at room temperature for five mins at 1200 x g. The supernatant was removed, and the sporangiospore pellet was resuspended in either 1 mL of PBS + 0.05% tween for short-term storage at 4˚C or in 1 mL of 20% glycerol in sterile deionized water for long-term storage at −80˚C. Titers were determined via hemocytometer counts. Sporangiospores stored at 4˚C remained 99% viable for one to two months.

Liposome Preparations and Fluorescent Tagging of Dectin-1

We prepared 100 nanometer (nm)-diameter pegylated AmB-LLs that contained 11 mole % AmB and 2 mole % rhodamine relative to moles of liposomal lipid as previously described[25]. Pegylation extends the half-life of packaged drugs by significantly reducing opsonization and phagocytosis[26,27]. We previously showed that our pegylated AmB-LLs significantly outperformed commercial AmBisome® at reducing fungal burden in a mouse model of candidiasis[23], presumably because of pegylation. The AmB-LLs were then coated with either 1 mole % Dectin-1 or 0.33 mole % bovine serum albumin (BSA; Sigma-Aldrich, Cat# A-8022, St. Louis, MO, USA), also as described, which achieves the same microgram protein concentration on the surface of the two liposome preparations[25]. Liposomes were stored at 4˚C in RN#5 buffer (0.1 M NaH_2PO_4, 10 mM triethanolamine pH 8.0, 1 M L-arginine, 100 mM NaCl, 5 mM EDTA, and fresh 5 mM 2-mercaptoethanol)[25], and all preparations were adjusted to contain 600 μM AmB. Each liposome preparation was freshly reduced with 1 mM 2-mercaptoethanol (BME; Sigma-Aldrich, Cat# M7522, St. Louis, MO, USA) on a monthly basis and again just prior to use. Rhodamine B-conjugated Dectin-1 protein, DEC1-Rhod, was prepared following the protocol we described previously for rhodamine-tagging Dectin-2[28].

Liposome Binding Activity

In order to prepare fixed agar plugs for microscopy (**Supplemental Figure S2.1**), *R. delemar* sporangiospores were plated on 1.5% agar plates made with RPMI-1640 media lacking phenol red dye (Sigma-Aldrich, Cat# R8755, St. Louis, MO, USA) + 0.165 M MOPS (3-(N-morpholino)propanesulfonic acid) (Sigma-Aldrich, Cat# M1254, St. Louis, MO, USA)[29] adjusted to pH 7 and incubated at 37 ˚C for either 6 to 8 h to sample swollen sporangiospores and germlings or overnight until the hyphal colonies were approximately 6 cm in diameter. A sterile 7 mm-diameter cork-borer was used to remove plugs from the plate with germlings or from the periphery of hyphal colonies to obtain elongating hyphae. Plugs were deposited into a 24-well plate containing 1 mL of 1× PBS and washed once. Plugs were fixed for one hour in freshly-prepared 3.7% formaldehyde (J.T. Baker, Cat# 2106-01, Phillipsburg, NJ, USA) and washed 3 times in PBS before being stored overnight at 4˚C. Plugs were blocked in liposome dilution buffer 1 (LDB1; 1× PBS + 0.5% BSA + 1 mM BME) for one hour. Dectin-1- and BSA-coated liposomes were diluted to 1:100 w/v (protein/buffer). AmB-LLs were similarly diluted. Plugs were incubated with liposomes for two hours at room temperature with shaking at 50 rpm and washed once with the LDB1 buffer in the dark. A 25 mM stock of calcofluor white (CW; Bayer Corp., Blankophor BBH, CAS 4193-55-9, Pittsburgh, PA, USA) stored in dimethyl sulfoxide (DMSO; Sigma-Aldrich, Cat# D8418, St. Louis, MO, USA) was diluted 1:5000 in 1× PBS + 5% DMSO, added to the wash, and incubated with the agar plugs for 30 min. After one more wash, plugs were placed on a microscope slide with the hyphal colony facing upward, fitted with a cover slip, and imaged under epifluorescence on a Leica DM6000 compound microscope at 5× or at 63× under oil immersion[25]. CW cell staining was imaged in the DAPI channel (Ex360/Em470) and rhodamine B-tagged liposomes in the Texas red channel

(Ex560/Em645). The area of red fluorescent liposome binding was quantified using ImageJ (imagej.nih.gov/ij, v. 1.53a; accessed on 4 May 2020). The following sequence of commands was used: Image > (8 bit), followed by Image > Adjust > Threshold > Apply. The commands Analyze > Measure were used to place the area data for each image in a file in Excel (v. 16.16.27). Live hyphal plugs were prepared by omitting the formaldehyde and subsequent wash steps.

In order to assess the specificity of DEC1-AmB-LL binding, fixed hyphal plugs were prepared as described above. DEC1-AmB-LLs were preincubated with either 0.5 mg/mL of laminarin (Sigma-Aldrich; Cat# L-9634, St. Louis, MO, USA) or 0.5 mg/mL yeast mannans (Sigma-Aldrich; Cat# M3640, St. Louis, MO, USA) for 30 min at room temperature. These liposomes were added to the hyphal plugs and incubated for two hours at room temperature with 50 rpm shaking in the dark. The plugs were then processed and imaged as described above.

Liposome Inhibition Activity

In order to determine the inhibitory concentration of AmB delivered by DEC1-AmB-LLs relative to AmB-LLs, two variations of the following assay were performed. Eight hundred *R. delemar* sporangiospores were plated in 90 uL of liquid RPMI + 0.165 M MOPS (pH 7) in individual wells of 96-well microtiter plates. Ten uL of each liposome type (AmB-LLs, BSA-AmB-LLs, and DEC1-AmB-LLs) delivering different concentrations of AmB were immediately added to the respective wells, and the plates were incubated for 24 or 48 h at 37°C with 120 rpm shaking. In one variation, after the first 24 h, the center of each well was imaged with an EVOS imaging system (AMG F1) at 10× magnification. After 48 h, an overview picture of the entire 96-well plate was taken. In the second variation, the cell density (OD at A_{610}) and metabolic

activity were measured at 24 h using a Bio-Tek Synergy HT fluorescent microtiter plate reader. Twenty microliters of the CellTiter-Blue (CTB, Promega; Cat.# G8080; Madison, WI, USA) resazurin reagent was added to each well according to the manufacturer's instructions. The plate was incubated at 37°C for two hours. The pink fluorescence in each well was quantified (Ex485/Em590). The background fluorescence in wells lacking cells was subtracted.

To determine metabolic activity following a short exposure to targeted and untargeted AmB-LLs, 5000 *R. delemar* sporangiospores were plated in 90 uL of liquid RPMI + 0.165 M MOPS (pH 7) in a 96-well microtiter plate. The plate was incubated at 37°C for eight hours until uniform germination and mature hyphae were observed. The liposome treatments were added as described above, and the plate was incubated for three hours at 37°C. The CTB assay was then performed as described above.

Data Management

Quantitative imaging data from ImageJ were initially managed in Excel. Imaging data were then moved to Graph Pad Prism 9 (v. 9.3.1), where scatter bar plots were prepared and standard errors were estimated. p values were estimated in Excel using the Student's two-tailed t test, T.TEST, for various comparisons.

Results

Dectin-1 Targeted DEC1-AmB-LLs Bind to R. delemar

To determine if Dectin-1 would target liposomes to *R. delemar*, we grew *R. delemar* on the surface of agar plates and stained the cells with rhodamine B-tagged liposomes. Liposome staining was viewed top down by epifluorescence. **Figure 2.1** shows the binding of BSA-AmB-

LLs, AmB-LLs, or DEC1-AmB-LLs to early stages of germinating *R. delemar* sporangiospores. Cells are visible due to the fluorescent stain CW. DEC1-AmB-LLs bound efficiently to the exopolysaccharide matrix and, to a lesser extent, the cell wall of swollen and germinating sporangiospores (**Figure 2.1C**), while BSA-AmB-LLs and AmB-LLs did not bind efficiently (**Figure 2.1A,B**). DEC1-AmB-LLs also bound efficiently to the exopolysaccharide matrix of germlings (**Figure 2.1F**), while BSA-AmB-LLs and AmB-LLs did not bind efficiently (**Figure 2.1D,E**). By measuring the area of red fluorescent liposome binding to randomly photographed fields of CW-stained germlings, we quantified the binding efficiency. DEC1-AmB-LLs bound 126-fold ($p = 7.4 \times 10^{-4}$) more efficiently than AmB-LLs (**Figure 2.1G**). The fact that essentially all germlings efficiently bound to DEC1-AmB-LLs is made evident by examining the distribution of data in the scatter bar plot.

Figure 2.2 examines liposome binding to hyphae grown on agar. DEC1-AmB-LLs (**Figure 2.2C**) bound efficiently to exopolysaccharide distributed all along the majority of the hyphae, while control liposome binding was barely detectable (**Figure 2.2A,B**). **Figure 2.2D** quantifies these data, showing that DEC1-AmB-LLs bound approximately 1900-fold ($p = 1.3 \times 10^{-10}$) more strongly than AmB-LLs. At 63× magnification (**Figure 2.2E**) we observed that DEC1-AmB-LLs bound along the cell wall (see arrows) and even more strongly to extracellular deposits of exopolysaccharide. We could not confirm if binding that appeared to be on the cell wall was to the cell wall itself or to small deposits of exopolysaccharide on the wall surface. We performed a parallel binding experiment on live hyphae (**Figure 2.2F**) and observed that DEC1-AmB-LLs bound 368-fold more strongly than AmB-LLs ($p = 0.002$). It is likely that the water solubility of some exopolysaccharides in unfixed cell preparations removed a portion of their beta-glucans, accounting for the slightly lower level of binding relative to that observed for fixed

cells[30]. The remodeling of the exopolysaccharide matrix in live cells could also account for some loss of binding. Complete biological replicates gave similar results for both fixed and live cells (**Supplemental Figure S2.2**). It is worth noting that coating AmB-LLs with BSA (BSA-AmB-LLs) did not significantly alter binding (**Figures 2.1G and 2.2D,F**). Hence, there does not appear to be a significant non-specific affinity of protein-coated liposomes for *Rhizopus.*

It seemed possible that the 100 nm-diameter size of our DEC1-AmB-LLs limited penetration and binding to cell wall beta-glucans. Therefore, we labeled hyphae with rhodamine-conjugated Dectin-1 protein. Dectin-1 is projected to have a diameter measured in tens of angstroms[21]. We labeled fixed hyphae with DEC1-Rhod. The exopolysaccharide staining pattern was indistinguishable from that of DEC1-AmB-LLs (**Supplemental Figure S2.2C**).

The glycan specificity of Dectin-1-targeted liposome binding to *R. delemar* was evaluated by a competitive inhibition study with laminarin (6 kDa), which contains cognate beta-glucan ligands, and yeast mannan (133 kDa), which is composed of various oligomannans (**Figure 2.3**). Dectin-1 binds to various beta-glucan crosslink variants with dissociation constants (e.g., Kds) ranging from mM to pM[31]. Laminarin is expected to contain many, but certainly not all, of the variously crosslinked oligoglucan structures found among fungal polysaccharides. DEC1-AmB-LLs were preincubated with laminarin or yeast mannan before being bound to mature *R. delemar* hyphae. Relative to the DEC1-AmB-LL untreated control (**Figure 2.3A**), laminarin inhibited DEC1-AmB-LL binding (**Figure 2.3C**), whereas yeast mannan did not (**Figure 2.3B**). We quantified the area of red fluorescent liposome binding from multiple images. Laminarin inhibited DEC1-AmB-LL binding 4.2-fold ($p = 4.7 \times 10^{-8}$) relative to the DEC1-AmB-LL untreated control (**Figure 2.3D**). A biological replicate of this experiment is shown in **Supplemental Figure S2.3**.

DEC1-AmB-LLs Efficiently Inhibit and/or Kill R. delemar

Multiple assays were used to examine the ability of liposomal AmB to reduce the viability and/or growth of *R. delemar*. First, we inoculated 96-well microtiter plates with *R. delemar* sporangiospores and immediately added BSA-AmB-LLs, AmB-LLs, and DEC1-AmB-LLs, delivering final concentrations of AmB ranging from 6.4 μM in a two-fold dilution series down to 0.0125 μM (**Figure 2.4**). Visual inspection of the plate revealed that the minimum inhibitory concentration (MIC) after 48 h of growth for DEC1-AmB-LLs was 0.4 μM, while that for AmB-LLs and BSA-AmB-LLs was 3.2 μM, an 8-fold difference (**Figure 2.4A**). It was possible to take a closer look at each well after only 24 h of growth, when the hyphae were less densely packed; images taken at 10× magnification revealed a similar result (**Figure 2.4B**). DEC1-AmB-LLs delivering 0.4 μM AmB effectively inhibited growth, while AmB-LLs and BSA-AmB-LLs delivering 1.6 and 6.4 μM, respectively, inhibited growth. A complete biological replicate of this experiment, shown in **Supplemental Figure S2.4**, suggests a similar reduction in the MIC by DEC1-AmB-LLs relative to AmB-LLs.

Secondly, using the same regimen for growing and treating cells as in **Figure 2.4**, we quantified cell density and metabolic activity (**Figure 2.5**). We found that DEC1-AmB-LLs delivering a range of concentration from 0.2 μM to 1.6 μM AmB were significantly more effective at reducing cell density and metabolic activity than AmB-LLs. For example, at 0.4 μM, DEC1-AmB-LLs reduced cell density 23.6-fold ($p = 5.8 \times 10^{-4}$) (**Figure 2.5A**) and metabolic activity 75-fold ($p = 3.9 \times 10^{-12}$) (**Figure 2.5B**) relative to AmB-LLs. CTB is a metabolic activity assay that measures the reduction of resazurin to fluorescent resorufin, which is dependent upon an intact electron transport chain in living cells. Preliminary experiments using this CTB assay design had shown improved dose-dependent inhibition and killing activity for

DEC1-AmB-LLs in this range of AmB concentrations relative to AmB-LLs (**Supplemental Figure S2.5A**). Replicates of these experiments are shown in **Supplemental Figure S2.5B,C**.

Third, we wished to determine how rapidly targeted liposomes had an impact on metabolic activity. Sporangiospores were germinated to early hyphal stage, treated for three hours with BSA-AmB-LLs, AmB-LLs, and DEC1-AmB-LLs delivering 1.56 μM, 3.12 μM, and 6.25 μM AmB, and assayed with CTB reagent (**Figure 2.5C**). At 3.12 and 6.25 μM AmB, DEC1-AmB-LLs were 1.9-fold ($p = 0.003$) and 3.2-fold ($p = 1.5 \times 10^{-4}$) more effective at reducing metabolic activity than AmB-LLs, respectively. A biological replicate gave a similar result (**Supplemental Figure S2.5D**).

Discussion

Dectin-1 recognizes beta-glucans that are present in fungal cell walls and exopolysaccharide matrices but are sometimes masked by other molecular components. We showed that Dectin-1 was extremely efficient at targeting AmB-loaded liposomes, DEC1-AmB-LLs, to *R. delemar* swollen sporangiospores, germlings, and mature hyphae. We observed DEC1-AmB-LLs bound primarily to the exopolysaccharide matrix and less so to the cell wall or to exopolysaccharide deposited close to the cell wall. Rhodamine-tagged Dectin-1 protein bound with the same specificity to *R. delemar*'s exopolysaccharide. Hence, it appears that the 100 nm-size of DEC1-AmB-LLs did not significantly limit liposome access to its cognate ligands. DEC1-AmB-LLs were significantly and dramatically more effective at inhibiting and/or killing *Rhizopus* in vitro than untargeted AmB-LLs or BSA-AmB-LLs. Using both cell growth and metabolic assays, we observed that DEC1-AmB-LLs delivering sub-micromolar concentrations of AmB were significantly more efficient at inhibiting and/or killing *R. delemar* than untargeted

AmB-LLs. We were able to detect significant loss of metabolic activity within three hours of treatment.

AmB has several partially validated antifungal activities related to its affinity for ergosterol (Erg) in the fungal bilipid membrane, including opening ion channels in the membrane to cause lethal ion leakage and extracting Erg from the lipid bilayer to the membrane surface, which also compromises the membrane[32]. Our results do not distinguish among the various mechanisms of AmB's activity. Yet, our data robustly demonstrate that that Dectin-1-targeted DEC1-AmB-LLs were more efficiently associated with *R. delemar*'s exopolysaccharides and had greater antifungal activity than either AmB delivered in AmB-LLs or our protein-coated control BSA-AmB-LLs. Therefore, it does not appear that AmB itself plays a measurable role in the enhanced efficacy of targeted liposomes.

Each DEC1-AmB-LL DectiSome contains several thousand molecules of rhodamine B that enhance signal intensity and more than a thousand Dectin-1 receptor molecules on its surface, enabling multimer formation that enhances the avidity of binding to cognate oligoglycans[25]. If a C-type lectin receptor protein was used alone in a fungal cell binding study and assayed by immunofluorescence, signal intensities might be reduced by orders of magnitude relative to that achieved by a fluorescent DectiSome. This makes DectiSomes excellent reagents for examining the direct binding of different C-type lectins to various pathogens[22-25,28].

The Mucoromycota is an ancient division of the fungal kingdom that contains a large number of morphologically diverse human pathogens that cause mucormycosis[33,34]. They are estimated to have diverged from a common ancestor in the fungal tree of life nearly 1.3 billion years ago[35,36]. Hence, it is not surprising that the glycan composition of the Mucoromycota cell wall and exopolysaccharide matrix[19,37-39] appear to be distinct from other pathogenic fungi[30,40-42].

The sporangiospore and hyphal cell wall[38] and the exopolysaccharide matrix[39] each are composed of approximately 43% glucose; other components include lower amounts of N-acetyl-glucosamine, mannose, fructose, lipids, proteins, and phosphate[38,39]. Considering that Dectin-1 recognizes oligo-beta-glucans, it is not surprising that Dectin-1-targeted liposomes bound to *Rhizopus*. The weaker binding we observed to the cell wall relative to the exopolysaccharide of *Rhizopus* suggests that most of the cell wall oligoglucans were masked from DEC1-AmB-LL binding. Experiments with DectiSomes targeted by the oligo-mannan-specific C-type lectin Dectin-2 are ongoing.

While liposomal AmB formulations such as AmBisome® delivering as much as 10 mg/kg/day are significantly less toxic than alternative AmB therapies, the several-months-long therapies needed to clear mucormycosis still result in infusion-related reactions and nephrotoxicity[43-45]. If DEC1-AmB-LLs can reduce the effective dose of liposomal AmB and/or reduce the duration of treatment in the clinic, this should reduce the risk of patients developing toxic effects from AmB. Salvage therapies after patients become intolerant to AmB include very high doses of posaconazole (POS) or isavuconazole (ISZ) on the order of hundreds of mg/kg/day[46-50]. Even if Dectin-1-targeted liposomes improve the performance of POS or ISZ by 10-fold in the clinic, it may not be cost-effective to prepare targeted liposomes that deliver tens of mg/kg/day doses of these drugs. However, our data also suggest that DEC1-AmB-LLs kill *Rhizopus* faster than untargeted therapies. Enhanced speed of killing may enable patients to clear *Rhizopus* infections with drug regimens of shorter duration or with fewer treatments, reducing the risk of AmB toxicity.

Immunoliposomes have been used in the clinic for some time to target anti-cancer drugs to cancer cells and tumors. They generally improve drug efficacy several-fold over untargeted

drugs[51-53]. Although conceptually DectiSomes function similarly to immunoliposomes by targeting drugs to pathogenic cells, DectiSomes have some distinct advantages[24]. C-type lectin receptors such as Dectin-1 generally recognize a much wider variety of target ligands than monoclonal antibodies, which supports their development as pan-antifungal reagents. Dectin-1 in particular recognizes the beta-glucans produced by nineteen of the twenty genera of pathogenic fungi[12]. Once developed for one fungal pathogen in the clinic, it should not be difficult to broaden their application to other pathogens. In addition, C-type lectins are much less expensive to produce than monoclonal antibodies, which will favor their development as reagents to treat fungal diseases in less wealthy countries[54-57]. Finally, low production costs may encourage the pharmaceutical industry to expend the large amounts of capital needed to develop DectiSomes.

In conclusion, there is a pressing demand for more effective therapeutics to treat mucormycosis because even after surgery and drug treatment, there is still a high mortality rate. We have shown order of magnitude improvements in the in vitro performance of AmB against *R. delemar* when delivered by Dectin-1-targeted liposomes. It appears that targeting liposomal AmB to the exopolysaccharide matrix of *Rhizopus* is sufficient to significantly improve liposomal drug performance. Future experiments will focus on mouse models of mucormycosis, including determining if Dectin-1-targeted liposomes bind to *R. delemar* at infection sites in the lung, reduce fungal burden in the lungs, and improve mouse survival. We also will need to confirm that Dectin-1-targeted liposomes work effectively against other clinically relevant members of Mucoromycota[58] in light of their ancient diversity[34].

Supplementary Materials

The following supporting information can be downloaded at: https://www.mdpi.com/article/10.3390/jof8040352/s1, **Figure S2.1**: Preparing samples of *R. delemar* growing on the surface of agar plugs for top-down epifluorescence microscopy. **Figure S2.2**: The quantification of DEC1-AmB-LL binding to fixed and live cells and images of DEC1-Rhod binding. **Figure S2.3**: The beta-glucan specificity of Dectin-1-targeted liposome binding to *R. delemar*. **Figure S2.4**: Inhibition and killing assays based on cell growth and density. **Figure S2.5**: Inhibition and killing assays based on metabolic activity.

Author Contributions

Conceptualization, R.B.M. and Z.A.L.; methodology, Q.J.C., Z.A.L. and R.B.M.; validation, Q.J.C., S.A. and R.B.M.; formal analysis, Q.J.C., S.A. and R.B.M.; investigation, Q.J.C., S.A., Z.A.L. and R.B.M.; resources, Z.A.L. and R.B.M.; data curation, Q.J.C.; writing—original draft preparation, Q.J.C. and R.B.M.; writing—review & editing, Q.J.C., S.A., Z.A.L. and R.B.M.; visualization, Q.J.C. and R.B.M.; supervision, Z.A.L. and R.B.M.; project administration, Z.A.L. and R.B.M.; funding acquisition, Z.A.L. and R.B.M. Authorship was limited to those who contributed substantially to the work reported. All authors have read and agreed to the published version of the manuscript.

Funding

S.A. and R.B.M. received funding from the University of Georgia Research Foundation, Inc. (UGARF). R.B.M. and Z.A.L. received funding from the National Institutes of Health,

NIAID (R21 AI148890 and R01 AI162989), and R.B.M. from the Georgia Research Alliance Ventures. These funding agencies are not responsible for the content of this article.

Data Availability Statement

All new data that are discussed are presented within this publication and its data supplement, and any data obtained from other publications were appropriately cited.

Acknowledgements

We thank Xiaorong Lin for her suggesting the importance of our working on *Rhizopus*, providing us with the *R. delemar* strain employed, and for her helpful advice. We thank Ashraf Ibrahim and Teclegiorgis Gebremariam for kindly recommending the use of RPMI + MOPS media, which dramatically simplified our culturing of *R. delemar* on plastic plates and on agar surfaces.

Conflicts of Interest

The University of Georgia has submitted a provisional patent to the United States Patent and Trademark Office. The sponsors had no role in the design, execution, interpretation, or writing of the study.

References

1. Prakash, H.; Chakrabarti, A. Global Epidemiology of Mucormycosis. *J. Fungi* **2019**, *5*, 26.
2. Bongomin, F.; Gago, S.; Oladele, R.O.; Denning, D.W. Global and Multi-National Prevalence of Fungal Diseases—Estimate Precision. *J. Fungi* **2017**, *3*, 57.
3. Kontoyiannis, D.P.; Lewis, R. Invasive Zygomycosis: Update on Pathogenesis, Clinical Manifestations, and Management. *Infect. Dis. Clin. N. Am.* **2006**, *20*, 581–607.

4. Pyrgos, V.; Shoham, S.; Walsh, T. Pulmonary Zygomycosis. *Semin. Respir. Crit. Care Med.* **2008**, *29*, 111–120.
5. Hassan, M.A.; Voigt, K. Pathogenicity patterns of mucormycosis: Epidemiology, interaction with immune cells and virulence factors. *Med. Mycol.* **2019**, *57*, S245–S256.
6. Jeong, W.; Keighley, C.; Wolfe, R.; Lee, W.L.; Slavin, M.A.; Kong, D.C.M.; Chen, S.C.-A. The epidemiology and clinical manifestations of mucormycosis: A systematic review and meta-analysis of case reports. *Clin. Microbiol. Infect.* **2019**, *25*, 26–34.
7. Song, Y.; Qiao, J.; Giovanni, G.; Liu, G.; Yang, H.; Wu, J.; Chen, J. Mucormycosis in renal transplant recipients: Review of 174 reported cases. *BMC Infect. Dis.* **2017**, *17*, 283.
8. Banerjee, I.; Robinson, J.; Asim, M.; Sathian, B.; Banerjee, I. Mucormycosis and COVID-19 an epidemic in a pandemic? *Nepal J. Epidemiol.* **2021**, *11*, 1034–1039.
9. Ibrahim, A.S.; Spellberg, B.; Walsh, T.J.; Kontoyiannis, D.P. Pathogenesis of Mucormycosis. *Clin. Infect. Dis.* **2012**, *54*, S16–S22.
10. Prakash, H.; Skiada, A.; Paul, R.; Chakrabarti, A.; Rudramurthy, S. Connecting the Dots: Interplay of Pathogenic Mechanisms between COVID-19 Disease and Mucormycosis. *J. Fungi* **2021**, *7*, 616.
11. Garre, V. Recent Advances and Future Directions in the Understanding of Mucormycosis. *Front. Cell. Infect. Microbiol.* **2022**, *12*, 850581.
12. Goyal, S.; Castrillón-Betancur, J.C.; Klaile, E.; Slevogt, H. The Interaction of Human Pathogenic Fungi with C-Type Lectin Receptors. *Front. Immunol.* **2018**, *9*, 1261.
13. Howard, D. (Ed.) *Fungi Pathogenic for Humans and Animals*; Dekker Incorporated, Marcel: New York, NY, USA, 1983; p. 652.
14. Klimko, N.; Khostelidi, S.; Shadrivova, O.; Volkova, A.; Popova, M.; Uspenskaya, O.; Shneyder, T.; Bogomolova, T.; Ignatyeva, S.; Zubarovskaya, L.; et al. Contrasts between mucormycosis and aspergillosis in oncohematological patients. *Med. Mycol.* **2019**, *57*, S138–S144.
15. Cornely, O.A.; Alastruey-Izquierdo, A.; Arenz, D.; Chen, S.C.A.; Dannaoui, E.; Hochhegger, B.; Hoenigl, M.; Jensen, H.E.; Lagrou, K.; Lewis, R.E.; et al. Global guideline for the diagnosis and management of mucormycosis: An initiative of the European Confederation of Medical Mycology in cooperation with the Mycoses Study Group Education and Research Consortium. *Lancet Infect. Dis.* **2019**, *19*, e405–e421.
16. Patel, A.; Kaur, H.; Xess, I.; Michael, J.; Savio, J.; Rudramurthy, S.; Singh, R.; Shastri, P.; Umabala, P.; Sardana, R.; et al. A multicentre observational study on the epidemiology, risk factors, management and outcomes of mucormycosis in India. *Clin. Microbiol. Infect.* **2019**, *26*, 944.e9–944.e15.
17. Hamilos, G.; Samonis, G.; Kontoyiannis, D.P. Pulmonary Mucormycosis. *Semin. Respir. Crit. Care Med.* **2011**, *32*, 693–702.
18. Hong, H.-L.; Lee, Y.-M.; Kim, T.; Lee, J.-Y.; Chung, Y.-S.; Kim, M.-N.; Kim, S.-H.; Choi, S.-H.; Kim, Y.S.; Woo, J.H.; et al. Risk Factors for Mortality in Patients with Invasive Mucormycosis. *Infect. Chemother.* **2013**, *45*, 292–298.
19. Chamilos, G.; Ganguly, D.; Lande, R.; Gregorio, J.; Meller, S.; Goldman, W.E.; Gilliet, M.; Kontoyiannis, D.P. Generation of IL-23 Producing Dendritic Cells (DCs) by Airborne Fungi Regulates Fungal Pathogenicity via the Induction of TH-17 Responses. *PLoS ONE* **2010**, *5*, e12955.

20. Camargo, J.F.; Bhimji, A.; Kumar, D.; Kaul, R.; Pavan, R.; Schuh, A.; Seftel, M.; Lipton, J.H.; Gupta, V.; Humar, A.; et al. Impaired T Cell Responsiveness to Interleukin-6 in Hematological Patients with Invasive Aspergillosis. *PLoS ONE* **2015**, *10*, e0123171.
21. Brown, J.; O'Callaghan, C.A.; Marshall, A.; Gilbert, R.; Siebold, C.; Gordon, S.; Brown, G.; Jones, E.Y. Structure of the fungal β-glucan-binding immune receptor dectin-1: Implications for function. *Protein Sci.* **2007**, *16*, 1042–1052.
22. Ambati, S.; Pham, T.; Lewis, Z.A.; Lin, X.; Meagher, R.B. DC-SIGN targets amphotericin B-loaded liposomes to diverse pathogenic fungi. *Fungal Biol. Biotechnol.* **2021**, *8*, 22.
23. Ambati, S.; Pham, T.; Lewis, Z.A.; Lin, X.; Meagher, R.B. DectiSomes: Glycan Targeting of Liposomal Drugs Improves the Treatment of Disseminated Candidiasis. *Antimicrob. Agents Chemother.* **2022**, *66*, e01467-21.
24. Meagher, R.B.; Lewis, Z.A.; Ambati, S.; Lin, X. Aiming for a bull's-eye: Targeting antifungals to fungi with dectin-decorated liposomes. *PLoS Pathog.* **2021**, *17*, e1009699.
25. Ambati, S.; Ferarro, A.R.; Khang, S.E.; Lin, J.; Lin, X.; Momany, M.; Lewis, Z.A.; Meagher, R.B. Dectin-1-Targeted Antifungal Liposomes Exhibit Enhanced Efficacy. *mSphere* **2019**, *4*, e00025-19.
26. Ramana, L.N.; Sharma, S.; Sethuraman, S.; Ranga, U.; Krishnan, U.M. Stealth anti-CD4 conjugated immunoliposomes with dual antiretroviral drugs—Modern Trojan horses to combat HIV. *Eur. J. Pharm. Biopharm.* **2015**, *89*, 300–311.
27. Tenchov, R. Understanding the Nanotechnology in COVID-19 Vaccines. *CAS*. 18 February 2021, pp. 1–15. Available online: https://www.cas.org/resource/blog/understanding-nanotechnology-covid-19-vaccines (accessed on 18 February 2021).
28. Ambati, S.; Ellis, E.C.; Lin, J.; Lin, X.; Lewis, Z.A.; Meagher, R.B. Dectin-2-Targeted Antifungal Liposomes Exhibit Enhanced Efficacy. *mSphere* **2019**, *4*, e00715-19.
29. Andrianaki, A.M.; Kyrmizi, I.; Thanopoulou, K.; Baldin, C.; Drakos, E.; Soliman, S.S.M.; Shetty, A.C.; McCracken, C.; Akoumianaki, T.; Stylianou, K.; et al. Iron restriction inside macrophages regulates pulmonary host defense against *Rhizopus* species. *Nat. Commun.* **2018**, *9*, 3333.
30. Hamidi, M.; Okoro, O.V.; Milan, P.B.; Khalili, M.R.; Samadian, H.; Nie, L.; Shavandi, A. Fungal exopolysaccharides: Properties, sources, modifications, and biomedical applications. *Carbohydr. Polym.* **2022**, *284*, 119152.
31. Adams, E.L.; Rice, P.J.; Graves, B.; Ensley, H.E.; Yu, H.; Brown, G.D.; Gordon, S.; Monteiro, M.A.; Papp-Szabo, E.; Lowman, D.W.; et al. Differential High-Affinity Interaction of Dectin-1 with Natural or Synthetic Glucans Is Dependent upon Primary Structure and Is Influenced by Polymer Chain Length and Side-Chain Branching. *J. Pharmacol. Exp. Ther.* **2008**, *325*, 115–123.
32. Anderson, T.M.; Clay, M.C.; Cioffi, A.G.; Diaz, K.A.; Hisao, G.S.; Tuttle, M.D.; Nieuwkoop, A.; Comellas, G.; Maryum, N.; Wang, S.; et al. Amphotericin forms an extramembranous and fungicidal sterol sponge. *Nat. Chem. Biol.* **2014**, *10*, 400–406.
33. Ribes, J.A.; Vanover-Sams, C.L.; Baker, D.J. Zygomycetes in Human Disease. *Clin. Microbiol. Rev.* **2000**, *13*, 236–301.
34. Spatafora, J.W.; Chang, Y.; Benny, G.L.; Lazarus, K.; Smith, M.E.; Berbee, M.L.; Bonito, G.; Corradi, N.; Grigoriev, I.; Gryganskyi, A.; et al. A phylum-level phylogenetic classification of zygomycete fungi based on genome-scale data. *Mycologia* **2016**, *108*, 1028–1046.

35. Spatafora, J.W.; Aime, M.C.; Grigoriev, I.V.; Martin, F.; Stajich, J.E.; Blackwell, M. The Fungal Tree of Life: From Molecular Systematics to Genome-Scale Phylogenies. *Microbiol. Spectr.* **2017**, *5*, 3–34.
36. Padovan, A.C.B.; Sanson, G.F.; Brunstein, A.; Briones, M.R. Fungi Evolution Revisited: Application of the Penalized Likelihood Method to a Bayesian Fungal Phylogeny Provides a New Perspective on Phylogenetic Relationships and Divergence Dates of Ascomycota Groups. *J. Mol. Evol.* **2005**, *60*, 726–735.
37. Bartnicki-Garcia, S.; Reyes, E. Chemistry of spore wall differentiation in *Mucor rouxii*. *Arch. Biochem. Biophys.* **1964**, *108*, 125–133.
38. Lecointe, K.; Cornu, M.; Leroy, J.; Coulon, P.; Sendid, B. Polysaccharides Cell Wall Architecture of Mucorales. *Front. Microbiol.* **2019**, *10*, 469.
39. Yu, W.; Chen, G.; Zhang, P.; Chen, K. Purification, partial characterization and antitumor effect of an exopolysaccharide from *Rhizopus nigricans*. *Int. J. Biol. Macromol.* **2016**, *82*, 299–307.
40. Gow, N.A.R.; Latge, J.-P.; Munro, C.A. The Fungal Cell Wall: Structure, Biosynthesis, and Function. *Microbiol. Spectr.* **2017**, *5*, 28513415.
41. Reichhardt, C.; A Stevens, D.; Cegelski, L. Fungal biofilm composition and opportunities in drug discovery. *Future Med. Chem.* **2016**, *8*, 1455–1468.
42. Lagree, K.; Mitchell, A.P. Fungal Biofilms: Inside Out. *Microbiol. Spectr.* **2017**, *5*, 873–886.
43. Hamill, R.J. Amphotericin B Formulations: A Comparative Review of Efficacy and Toxicity. *Drugs* **2013**, *73*, 919–934.
44. Deray, G. Amphotericin B nephrotoxicity. *J. Antimicrob. Chemother.* **2002**, *49*, 37–41.
45. Stanzani, M.; Vianelli, N.; Cavo, M.; Maritati, A.; Morotti, M.; Lewis, R.E. Retrospective Cohort Analysis of Liposomal Amphotericin B Nephrotoxicity in Patients with Hematological Malignancies. *Antimicrob. Agents Chemother.* **2017**, *61*, e02651-16.
46. Jeong, W.; Keighley, C.; Wolfe, R.; Lee, W.L.; Slavin, M.A.; Chen, S.C.-A.; Kong, D.C. Contemporary management and clinical outcomes of mucormycosis: A systematic review and meta-analysis of case reports. *Int. J. Antimicrob. Agents* **2019**, *53*, 589–597.
47. Floros, L.; Kuessner, D.; Posthumus, J.; Bagshaw, E.; Sjölin, J. Cost-effectiveness analysis of isavuconazole versus voriconazole for the treatment of patients with possible invasive aspergillosis in Sweden. *BMC Infect. Dis.* **2019**, *19*, 134.
48. Skiada, A.; Lass-Floerl, C.; Klimko, N.; Ibrahim, A.; Roilides, E.; Petrikkos, G. Challenges in the diagnosis and treatment of mucormycosis. *Med. Mycol.* **2018**, *56*, S93–S101.
49. Dannaoui, E. Antifungal resistance in mucorales. *Int. J. Antimicrob. Agents* **2017**, *50*, 617–621.
50. Riley, T.T.; Muzny, C.; Swiatlo, E.; Legendre, D.P. Breaking the Mold: A Review of Mucormycosis and Current Pharmacological Treatment Options. *Ann. Pharmacother.* **2016**, *50*, 747–757.
51. Merino, M.; Zalba, S.; Garrido, M.J. Immunoliposomes in clinical oncology: State of the art and future perspectives. *J. Control. Release* **2018**, *275*, 162–176.
52. Eloy, J.O.; Petrilli, R.; Trevizan, L.N.F.; Chorilli, M. Immunoliposomes: A review on functionalization strategies and targets for drug delivery. *Colloids Surf. B Biointerfaces* **2017**, *159*, 454–467.
53. Wang, D.; Sun, Y.; Liu, Y.; Meng, F.; Lee, R.J. Clinical translation of immunoliposomes for cancer therapy: Recent perspectives. *Expert Opin. Drug Deliv.* **2018**, *15*, 893–903.

54. Suvvari, T.K.; Arigapudi, N.; Kandi, V.R.; Kutikuppala, L.S. Mucormycosis: A killer in the shadow of COVID-19. *J. Mycol. Med.* **2021**, *31*, 101161.
55. Selarka, L.; Sharma, S.; Saini, D.; Sharma, S.; Batra, A.; Waghmare, V.T.; Dileep, P.; Patel, S.; Shah, M.; Parikh, T.; et al. Mucormycosis and COVID-19: An epidemic within a pandemic in India. *Mycoses* **2021**, *64*, 1253–1260.
56. Pal, R.; Singh, B.; Bhadada, S.K.; Banerjee, M.; Bhogal, R.S.; Hage, N.; Kumar, A. COVID-19-associated mucormycosis: An updated systematic review of literature. *Mycoses* **2021**, *64*, 1452–1459.
57. Bhanuprasad, K.; Manesh, A.; Devasagayam, E.; Varghese, L.; Cherian, L.M.; Kurien, R.; Karthik, R.; Deodhar, D.; Vanjare, H.; Peter, J.; et al. Risk factors associated with the mucormycosis epidemic during the COVID-19 pandemic. *Int. J. Infect. Dis.* **2021**, *111*, 267–270.
58. Walther, G.; Wagner, L.; Kurzai, O. Updates on the Taxonomy of Mucorales with an Emphasis on Clinically Important Taxa. *J. Fungi* **2019**, *5*, 106.

Figures

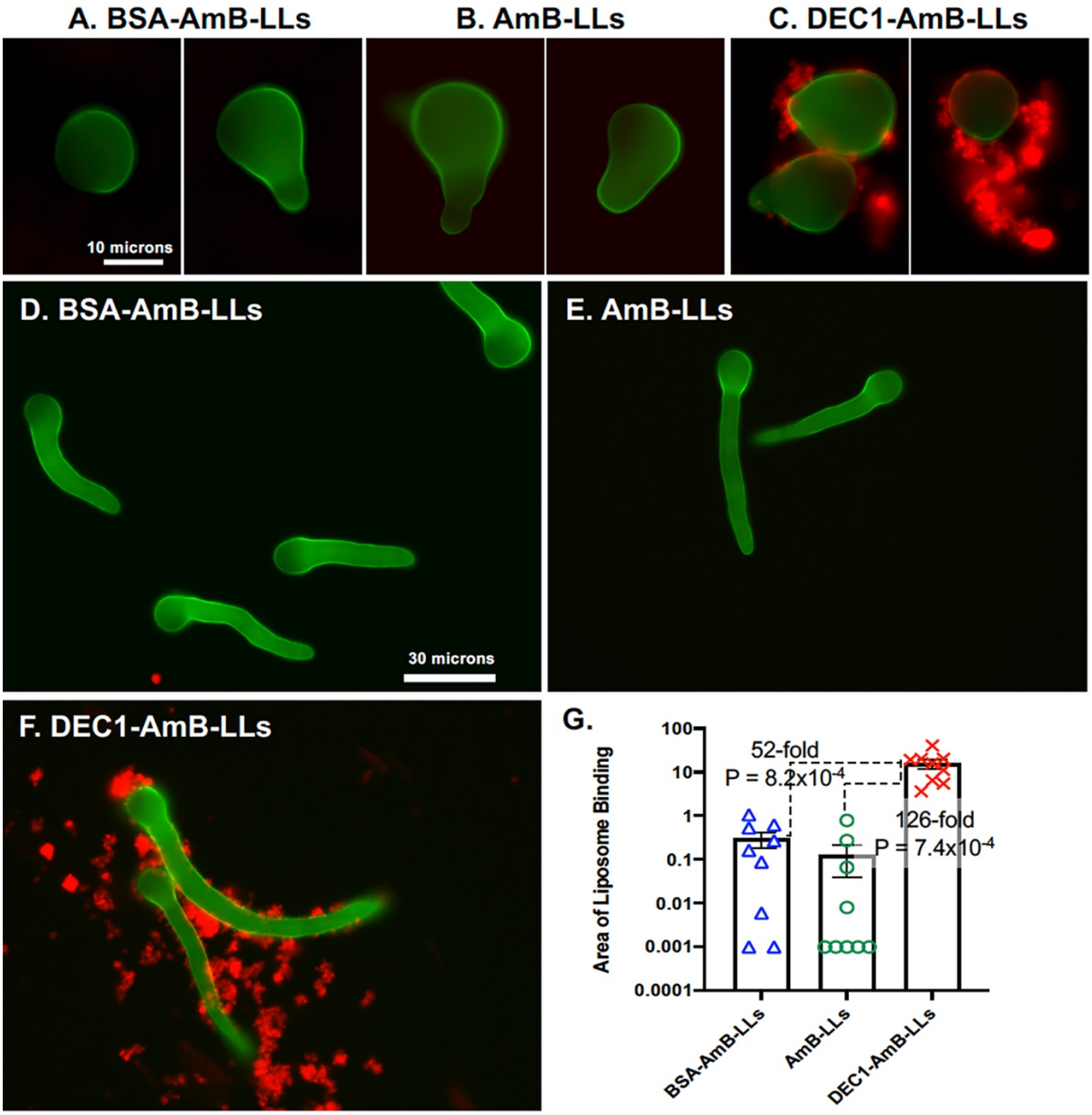

Figure 2.1. Dectin-1-targeted AmB-loaded liposomes, DEC1-AmB-LLs, bind efficiently to germinating sporangiospores and germlings of *R. delemar*. (**A-C**) Representative fluorescence images of swollen *R. delemar* sporangiospores (63× magnification) on an agar surface are shown. Sporangiospores were either treated with BSA-AmB-LLs (**A**), AmB-LLs (**B**), or DEC1-AmB-LLs (**C**). (**D-F**) Representative fluorescence images of *R. delemar* germlings (63× magnification) are shown. Germlings were either treated with BSA-AmB-LLs (**D**), AmB-LLs (**E**), or DEC1-AmB-LLs (**F**). (**G**) The area of red liposome binding (log_{10}) was quantified as shown (N = 9). Standard errors and *p*-values are included. Size bars indicate 10 and 30 micron scales.

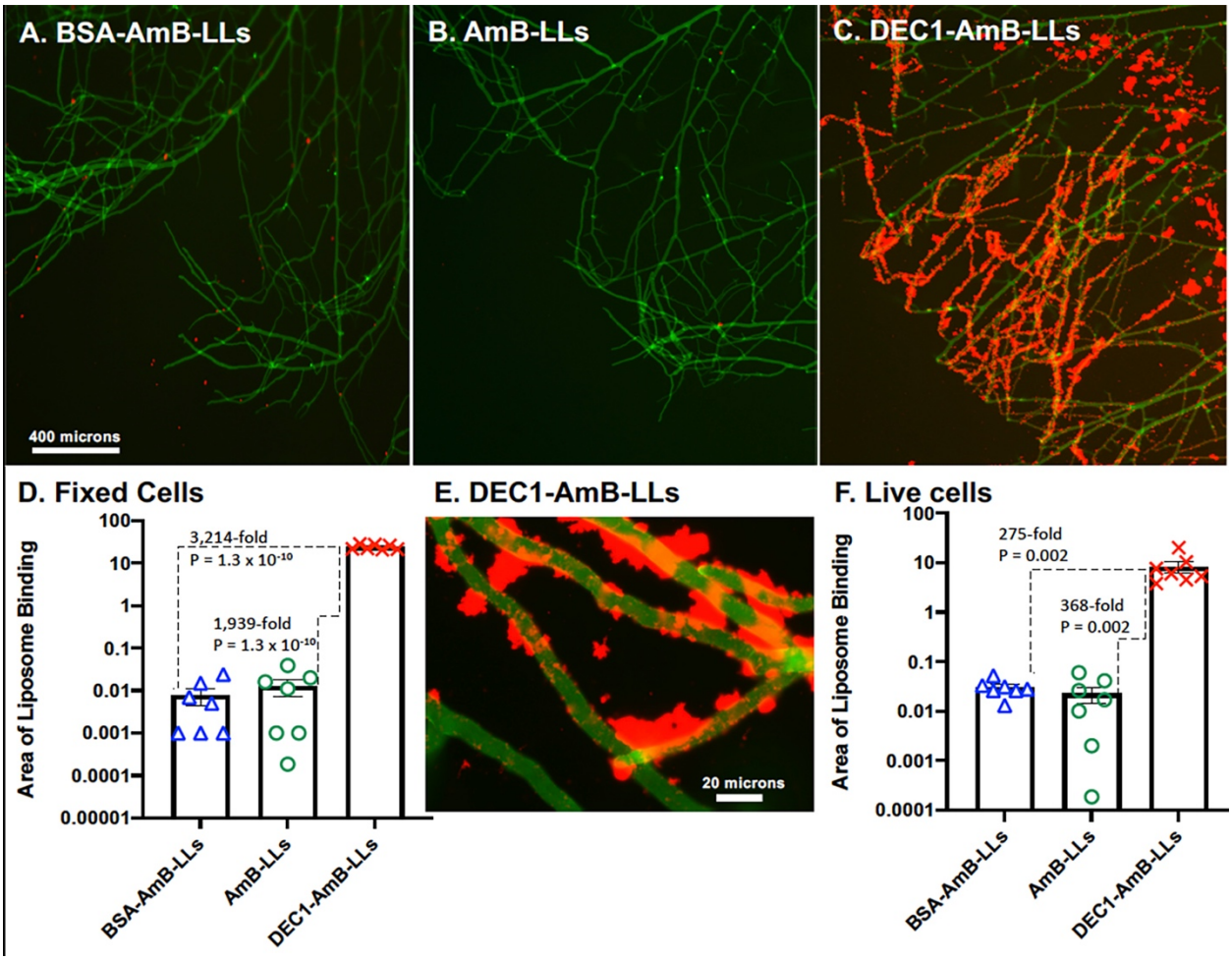

Figure 2.2. Dectin-1-targeted liposomes bind efficiently to *R. delemar* hyphae. (**A-C**) Representative fluorescence images of *R. delemar* hyphae (5× magnification) are shown. Hyphae grown on an agar surface were fixed and either treated with BSA-AmB-LLs (**A**), AmB-LLs (**B**), or DEC1-AmB-LLs (**C**). (**D**) The area of red liposome binding (log_{10}) for fixed cells was quantified as shown (N = 7). (**E**) A fluorescence image of DEC1-AmB-LLs binding to fixed *R. delemar* hyphae at 63× magnification is shown. (**F**) The area of red liposome binding (log_{10}) for live hyphae was quantified as shown (N = 7). Standard errors and *p*-values are included. Size bars indicate 400 and 20 micron scales for the 5× and 63× images, respectively.

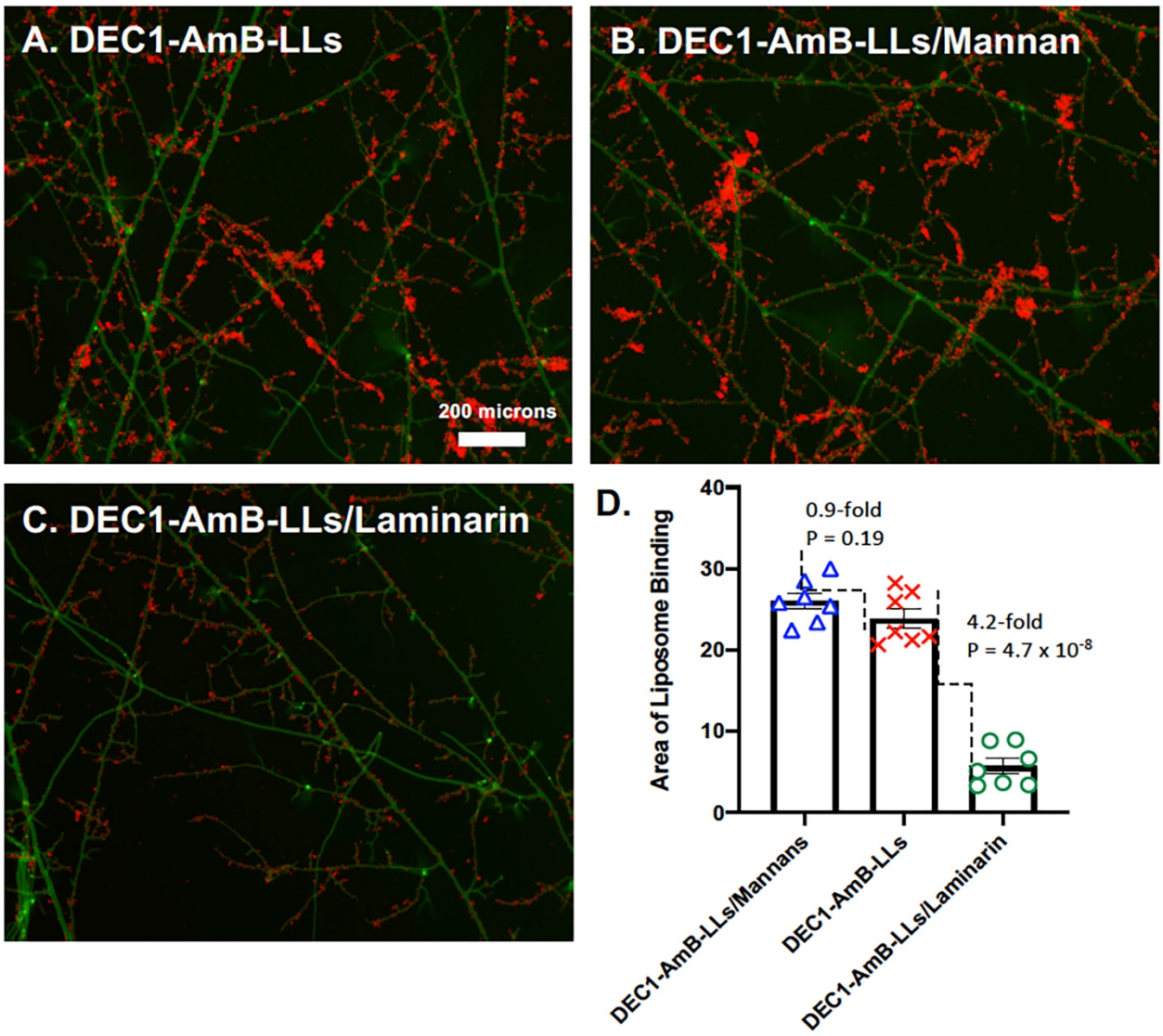

Figure 2.3. DEC1-AmB-LL binding to *R. delemar* is beta-glucan specific. (**A-C**) Representative fluorescence images of *R. delemar* hyphae (5× magnification) on an agar surface are shown. Hyphae were treated with DEC1-AmB-LLs that had been preincubated either with control buffer (**A**), yeast mannans (**B**), or the beta-glucan laminarin (**C**). The size bar indicates 200 microns. (**D**) The area of red liposome binding (linear plot) was quantified (N = 7). Standard errors and *p*-values are included.

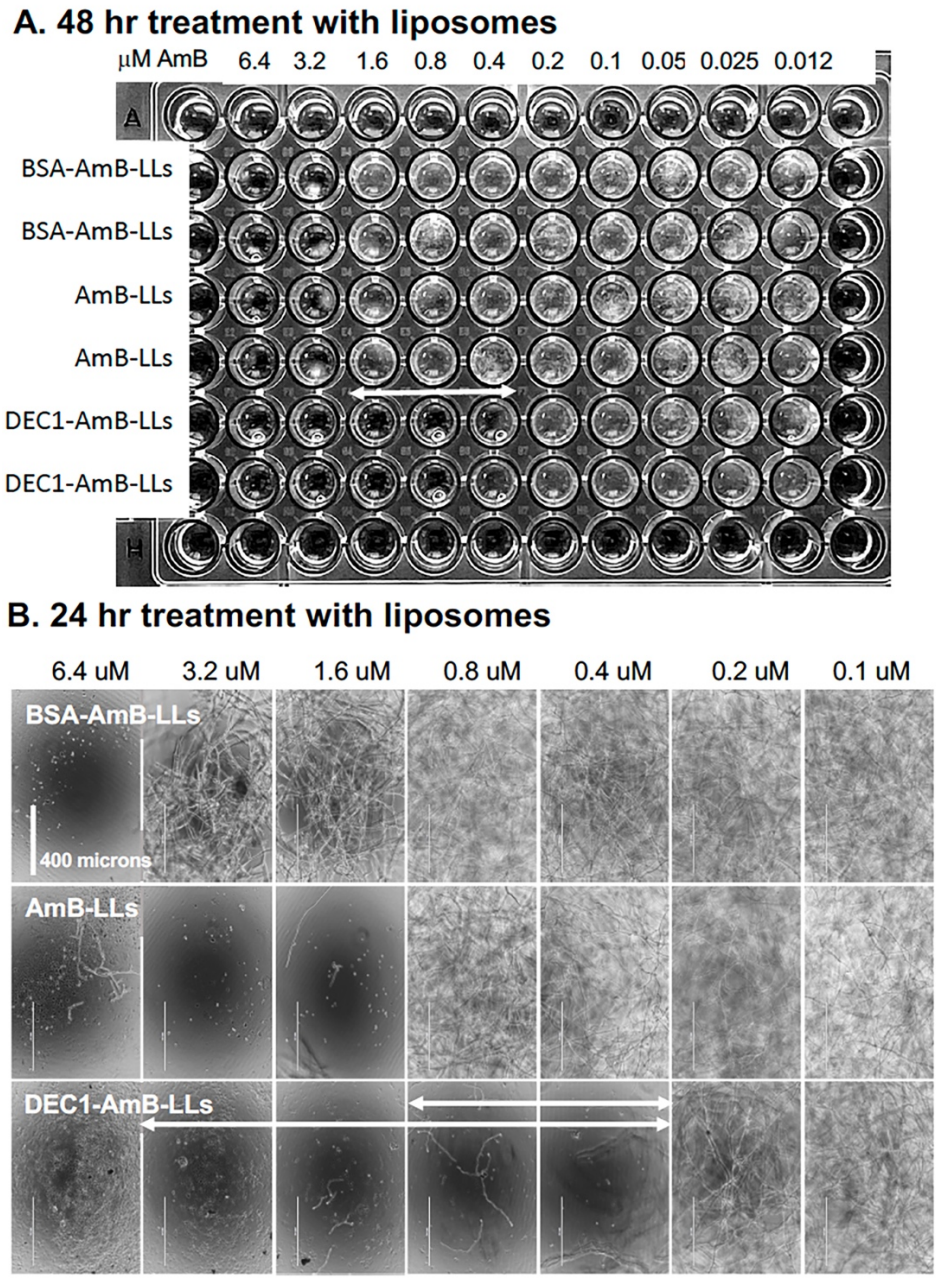

Figure 2.4. Qualitative DEC1-AmB-LL inhibition and killing assays based on cell growth and density. (**A**) *R. delemar* sporangiospores diluted into liquid RPMI + MOPS media were immediately treated with either BSA-AmB-LLs, AmB-LLs, or DEC1-AmB-LLs delivering the indicated AmB concentrations and incubated at 37˚C. An overview image showing hyphal density was taken 48 h after treatment. The two-headed arrow indicates the range at which DEC1-AmB-LLs significantly inhibited *R. delemar* growth as compared to the control liposome treatments. (**B**) Images of the center of each well from the same plate had been taken 24 h after treatment at 10× magnification. The two two-headed arrows indicate the ranges at which DEC1-AmB-LLs significantly inhibited *R. delemar* growth compared to the controls at this earlier time point. The size bar indicates 400 microns.

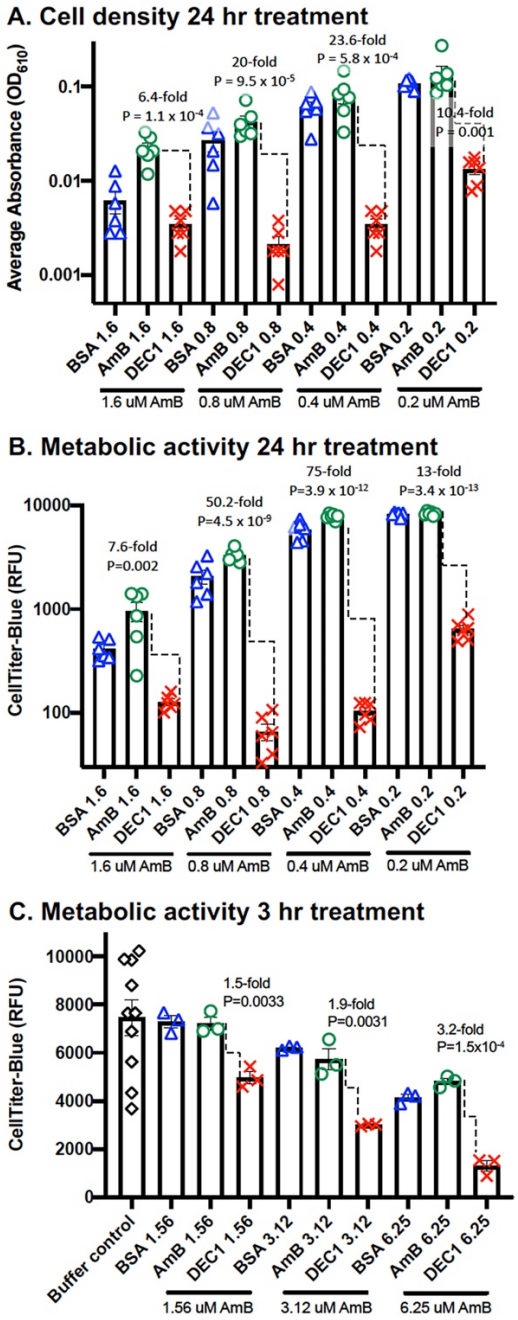

Figure 2.5. Quantitative DEC1-AmB-LL inhibition and killing assay based on cell density and metabolic activity. (**A**) Microtiter plate-grown cells were treated with liposomes delivering the indicated concentrations of AmB for 24 h and cell density was quantified. (**B**) The same 24 h microtiter plate-grown cells were incubated with CTB reagent and metabolic activity was quantified. (**C**) *R. delemar* sporangiospores were diluted into liquid RPMI + MOPS media and incubated at 37˚C for 8 h. *R. delemar* hyphae were then treated for 3 h with either BSA-AmB-LLs, AmB-LLs, or DEC1-AmB-LLs at the noted AmB concentrations or treated with buffer alone (buffer control). The residual metabolic activity was quantified as relative fluorescence units (RFU) generated from the electrochemical reduction of the CellTiter-Blue reagent to a fluorescent product (N = 3). Standard errors, fold differences, and *p*-values are indicated.

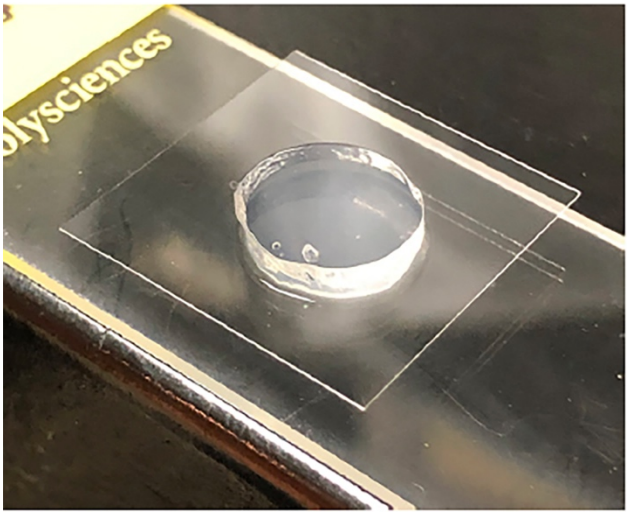

Supplementary Figure S2.1. Preparing samples of *R. delemar* growing on the surface of agar plugs for top down epifluorescence microscopy. Sporangiospores were germinated and grown to different developmental stages on the surface of agar plates in RPMI-MOPS media. Seven-mm circular plugs were removed with a sterile cork-borer, transferred to 24-well microtiter plates, and washed once submerged in PBS. The cells were fixed in 3.7% formaldehyde in PBS for 1 hr or left live, and washed thrice in PBS. The details of the liposome staining protocol is given in the text.

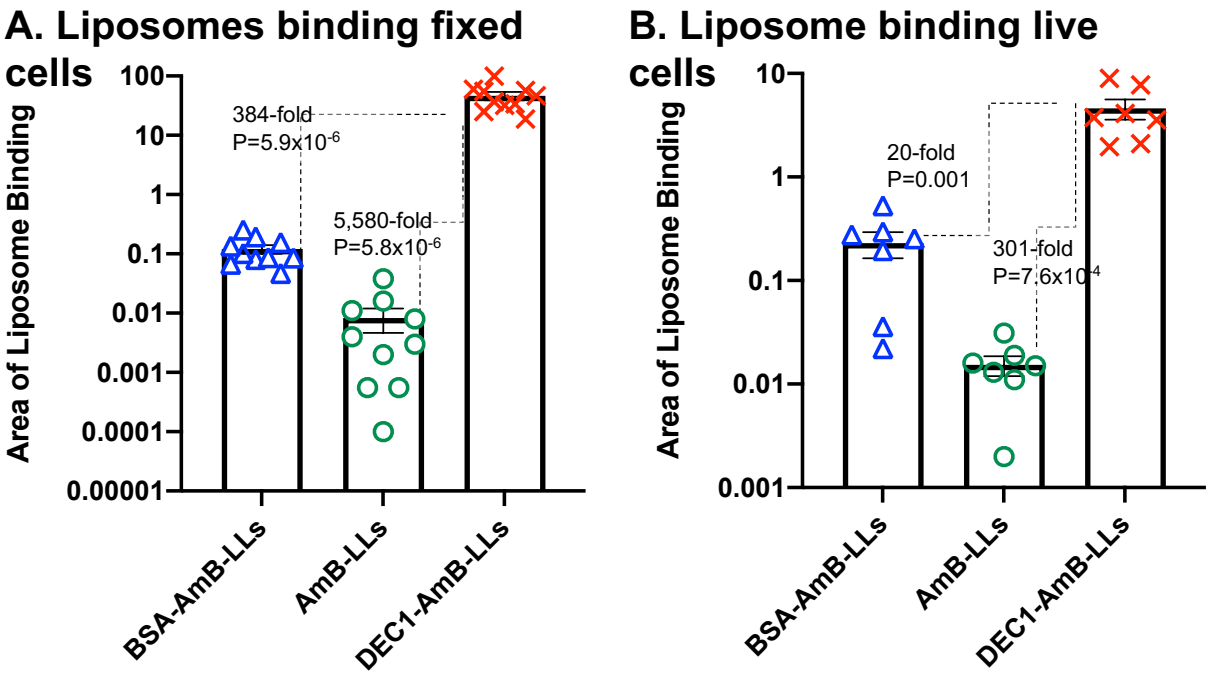

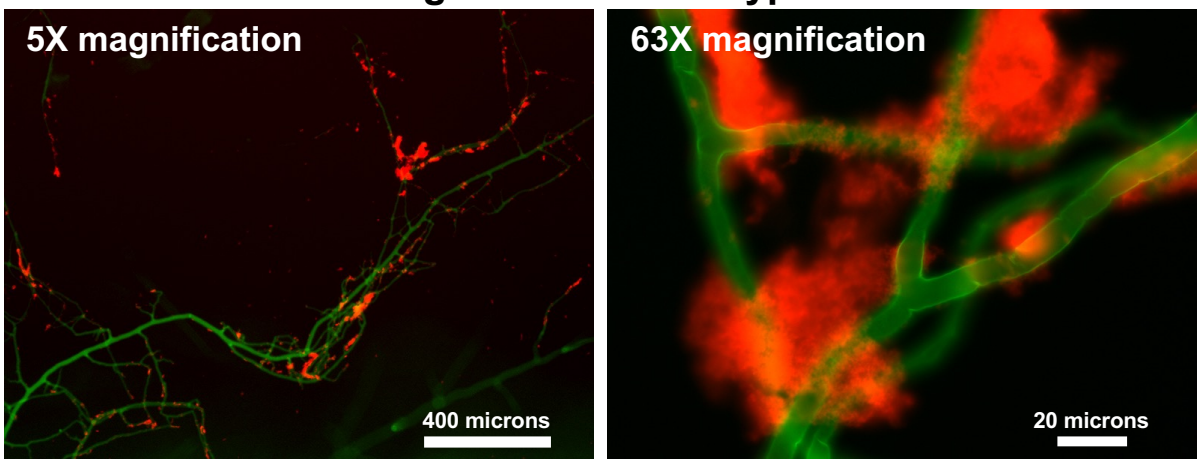

Supplementary Figure S2.2. The quantification of DEC1-AmB-LL binding to fixed and live cells relative to control liposome binding. Panels **A** and **B** in this figure show biological replicates of the experiments in **Figure 2.2D** and **2.2F.** See the legend to **Figure 2.2** for details. Panel **C** shows the labeling of *R. delemar* hyphae with rhodamine B-conjugated Dectin-1, DEC1-Rhod, photographed at 5x and 63x using epifluorescence. CW-stained hyphae are shown in green, and DEC1-Rhod staining is shown in red. Size bars indicate 400 and 20 micron scales for the 5x and 63x images, respectively.

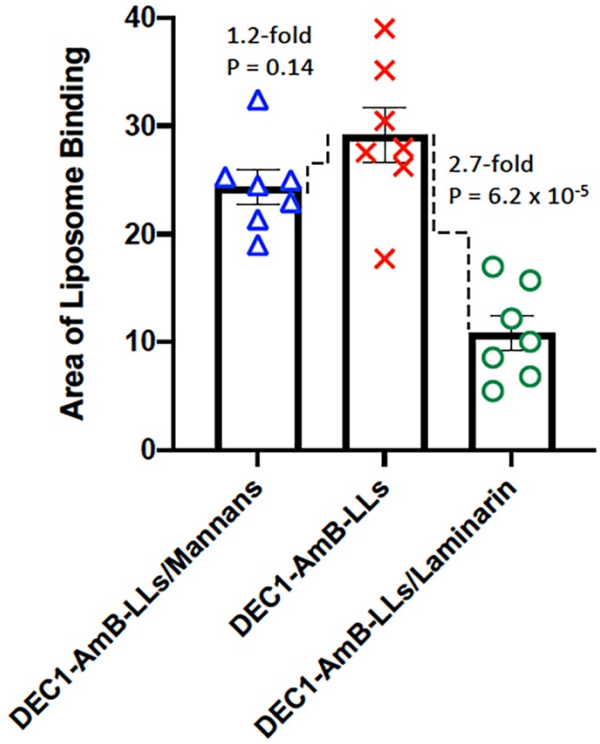

Supplementary Figure S2.3. The beta-glucan specificity of Dectin-1-targeted liposomes, DEC1-AmB-LLs, binding to *R. delemar*. This figure shows a biological replicate of the experiment in **Figure 2.3D**. See the legend to **Figure 2.3** for details.

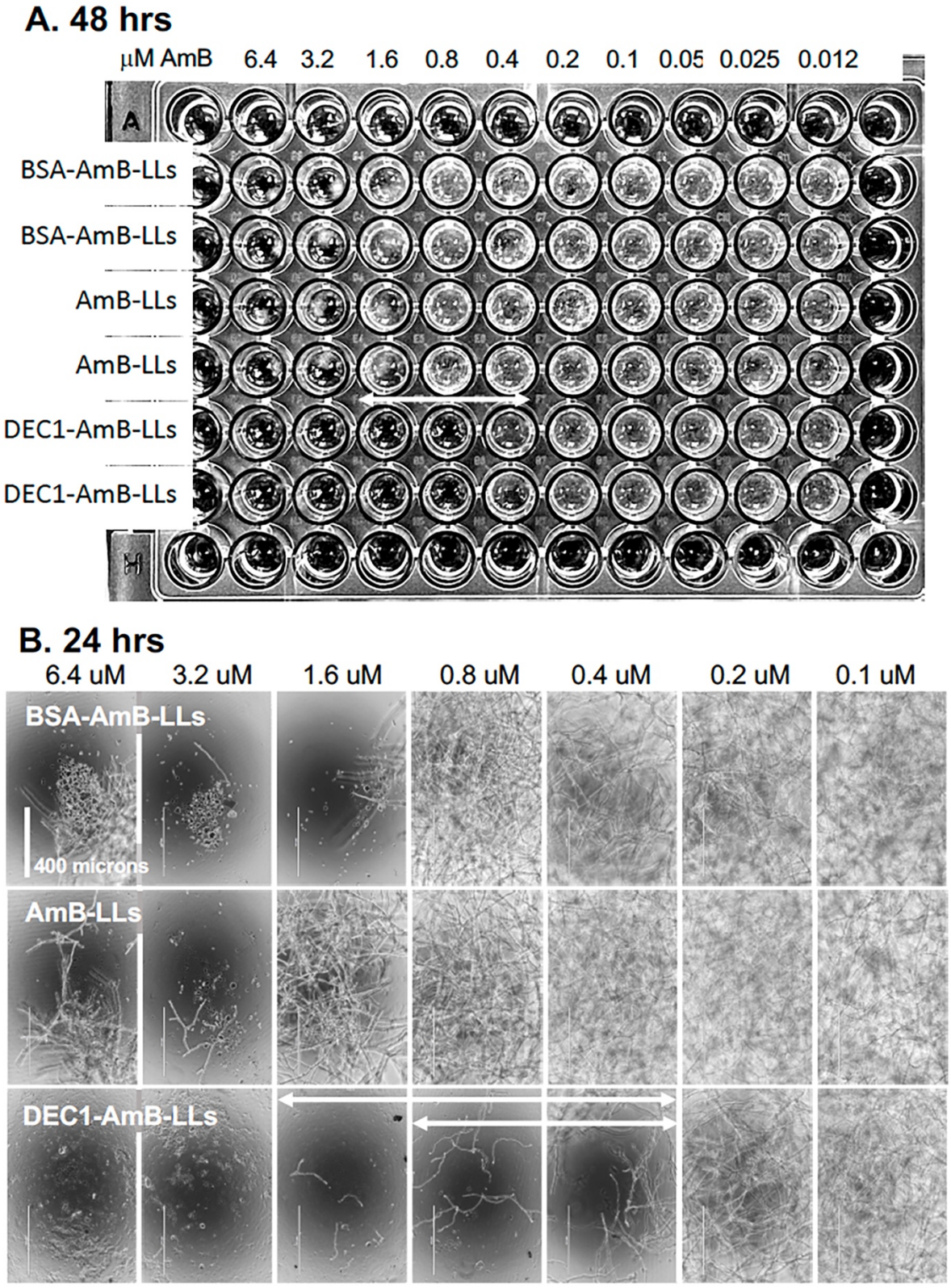

Supplementary Figure S2.4. Inhibition and killing assays based on cell growth and density. Panels **A** and **B** in this figure show biological replicates of the experiments in **Figure 2.4A** and **2.4B**, respectively. See the legend to **Figure 2.4** for details.

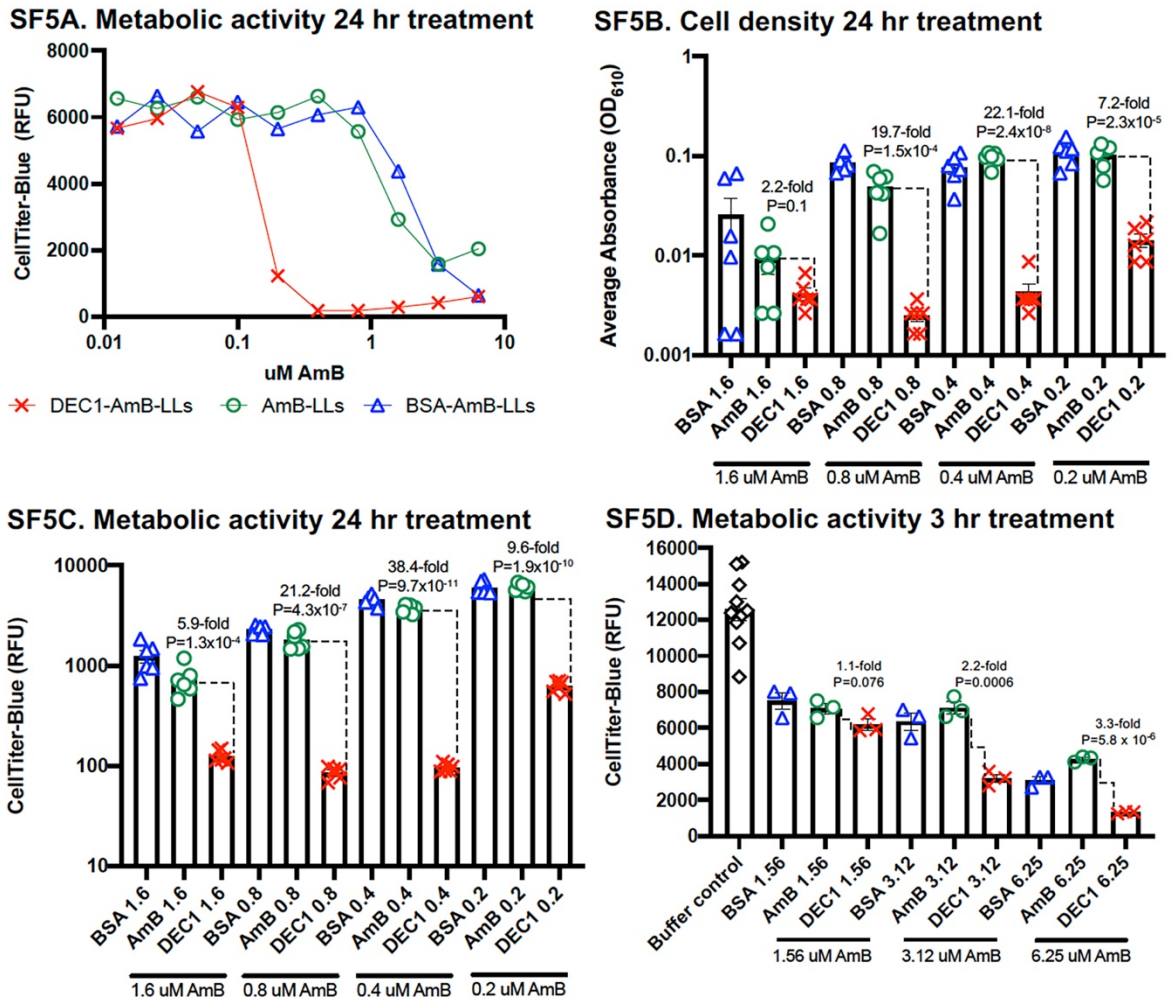

Supplementary Figure S2.5. Inhibition and killing assays based on cell density and metabolic activity. Panel **A** shows the residual metabolic activity of cells treated with targeted and untargeted liposomes delivering a wide range of AmB concentrations for 24 hrs. Panels **B** and **C** show replicates of the cell density and CTB assay experiments in **Figure 2.5A** and **2.5B**. Panel **D** shows a replicate of the CTB assay in **Figure 2.5C**. See the legends in the main text for details.

CHAPTER 3

DECTIN-3-TARGETED ANTIFUNGAL LIPOSOMES EFFICIENTLY BIND AND KILL DIVERSE FUNGAL PATHOGENS[1]

[1]Choudhury Q.J.*, Ambati S.*, Link C.D., Lin X., Lewis Z.A., and Meagher R.B. (2023). Dectin-3-targeted antifungal liposomes efficiently bind and kill diverse fungal pathogens. *Molecular Microbiology* 120 (5): 723-739. Paper link: https://onlinelibrary.wiley.com/doi/full/10.1111/mmi.15174. Reprinted here with permission of publisher. (*Co-first authors)

Abstract

DectiSomes are anti-infective drug-loaded liposomes targeted to pathogenic cells by pathogen receptors including the Dectins. We have previously used C-type lectin (CTL) pathogen receptors Dectin-1, Dectin-2, and DC-SIGN to target DectiSomes to the extracellular oligoglycans surrounding diverse pathogenic fungi and kill them. Dectin-3 (also known as MCL, *CLEC4D*) is a CTL pathogen receptor whose known cognate ligands are partly distinct from other CTLs. We expressed and purified a truncated Dectin-3 polypeptide (DEC3) comprised of its carbohydrate recognition domain and stalk region. We prepared amphotericin B (AmB)-loaded pegylated liposomes (AmB-LLs) and coated them with this isoform of Dectin-3 (DEC3-AmB-LLs), and we prepared control liposomes coated with bovine serum albumin (BSA-AmB-LLs). DEC3-AmB-LLs bound to the exopolysaccharide matrices of *Candida albicans*, *Rhizopus delemar* (formerly known as *R. oryzae*), and *Cryptococcus neoformans* from one to several orders of magnitude more strongly than untargeted AmB-LLs or BSA-AmB-LLs. The data from our quantitative fluorescent binding assays were standardized using a CellProfiler program, AreaPipe, that was developed for this purpose. Consistent with enhanced binding, DEC3-AmB-LLs inhibited and/or killed *C. albicans* and *R. delemar* more efficiently than control liposomes and significantly reduced the effective dose of AmB. In conclusion, Dectin-3 targeting has the potential to advance our goal of building pan-antifungal DectiSomes.

Introduction

In 2017, it was estimated that globally, there were approximately 750,000 cases of candidiasis, 900,000 cases of mucormycosis, and 220,000 cases of cryptococcosis (Bongomin et al., 2017). These three invasive fungal infections (IFIs) account for more than half of IFI-

associated deaths annually (Banerjee et al., 2021; Bongomin et al., 2017; Brown et al., 2012; Low & Rotstein, 2011; Varshney et al., 2017). Death rates are very high even following antifungal drug treatment, and in many cases of mucormycosis, the surgical removal of infected tissue is necessary. *Candida albicans, Rhizopus delemar* (*R. oryzae*), and *Cryptococcus neoformans* are the most common causative pathogens, respectively, and are the test species in the following study.

Our goal has been to design targeted pan-antifungal liposomes, DectiSomes, which greatly improve the delivery and performance of antifungal drugs. DectiSomes are defined as liposomes loaded with an anti-infective drug and targeted to pathogenic cells via a pathogen receptor protein such as a C-type lectin (CTL). DectiSomes have several distinct advantages over more classical antibody-targeted immunoliposomes, including a wider range of cognate ligands, lower cost, and greater avidity (Meagher et al., 2021, 2023). We have previously demonstrated the potential of three CTLs, Dectin-1 (*CLEC7A*), Dectin-2 (*CLEC6A*), and DC-SIGN (*CD209*), to efficiently target Amphotericin B-loaded DectiSomes to four human fungal pathogens: *C. albicans, R. delemar, C. neoformans*, and *Aspergillus fumigatus* (Ambati et al., 2022; Ambati, Ellis, et al., 2019, 2021; Ambati, Ferarro, et al., 2019; Ambati, Pham, et al., 2021; Choudhury et al., 2022; Meagher et al., 2021). One or more of the CTL-targeted DectiSomes dramatically lowered the effective dose of Amphotericin B (AmB) when these pathogens were grown in vitro. DectiSomes were also shown to be effective at reducing fungal burden and/or improving mouse survival in murine models of aspergillosis and candidiasis (Ambati et al., 2022; Ambati, Ellis, et al., 2021; Ambati, Pham, et al., 2021).

We hoped to enhance the pan-antifungal performance of DectiSomes by employing Dectin-3 (MCL, Macrophage C-type Lectin, *CLEC4D*) (Flornes et al., 2004; Goyal et al., 2018;

Wilson et al., 2015). Dectin-3 is expressed by several lymphoid cell types, particularly dendritic cells and macrophages. It is less well studied than the other CTLs. Dectin-3 was initially reported to recognize the Ascomycete *Candida* spp. and the Basidiomycete *Cryptococcus* spp. (Goyal et al., 2018; Hole et al., 2016; Huang et al., 2018), and shortly thereafter the Ascomycetes *Paracoccidioides brasiliensis* (Preite et al., 2018) and *Pneumocystis carinii* (Kottom et al., 2019). When expressed in the membrane of lymphoid cell types, dimers of Dectin-3's extracellular carbohydrate recognition domain (CRD) bind to fungal glycans. Then its intracellular immunoreceptor tyrosine-based activation motif (ITAM) signals a fungal infection. Similar to Dectin-2, Dectin-3's CRD binds yeast alpha-mannans. Evidence for Dectin-3 recognition of a more expanded set of ligands comes primarily from analysis of artificial ligands (Decote-Ricardo et al., 2019; Fonseca et al., 2009; Huang et al., 2018; Marr et al., 2004; Martinez & Casadevall, 2007). Its potential to recognize diverse novel fungal glycan and lipoglycan ligands was the rationale for building Dectin-3-targeted DectiSomes.

We cloned and expressed a truncated isoform of murine Dectin-3 containing its extracellular CRD and stalk region (DEC3) and used it to coat Amphotericin B-loaded liposomes to make the DectiSome DEC3-AmB-LL. We compared the ability of DEC3-AmB-LLs to bind, inhibit, and/or kill three highly evolutionarily divergent and morphologically distinct fungal pathogens—*C. albicans* (Ascomycete), *R. delemar* (Mucormycete, Zygomycete), and *C. neoformans* (Basidiomycete)—as compared to untargeted control liposomes.

Results

Preparation of Dectin-3-targeted DectiSomes

We prepared Amphotericin B-loaded pegylated liposomes (AmB-LLs) with 11 to 12 moles percent AmB relative to 100 moles percent liposomal lipid, wherein AmB is intercalated into the liposomal membrane (Ambati, Ferarro, et al., 2019). They have a similar AmB concentration to the analogous commercial FDA-approved un-pegylated liposomal drug AmBisome (U.S. Food and Drug Administration, 1997). We cloned the N-terminal portion of the sequence encoding the CRD and stalk region of murine Dectin-3, which was codon optimized for *E. coli* expression (hereafter referred to as truncated Dectin-3 or DEC3, **Figure SF3.1**). For this liposomal presentation, we omitted the transmembrane and intracellular ITAM signaling domains of Dectin-3. The *E. coli*-produced DEC3 polypeptide was affinity purified (**Figure SF3.2a,b**) and coupled to a pegylated lipid to make DEC3-PEG-DSPE. The DEC3-PEG-DSPE polypeptide was inserted via its DSPE lipid moiety into the AmB-LLs at 1 mole percent to make the DectiSome DEC3-AmB-LL by methods we have described previously for other DectiSomes (Ambati, Ellis, et al., 2019; Ambati, Ferarro, et al., 2019; Ambati, Pham, et al., 2021). The construct allows the CRD and stalk region of DEC3 to float freely in the liposomal membrane and to form functional homodimers and multimers (Meagher et al., 2021, 2023). Bovine serum albumin (BSA) was also lipid-modified and inserted via its DSPE moiety, but at 0.3 moles percent, accounting for its 3-fold higher molecular weight relative to our truncated Dectin-3 polypeptide (Ambati, Ferarro, et al., 2019). AmB-LLs and BSA-AmB-LLs served as negative, untargeted liposome controls for non-specific binding and killing. It was assumed that the protein coating of BSA-AmB-LLs would interfere with the untargeted interaction of AmB-LLs with

fungal cells (LaMastro et al., 2023). All three types of liposomes were fluorescently tagged with 2 moles percent Rhodamine-B-DHPE loaded into the liposomal membrane.

Qualitative and quantitative assessment of DectiSome binding to three fungal pathogens

C. albicans, *R. delemar*, and *C. neoformans* were grown in vitro, treated with rhodamine B-labeled DEC3-AmB-LLs, BSA-AmB-LLs, or AmB-LLs, washed, and then photographed using fluorescence microscopy. Under the in vitro growth conditions used, *C. albicans* cells exhibited both yeast and hyphal morphologies; *R. delemar* grew with a hyphal morphology; and *C. neoformans* was in the yeast form. These experiments allowed the qualitative assessment of liposome binding to various fungal cells of different morphotypes. The areas of rhodamine B red fluorescence were measured from multiple photographs to quantify these binding data. We began assessing fluorescent liposome binding area data by manually processing each image through ImageJ as done previously (Ambati, Ellis, et al., 2019; Ambati, Ferarro, et al., 2019; Ambati, Pham, et al., 2021; Choudhury et al., 2022). To reduce the labor involved in quantifying fluorescent liposome binding data and standardize the process, we created a CellProfiler pipeline, AreaPipe, that automates quantitative image analysis (**Figure SF3.3**).

C. albicans

Dendritic cell Dectin-3 and purified epitope-tagged Dectin-3 polypeptides are reported to recognize *C. albicans*, at least in part, via their binding to extracellular oligo-mannans (Goyal et al., 2018; Wang et al., 2016; Zhu et al., 2013). Because Dectin-3's interactions with *C. albicans* are the best characterized for any fungal pathogen, we began our analysis of DEC3-AmB-LLs with this species. In our first experiment, *C. albicans* yeast cells were grown on microscope

chamber slides for only 1.5 h in hyphal growth-inducing media, wherein they just reached the yeast–hyphal transition stage of development. Fixed cells were stained with DEC3-AmB-LLs and control liposomes and viewed top-down at high magnification (60×) using combined epifluorescence and phase contrast microscopy (**Figure 3.1**). DEC3-AmB-LLs bound efficiently to the exopolysaccharide (EPS) matrices surrounding all yeast–hyphal stage cells (**Figure 3.1a**), while binding by control BSA-AmB-LLs and AmB-LLs was not detected (**Figure 3.1b,c**). Five pixels were substituted for the zero values of liposome binding in some control images, which was equivalent to the smallest numbers we had detected out of the 5×10^6 total pixel area in some experiments. The area of DEC3-AmB-LL binding was approximately 9,700-fold larger than for BSA-AmB-LLs or AmB-LLs ($p < 0.0001$, **Figure 3.1d**). The data are presented in a $\log_{10}$ scale scatter bar plot to reveal the dispersion of individual data points over a large dynamic range that would have been obscured in a linear plot.

In our next experiment, *C. albicans* was grown on plastic microtiter plates until they produced mature hyphal colonies a few hundred microns in diameter, fixed, treated with liposomes, and viewed bottom-up using combined epifluorescence and bright field microscopy (**Figure 3.2**). DEC3-AmB-LLs bound strongly (**Figure 3.2a**). Most of the binding appeared to be to patches of hyphal-associated EPS at the periphery of the colonies, where hyphae had been growing most rapidly, and less binding was associated with older cells at the center of colonies. Control liposomes bound rarely (**Figure 3.2b,c**). The area of DEC3-AmB-LL binding was 1,150-fold larger ($P_{MW} < 0.0001$) than for BSA-AmB-LLs and 43-fold larger ($P_{MW} < 0.0001$) than for AmB-LLs (**Figure 3.2d**). We speculate that the stronger binding of AmB-LLs relative to BSA-AmB-LLs may be attributed to non-specific binding of the liposomal membrane with hydrophobic components on the cells, such as cellular membranes (LaMastro et al., 2023),

wherein a coating of BSA interfered with this interaction. Biological replicates of these two experiments with *C. albicans* showed similar results (**Figure SF3.4a,b**, respectively).

R. delemar

Dectin-3 has not previously been reported to recognize Mucormycetes such as *R. delemar*. Because *R. delemar* does not stick efficiently to plastic or glass growth substrates (Ibrahim et al., 2005), we cultured the cells on agar media in petri dishes, where we have shown that they stick efficiently (Choudhury et al., 2022). Agar plugs were removed, fixed, washed, stained with rhodamine B-labeled DEC3-AmB-LLs, AmB-LLs, and BSA-AmB-LLs, and in some cases also with calcofluor white (CW) for chitin, and washed extensively to remove unbound liposomes and CW (Choudhury et al., 2022). Stained cells were viewed top-down by epifluorescence and, in some experiments, also by phase contrast.

R. delemar cells were grown for 6 h to the germling stage or 15 h to the mature hyphal stage. We found that DEC3-AmB-LLs bound strongly to fixed swollen sporangiospores and germ tubes of germling stage cells (**Figure 3.3a**). By contrast, binding by the control liposomes was rarely observed (**Figure 3.3b,c**). DEC3-AmB-LL binding was heavily concentrated in the EPS deposits (yellow arrows). There was some staining that appeared to be tightly associated with the cell wall (white arrows), but it was not possible to distinguish binding to the cell wall itself from EPS that was closely allied with the cell wall. The patchy nature of the staining along the cell wall may be accounted for either by the deposition of small amounts of EPS proximal to the cell wall or by small regions in the cell wall containing cognate ligands of Dectin-3 that are exposed, thus enabling DEC3-AmB-LL staining. The area of red fluorescent DEC3-AmB-LL binding was 164- fold larger ($P_{MW} = 0.0022$) than that for BSA-AmB-LLs and 188-fold larger

(P_{MW} = 0.0022) than that for AmB-LLs (**Figure 3.3d**). We did not observe preferential binding by AmB-LLs relative to BSA-AmB-LLs.

When fixed hyphal colonies of *R. delemar* were examined (**Figure 3.4**), we again observed that DEC3-AmB-LLs bound to cell-associated EPS deposits (**Figure 3.4a**), which are more obvious in a higher magnification image (**Figure 3.4b**). Control liposomes seldom bound (**Figure 3.4c,d**). The area of DEC3-AmB-LL binding was 614-fold larger (P_{MW} < 0.0001) than for BSA-AmB-LLs and 39-fold larger (P_{MW} < 0.0001) than for AmB-LLs (**Figure 3.4e**). Consistent with the data for *C. albicans*, the AmB-LLs showed higher levels of non-specific binding than the BSA-AmB-LLs.

When live mature hyphal colonies were examined (**Figure 3.5a–d**), we observed that DEC3-AmB-LLs bound to hyphal-associated EPS deposits in a pattern similar to fixed hyphae (**Figure 3.5a**) and control liposomes seldom bound (**Figure 3.5b,c**). The relative area of DEC3-AmB-LL binding was less dramatic than for fixed cells. The area of DEC3-AmB-LL binding was 21-fold larger (P_{MW} = 0.0012) than for BSA-AmB-LLs and 73-fold larger (P_{MW} = 0.0006) than for AmB-LLs. Perhaps the dynamic nature and turnover of cognate ligand sites in the EPS of live cells turn over DectiSome binding during the binding and washing steps, resulting in the weaker binding observed in live cells relative to fixed cells. Biological replicates of these three *R. delemar* liposome binding experiments showed similar results (**Figure SF3.4c–e**).

C. neoformans

Dendritic cell Dectin-3 was previously reported to recognize *C. neoformans* (Goyal et al., 2018; Hole et al., 2016). Therefore, we anticipated that DEC3-AmB-LLs would bind to this species. Colonies of *C. neoformans* were grown on minimal agar plates for 6 or 18 h. Agar plugs

were removed, fixed, washed, stained with rhodamine B-labeled DEC3-AmB-LLs, AmB-LLs, BSA-AmB-LLs, and CW, and washed extensively. Colonies were observed using top-down epifluorescence (**Figure 3.6**).

Six-hr-old *C. neoformans* colonies were composed of only three cells to two dozen cells (**Figure 3.6**). DEC3-AmB-LLs bound strongly to the EPS matrices associated with almost every colony (**Figure 3.6a**), even those composed of only a few cells, while binding by control liposomes was rarely observed (**Figure 3.6b,c**). DEC3-AmB-LLs bound to a 409-fold larger area ($P_{MW} < 0.0001$) than BSA-AmB-LLs and a 155-fold larger area ($P_{MW} < 0.0001$) than AmB-LLs (**Figure 3.6d**).

Eighteen-hr-old *C. neoformans* colonies were approximately 200 to 300 microns in diameter (**Figure 3.7**) and composed of thousands of cells. DEC3-AmB-LLs bound to numerous patches both within and at the boundary of mature colonies (**Figure 3.7a**). Some binding appeared to be specific to the EPS matrix at the periphery of the colonies (yellow arrows), while the binding that completely surrounded some small groups of cells might be specific to the cell capsules or capsule-associated EPS of these spherical cells (white arrows). Binding by BSA-AmB-LLs and AmB-LLs was seldom detected (**Figure 3.7b,c**), but is indicated for AmB-LL binding by thin white arrows (**Figure 3.7c**). DEC3-AmB-LLs bound to a 6,160-fold larger area ($P_{MW} < 0.0001$) than BSA-AmB-LLs and to a 4,160-fold larger area ($P_{MW} < 0.0001$) than AmB-LLs (**Figure 3.7d**). Biological replicates of these two *C. neoformans* liposome binding experiments produced similar results (**Figure SF3.4f,g**). To confirm that DEC3-AmB-LLs exhibit specific binding to fungal glycans, we tested the ability of various oligoglycans to inhibit binding to 16-hr-old *C. neoformans* colonies and found modest inhibition by oligomannans as expected and by glucuronic acid (**Figure SF3.5**) as recently reported in an independent study

(Huang et al., 2018). The inhibition by laminarin shown in this experiment was unexpected and inconsistent among experimental replicates. Importantly, neither DEC3-AmB-LLs nor control liposomes BSA-AmB-LLs and AmB-LLs bound detectably to human HEK293T cells, as shown in **Figure SF3.6.**

Binding by Dectin-3 protein

The exterior portion of the cell wall of *C. albicans* is rich in variously crosslinked oligomannans and mannoproteins (Garcia-Rubio et al., 2020; Gow et al., 2017; Schiavone et al., 2014). The cell walls of Mucorales species contain small amounts of variously crosslinked mannans (Lecointe et al., 2019). The exterior portion of the *C. neoformans* capsule is rich in glucuronoxylomannans (GXMs), which are a known ligand of Dectin-3 (Garcia-Rubio et al., 2020, Gow et al., 2017). Therefore, we expected Dectin-3-targeted liposomes to bind to the cell wall or capsule of all three species. Yet, we did not observe DEC3-AmB-LLs to be unambiguously bound to their cell walls or capsules. We considered the possibility that the 100-nanometer diameter of DEC3-AmB-LLs was simply too large to physically access the cognate ligands of Dectin-3 within the highly crosslinked glycan matrices of the cell walls and/or capsules. We estimate the rotational diameter of the 23 kDa MW truncated Dectin-3 polypeptide (DEC3) to be only a few nanometers. To test this hypothesis of size limitation for liposome binding, we directly conjugated rhodamine B (MW 0.48 kDa) to the Dectin-3 polypeptide to make DEC3-Rhod. DEC3-Rhod bound to the EPS matrices surrounding the various developmental stages of all three species and has comparable spatial distributions to those of DEC3-AmB-LLs (**Figure SF3.7a–e**). The localization of both DEC3-AmB-LLs and DEC3-Rhod staining varied widely from *C. albicans* colony to colony, as revealed by the distribution of

data points in scatter bar plots, but no significant difference in binding was observed between the two reagents. As with the liposomal reagents, the DEC3-Rhod protein reagent did not exhibit clear, unambiguous binding to the cell walls or capsules. Thus, the binding pattern of DEC3-AmB-LLs does not appear to have been dramatically altered by the physical size of liposomes.

Quantitative assessment of the inhibition and/or killing of three fungal pathogens

C. albicans, *R. delemar*, and *C. neoformans* were grown in vitro and treated with the DEC3-AmB-LLs, BSA-AmB-LLs, and AmB-LLs using different temporal regimens, after which growth, viability, and/or metabolic activity were quantified.

C. albicans

An overnight culture of *C. albicans* yeast cells was suspended into RPMI +10% FBS hyphal-inducing media and aliquoted into 96-well microtiter plates. Shortly after hyphal development was initiated (1.5 h, 37°C; see morphology in **Figure 3.1**), cells were treated with the DEC3-AmB-LLs, BSA-AmB-LLs, or AmB-LLs at the indicated AmB concentrations. Seventeen hours later, residual metabolic activity was measured using the CellTiter-Blue (CTB) reagent (resazurin). Only live cells with an intact plasma membrane and a functional mitochondrial electron transport chain can reduce resazurin to the fluorescent product resorufin. The plate was incubated for approximately 60 min at 37°C, and the pink fluorescence of resorufin was quantified. The data are presented in a $\log_{10}$ scatter bar plot in **Figure 3.8a**. Cells receiving DEC3-AmB-LLs delivering 0.3, 0.2, and 0.1 μM AmB showed respectively, 24-fold ($P_{MW} = 0.0003$), 127-fold ($P_{MW} = 0.0002$), and 25-fold ($P_{MW} = 0.0002$) lower metabolic activity than the corresponding BSA-AmB-LL-treated controls. Statistically significant reductions in

metabolic activity were also observed relative to the AmB-LL-treated controls. Control liposomes delivering 0.3 μM AmB began to have strong inhibitory activity, thus limiting the resolution of differences at this and higher concentrations of AmB. A biological replicate produced similar results (**Figure SF3.8a**).

R. delemar

R. delemar sporangiospores were plated in RPMI + 0.165 M MOPS (pH 7) media in 96-well microtiter plates. DEC3-AmB-LLs, BSA-AmB-LLs, and AmB-LLs delivering different concentrations of AmB were immediately added to the respective wells, and the plates were incubated for 24 h at 37°C with shaking at 120 rpm. Cell density was measured as O.D. at A_{610}. Cells receiving DEC3-AmB-LLs delivering 0.8, 0.4, and 0.2 μM AmB were 10.8-fold ($p = 5.5 \times 10^{-6}$), 7.8-fold ($p = 2 \times 10^{-4}$) and 1.4-fold ($p = 0.024$) less dense than the respective BSA-AmB-LL-treated controls, and the 0.8 and 0.4 μM samples were similarly less dense than the respective AmB-LL-treated controls (**Figure 3.8b**). After the cell density measurements were taken, CTB reagent was added to each well, and the plate was incubated at 37°C for an additional two hours. The pink fluorescence in each well was quantified. Cells receiving DEC3-AmB-LLs delivering 1.6, 0.8, 0.4, and 0.2 μM AmB had 28-fold ($p = 1.7 \times 10^{-6}$), 105-fold ($p = 5.1 \times 10^{-7}$), 19-fold ($p = 2.9 \times 10^{-11}$), and 1.79-fold ($P_{MW} = 0.0079$) lower metabolic activity than the respective BSA-AmB-LL-treated cells (**Figure 3.8c**). DEC3-AmB-LLs-treated cells had similarly reduced levels of metabolic activity relative to the AmB-LL-treated controls. Biological replicates produced comparable results (**Figure SF3.8b,c**).

C. neoformans

C. neoformans yeast cells grown overnight in YPD were plated at 10,000 cells per well in 96-well microtiter plates in RPMI + 0.165 M MOPS (pH 7) at 30°C. After a few hours of incubation in YPD, when the cells had formed small colonies equivalent to those shown in **Figure 3.6**, they were treated with liposomes delivering the indicated concentrations of AmB, and the plates were incubated for 1 h at 30°C with shaking at 50 rpm. The media with unbound liposomes was removed, CTB reagent in RPMI + MOPS media was added to each well, and the plate was incubated for an extended period at 30°C. Cells receiving DEC3-AmB-LLs delivering 2.0 and 1.0 μM AmB showed only 1.32-fold ($P_{MW} = 0.0002$) and 1.26-fold ($P_{MW} = 0.0002$) lower metabolic activity than the respective BSA-AmB-LL-treated controls (**Figure 3.8d**). There were similar small reductions in CTB activity relative to the AmB-LL-treated controls. Because there was small variability in the results among eight individual samples, these results were highly statistically significant, but the fold improvements in inhibition by DEC3-AmB-LLs were clearly marginal. A biological replicate produced similar results for the comparison at 2.0 μM AmB but not for 1.0 or 0.5 μM (**Figure SF3.8d**). Variations in this CTB assay design, such as longer drug treatments or not removing unbound liposomes, did not improve the relative efficacy of DEC3-AmB-LLs. Attempts to measure the efficacy of DEC3-AmB-LLs at reducing cell viability by measuring reductions in cell density in microtiter plate assays, or reductions in CFUs in liquid suspension cultures, or increases in propidium iodide staining of dead cells all failed to give significant results. Apparently, these techniques were not sensitive or reproducible enough to detect the small changes in cell viability revealed by CTB assays.

Discussion

We have shown that Dectin-3's CRD targets DEC3-AmB-LLs specifically and efficiently to the yeast–hyphal transition stage and mature hyphal stage of the Ascomycete *C. albicans*, to the germling and mature hyphal stages of the Mucormycete *R. delemar*, and to small and large colonies of the Basidiomycete *C. neoformans*. We've added *R. delemar* to the list of fungal species recognized by Dectin-3's CRD and suggest the possibility that there are other target pathogens for Dectin-3 yet to be discovered. These three fungal pathogens diverged from common ancestral species several hundred million years ago and, hence, represent some of the extreme ancient diversity within the fungal kingdom (Kuramae et al., 2006; Spatafora et al., 2017; Taylor & Berbee, 2006). Fluorescent DectiSomes have tremendous power as probes for the novel binding of CTLs, such as Dectin-3, because each liposome has a few thousand rhodamine B molecules and each has more than a thousand DEC3 molecules, thus creating avidity for target ligands. DEC3-AmB-LLs bound to the EPS matrices of these species, and there was little, if any, binding to their cell walls and/or capsules. The much smaller DEC3-Rhod protein reagent also did not bind unambiguously to cell walls and/or capsules. Fungal pathogens are thought to produce EPS to adhere to host tissues and protect themselves from host immune defenses. EPS shed into host serum could decoy immune responses away from fungal cells. Dectin-3 may have evolved its ability to bind to the EPS associated with and shed from diverse pathogens in order to aid in the complex host innate immune responses to infection. Our results presented here on Dectin-3-targeted DectiSomes binding to and killing *C. albicans* and *R. delemar* compare reasonably well with our previous publications on Dectin-1-, Dectin-2-, and DC-SIGN-targeted DectiSomes (Meagher et al., 2023).

Many CTLs form homodimers that form their glycan ligand binding sites at the junction of the two CRDs (Cummings & McEver, 2022). In our previous studies, we constructed liposomes containing the truncated forms of Dectin-1, Dectin-2, and DC-SIGN alone, as we have done here with truncated Dectin-3. In each case, this resulted in the efficient targeting of antifungal liposomes to fungal pathogens, and this design must have enabled homodimers to form functional ligand binding sites. Each showed dramatically improved antifungal efficacy over untargeted liposomal AmB toward one or more fungal pathogens, including *Aspergillus fumigatus*, *C. albicans*, *C. neoformans*, and *R. delemar* grown in vitro (Ambati, Ellis, et al., 2019; Ambati, Ferarro, et al., 2019; Ambati, Pham, et al., 2021; Choudhury et al., 2022) and *A. fumigatus* and *C. albicans* in mouse models of pulmonary aspergillosis and invasive candidiasis (Ambati et al., 2022; Ambati, Ellis, et al., 2021). However, these and several other CTLs are co-expressed in mammalian dendritic cells and macrophages (Ariizumi et al., 2000; Hole et al., 2016; Kitai et al., 2021; Sun et al., 2013; Yoshikawa et al., 2021; Zhu et al., 2013) and, hence, have the potential to act cooperatively to enhance signaling. Dectin-2 and Dectin-3 appear to be on the same membrane rafts in bone marrow-derived macrophages or when co-transfected into monocyte/macrophage-like RAW264.7 cells. This view of their linked behavior stems from results showing that when either binds a cognate ligand or is treated with either Dectin-specific antibody, the two CTLs are co-endocytosed (Zhu et al., 2013). The study used bimolecular fluorescence complementation of Dectin-2 and Dectin-3 yellow fluorescent protein fusions in HEK293 cells to show that the co-expressed proteins physically interact on cell surfaces to form heterodimers that have enhanced and perhaps novel ligand binding and signaling properties. The implication is that physically connected heteromeric CRDs of the two CTLs are formed and have novel properties of ligand recognition. By contrast, when co-transfected into embryonic kidney

293T cells, Dectin-2 did not appear to form heteromeric complexes with Dectin-3 (Blankson et al., 2022). Thus, it is possible that other factors are required for their linked behavior. Now that we have shown that Dectin-3 functions efficiently when floating on a liposomal surface, we can construct liposomes co-presenting Dectin-3 and Dectin-2 and test their interaction in a cell-free system. If liposomal co-presentation of Dectin-2/Dectin-3 enhances and expands their ligand binding properties, this should make a more effective pan-antifungal delivery vehicle than either Dectin alone.

The superfamily of CTL genes contains more than 30 members and several subgroups based on the sequences of their CRDs and their functional structures and signaling domains when positioned in the cell membrane (Drickamer & Taylor, 2015). Among the fifteen members of structural group 2 CTLs, Dectin-3, Dectin-2, and DCSIGN (*CD209*) all recognize oligomannans. This is a well-represented class of glycans that form part of the cell walls and EPS matrices of most fungal pathogens (Briard et al., 2021; Drickamer & Taylor, 2015; Gow et al., 2017; Goyal et al., 2018). However, our previous studies showed that Dectin-2- and DC-SIGN-targeted liposomes stained fungal EPS matrices with little, if any, staining of fungal cell walls or capsules (Ambati, Ellis, et al., 2019; Ambati, Pham, et al., 2021; Meagher et al., 2023). In these previous studies, as herein, microscope observations showed that binding was primarily localized to the material closely associated with the cells, but there was minimal binding tightly associated with the cell wall. We have inferred that this material is EPS, which is also known to contain cognate ligands of various CTLs. At the outset, we suspected that Dectin-3 would recognize distinct fungal oligoglycans in both cell walls and EPS matrices and recognize diverse fungal pathogens. First, Dectin-3 has a relatively distinct and divergent CRD amino acid sequence when compared to the other two Dectins. Second, lymphoid cell Dectin-3 recognizes

glucuronoxylomannan (GXM), which is characterized as a major glycan component of *C. neoformans* capsules and a lesser component of their biofilms (Albuquerque et al., 2014; Huang et al., 2018). GXM is not a single compound. It is composed of a heterogenous mixture of polysaccharides that vary widely in their molecular weight from less than 10 kDa to 300 kDa (Albuquerque et al., 2014) and are often crosslinked to other glycans, thus generating different GXM variants. We previously stained in vitro-grown *C. neoformans* cells with the best-characterized anti-GXM antibody 18B7 and found robust staining of GXM within the capsule of most, but not all, individual cells and the EPS matrix associated with some cells (Ambati, Ellis, et al., 2019). Dectin-2 liposomal staining only partially overlapped with that of the GXM antibody. Using a variety of monoclonal antibodies to GXM, including 18B7, it was shown that GXM encompasses many different immuno-epitopes that are heterogeneously distributed in the *C. neoformans* capsule and EPS (Albuquerque et al., 2014). Because Dectin-3 is reported to specifically recognize GXM, and GXM is a major glycan component of *C. neoformans*, we anticipated the potential for highly preferential binding to *C. neoformans*, and in particular its capsule, over binding to our other two test species. But instead, we only observed staining of the EPS matrix in small colonies and sporadic staining of the EPS surrounding some cells in older colonies. While it is possible that our DEC3-AmB-LL reagent recognized a very small subset of *C. neoformans* GXMs in the cell capsule, proving this would require extensive immunochemical and/or biochemical analyses. It is also possible that lymphoid cell Dectin-3 recognition of GXM requires cooperation with other CTLs, and Dectin-3 itself does not itself bind GXM. Our study does not attempt to identify the particular glycans or glycolipids recognized by Dectin-3, and our results do suggest there is still much to be learned about Dectin-3's range of cognate ligands.

Based on the two to three orders of magnitude higher levels of DEC3-AmB-LL binding to *C. albicans*, *R. delemar*, and *C. neoformans* relative to control liposome binding, we anticipated orders of magnitude more efficient inhibition and/or killing of all three species. When delivering the low concentrations of AmB of 0.1–1.6 μM, we showed that DEC3-AmB-LLs reduced the viable cell metabolic activity of *C. albicans* and *R. delemar* one to two orders of magnitude more efficiently than untargeted AmB-loaded liposomal controls. Under the conditions of our assays, DEC3-AmB-LLs lowered the effective dose of liposomal AmB for inhibition and/or killing of these two species by at least two orders of magnitude. By contrast, and based on various assays, DEC3-AmB-LLs were much less effective at inhibiting or killing *C. neoformans*. This was unexpected based on DEC3-AmB-LL's efficient binding to this species. We cannot explain the lack of strong antifungal efficacy against *C. neoformans*.

As to the mechanism by which AmB-loaded DectiSomes, and DEC3-AmB-LLs in particular, increase inhibition and killing of fungal pathogens relative to untargeted control liposomes, AmB-LLs, our analog of AmBisome®, we propose the following. While it is known that AmBisome® liposomes pass through the cell wall and plasma membrane (Walker et al., 2018), it is reasonable to assume this transport process is relatively inefficient because the 60 to 90 nanometer diameter size of liposomes should impede movement through the cell wall and membrane. While a small fraction of the untargeted liposomes will make it through the cell wall and plasma membrane, most will diffuse far away from the cells or be washed away, and the AmB from these liposomes will be at much lower concentrations. By contrast, when AmB-loaded DectiSomes are bound to the EPS, their close proximity to fungal cells increases the concentration of AmB diffusing from DectiSomes to fungal cells. The dimensions of AmB are measured in 10's of Angstroms, and it is known to penetrate into the cell membrane. The

argument that AmB from DectiSomes will diffuse more rapidly to fungal cells than untargeted liposomal AmB is based on the Fokker–Planck equation showing that the rate of diffusion proceeds as the inverse square of the distance (Fokker, 1914; Planck, 1917). In the case of DectiSomes bound to the ligands in the EPS proximal to the fungal cells, there should be a more rapid and efficient diffusion of AmB to cells than by most of the untargeted liposomal AmB, which is more distant from fungal cells, and the rate of diffusion to fungal cells will be much slower. Additionally, the fact that various DectiSomes bind primarily to the EPS offers a big advantage to their antifungal activity. Depending upon their glycan compositions, the sheer size of the EPS should generate more available cognate ligand binding sites than the cell wall. Hence, EPS-bound DectiSomes should provide a larger reservoir of AmB than if they were bound only to the cell wall.

While the goal is to develop DectiSomes as powerful pan-antifungal therapeutics, this and our other recent studies leave many important issues unresolved (Meagher et al., 2023). We have only just begun to test DectiSomes in mouse models of invasive fungal disease (Ambati et al., 2022; Ambati, Ellis, et al., 2021; Ambati, Pham, et al., 2021). Extrapolating from in vitro binding and killing to in vivo studies is complicated by the fact that the glycan and lipoglycan ligands produced by fungi are dependent upon their growth environment. Dectins such as Dectin-3 have the advantage over antibody-targeted reagents in that a unique host Dectin sequence should have low immunogenicity relative to variable antibody sequences that often produce host-specific immunogenic responses. However, Dectin-1 and Dectin-3 recognize endogenous ligands that discriminate self from non-self (Mori et al., 2017; Saijo & Iwakura, 2011), and as more is known about Dectin-3, it may also be shown to recognize host ligands. Thus, there is the

potential that CTL-targeted reagents could have toxicity issues. Our ongoing research explores a wide variety of topics concerning the efficacy of DectiSomes as drug delivery agents.

Conclusions

We presented statistically well-supported data showing that Dectin-3-coated AmB-loaded liposomes, DEC3-AmB-LLs, were an order of magnitude or more effective at binding to *C. albicans*, *R. delemar*, and *C. neoformans* than either of our control liposomes, AmB-LLs and BSA-AmB-LLs. DEC3-AmB-LLs bound primarily to their EPS matrices and not to their cell walls or cell capsules. DEC3-AmB-LLs were similarly effective at inhibiting or killing *C. albicans* and *R. delemar*, but much less effective against *C. neoformans*. Our positive data showing the inhibition of hyphal stages of two highly divergent pathogens suggest that it would be worthwhile to explore the efficacy of DEC3-AmB-LLs in mouse models of candidiasis and mucormycosis and investigate the potential of Dectin-3 to act synergistically and perhaps form heterodimers with Dectin-2 on the same liposomes. The CellProfiler pipeline AreaPipe was introduced to automate and simplify the capture and quantification of fluorescent area data within TIFF or JPEG images, replacing the tedious, time-consuming manual processing of area data in ImageJ.

Experimental Procedures

Fungal strains and growth conditions

C. albicans strain SC5314 (Gillum et al., 1984) was grown in YPD (1% yeast extract, 2% peptone, 2% dextrose, ThermoFisher Cat#212750, #21677, Fisher Sci. Cat#D16-10, respectively) liquid culture starting from a single colony on an agar plate and grown at 37°C

overnight with vigorous shaking. Yeast cells were washed once into RPMI lacking phenol red dye (Sigma-Aldrich, Cat# R8755) + 10% Fetal Bovine Serum (FBS) (GIBCO Cat#10437–028) adjusted to pH 7.5, plated at 20,000 cells/well in 1 mL and 35,000 cells/per well in 0.1 mL, and grown at 37°C to the germling or hyphal stage in wells of plastic 24-well or 96-well polystyrene microtiter plates or on poly-L-lysine-coated glass microscope slides inside a glass chamber. When indicated, cells were fixed in 3.7% formalin (J.T. Baker, #2106–01) diluted in PBS for 1 h and washed three times in PBS before staining. The design of the reusable glass chambers and assembled chamber slides for growing cells is shown in **Figure SF3.9a,b**.

Sporangiospore stocks of *R. delemar* strain 99–880 (f.k.a. *R. oryzae* and *R. arrhizus*, ATCC MYA-4621) were prepared as described recently (Choudhury et al., 2022) and stored at 4°C, where they remained greater than 90% viable for more than a month. Sporangiospores were germinated and grown to germling or hyphal stages on 1.5% agar plates made with RPMI + 0.165 M MOPS (3-(N-morpholino) propane sulfonic acid; Sigma-Aldrich, Cat# M1254) (Andrianaki et al., 2018) adjusted to pH 7 and incubated at 37°C (Choudhury et al., 2022). Agar plugs were removed and processed for top-down microscopic imaging (Choudhury et al., 2022). For quantitative inhibition and killing experiments, cells were grown in liquid RPMI + MOPS media diluted to 800 cells per 90 μL per well in 96-well microtiter plates. Because *R. delemar* does not stick well to microtiter plates but does stick efficiently to micropipette tips, reagents were added but never removed during growth and inhibition assays.

C. neoformans clinical isolate H99-alpha (Montone, 2009) was grown at 30°C in liquid YPD (1% yeast extract, 2% peptone, 2% dextrose) with vigorous shaking overnight. Cells prepared for microscopy were then plated on RPMI + MOPS agar plates and incubated at 30°C, and agar plugs were later removed. Cells for viability assays were plated at 10,000 cells per 90

μL per well in YPD in 96-well microtiter plates, grown for 4.5 h, and treated with liposomes, after which the media was removed and replaced with RPMI + MOPS media containing CTB reagent at the manufacturer's recommended concentration.

Production of Dectin-3

Annotated Dectin-3-derived DNA and protein sequences are given in **Figure SF3.1**. The 219 amino acid (a.a.)-long sequence of the native murine Dectin-3 protein (NP_034949.3) was obtained from the National Center for Biotechnology Information (**Figure SF3.1a**). The sequence of the *E. coli* codon-optimized construct of murine Dectin-3 CRD and stalk region truncated and modified for cloning into pET-45B and lipidation is shown in **Figure SF3.1b** and was deposited at the U.S. National Center for Biotechnology Information (BankIT, HK-DEC3; accession number OQ366170). The sequence encodes a 199 a.a.-long modified truncated Dectin-3 polypeptide, DEC3, beginning at its N-terminus with a vector-encoded N-terminal $(His)_6$ affinity tag, an added flexible GlySerGly spacer, two lysine (K) residues, and another flexible GlySerGly spacer, followed by the 176 a.a.-long N-terminal end of murine Dectin-3 (**Figure SF3.1c**). The *E. coli* strain BL21 containing the murine Dectin-3-pET45B plasmid was grown in 1 L of Luria broth at 37°C overnight without IPTG induction (**Figure SF3.2**) or with IPTG induction at O.D. 0.7 A_{600}, followed by 4 more hours of growth. DEC3 was extracted from cell pellets using a 6 M guanidine hydrochloride (GuHCl) buffer and purified on nickel affinity resin in this buffer as described previously (Ambati, Ellis, et al., 2019; Ambati, Ferarro, et al., 2019). After affinity purification, the protein was approximately 80% pure (**Figure SF3.2b**). In various preparations, five to ten milligrams of affinity-purified protein were typically recovered per liter of Luria broth culture.

Production of Dectin-3-coated drug-loaded liposomes (DEC3-AmB-LLs)

AmB-loaded liposomes, AmB-LLs, were prepared as described previously, except that the drug loading was performed at 37°C instead of 60°C (Ambati, Ferarro, et al., 2019). Samples of Dectin-3 were coupled to DSPE-PEG-3400-NHS (Nanosoft Polymers, 1544–3400) in the same 6 M GuHCl buffer with the pH adjusted to 8.3 with triethanolamine and purified over Bio-Gel P-6 acrylamide molecular exclusion resin in a 1 M Arginine crowding buffer pH adjusted to 7.3 (Bio-Rad Cat#150–0740) as we described previously for other CTLs (Ambati, Ellis, et al., 2019; Ambati, Ferarro, et al., 2019; Ambati, Pham, et al., 2021). DSPE-PEG-BSA was prepared from BSA (Sigma, Cat#A-8022) by the same protocol, except that the coupling to DSPE-PEG-NHS was performed in 0.1 M pH 8.3 carbonate buffer, and it was subsequently desalted by P-6 gel exclusion chromatography in 0.1 M sodium phosphate buffered saline pH 7.4 (Corning, Cat#21-031-CV). Modified Dectin-3 and BSA were loaded into AmB-LLs at 1 and 0.33 moles percent, respectively, relative to moles of liposomal lipid via their DSPE lipid moiety as described previously (Ambati, Ellis, et al., 2019, Ambati, Ferarro, et al., 2019). Typical preparations produced 800 μL of protein-coated liposomes with 1.1 mg of modified Dectin-3 or BSA (~1.4 mg/mL) and AmB at 750 μM (0.69 mg/mL). For each new batch of AmB-loaded liposomes, the volumes of DEC3-AmB-LLs, BSA-AmB-LLs, and AmB-LLs were adjusted to have the same concentration of AmB, typically 750 μM, to simplify dilutions of the three samples in subsequent experiments.

Liposome dilutions for binding and inhibition studies

For all liposome-binding experiments, DEC3-AmB-LLs were diluted such that the Dectin-3 protein was at a concentration of 1 μg/100 μL (1:100 w/v) in respective growth media.

AmB-LLs and BSA-AmB-LLs were diluted equivalently. For binding inhibition experiments, DEC3-AmB-LLs (1:100 w/v) were preincubated for 30 min with the following oligoglycans at a concentration of 10 mg/mL: yeast mannans extracted via alkaline extraction (Sigma Cat# M7504) or detergent extraction (Sigma Cat# M3640), laminarin (Sigma Cat# L9634), glucuronic acid (Sigma Cat# G5269), or the liposome dilution buffer as a control. The oligoglycan/DectiSome mixes were then added to pre-blocked *C. neoformans* plugs. For killing studies, liposomes were diluted into growth media just before use, such that they delivered AmB final concentrations of 0.1 to 2 μM.

Liposome binding to a human cell line

The human embryonic kidney epithelial cell line HEK293T was obtained from the American Type Culture Collection (ATCC #CRL-3216). Cells were grown on 24-well plastic microtiter plates in RPMI media plus 10% fetal bovine serum at 37°C with 5% CO_2. Cells were washed with PBS, fixed for 30 min with 4% freshly prepared formalin, and washed thrice more with PBS. Cells were stained with rhodamine-tagged DEC3-AmB-LLs, BSA-AmB-LLs, and AmB-LLs as described for staining fungal cells. Images were taken bottom up on an inverted revolving microscope at 10× magnification, combining the visible light channel and the fluorescent Texas Red channel.

CellProfiler analysis of fluorescent liposome staining

All microscopy was performed on an ECHO Revolve microscope (model #RVSF1000/Revolve R4). Red fluorescent liposome staining was captured in the TRITC channel, CW chitin staining in the DAPI channel, visible light images using the Ph1 phase

condenser, and combined images as Revolve's zoverlay.jpg files. As we began this project, we manually captured the area of fluorescent staining image by image in ImageJ. The direct output from ImageJ presents fluorescence as a fraction of the image area, as we presented in our previous publications of DectiSomes and as shown in several supplemental figures herein (**SF3.4C through SF3.4G**). A CellProfiler (v. 4.2.4)-based pipeline, AreaPipe (v. 5), was developed to analyze photographic images (e.g., jpg, tiff) for the area of fluorescent reagent binding (e.g., fluorescent liposomes) to cells (Carpenter et al., 2006). AreaPipe (AreaPipe_V5.cppipe) was deposited at the CellProfiler repository of published pipelines at the Broad Institute (https://cellprofiler.org/published-pipelines). In short, the program eliminated the manual quantification of fluorescent imaging data. **Figure SF3.3** shows the original rhodamine red fluorescent jpeg image of DEC3-AmB-LLs binding to a *C. albicans* hyphal colony (**Figure SF3.3A1**) and compares the areas of fluorescence captured from the image using the manual analysis method in ImageJ (**Figure SF3.3A2**) as done previously (Ambati et al., 2022; Ambati, Ellis, et al., 2019, 2021; Ambati, Ferarro, et al., 2019; Ambati, Pham, et al., 2021; Choudhury et al., 2022) to that obtained using AreaPipe (**Figure SF3.3A3**). When using the manual method, each red fluorescent image (e.g., **Figure SF3.3A1**) jpeg or tiff was (1) loaded into ImageJ, (2) converted to an 8-bit black and white image under Image > Type, and (3) adjusted using threshold settings to capture the appropriate red liposome binding area under Image > Adjust > Threshold (30/255) > Apply. (4) These data were placed in a file using the Analyze>Measure functions, and (5) the ImageJ data were copied and pasted into an Excel file for subsequent quantitative analysis. To use AreaPipe, (1) CellProfiler was opened, (2) the jpeg or tiff images to be analyzed were pasted into the indicated window, (3) AreaPipe (AreaPipe_V5.cppipe) was dragged into the indicated window, and the operator answered “yes” to “load pipeline?”; (5) two

separate folders were designated for the output data files "SaveImages" and "ExportToSpreadsheet"; (6) Analyze Images was selected; and (7) the quantitative area output data was automatically loaded into a .csv file and the jpeg images of the segmented areas into a folder (e.g., **Figure SF3.3A3**). Some effort was devoted to ensuring that AreaPipe accurately captured even trace images with only a few pixels of liposomal fluorescence or could report zero pixels of fluorescence, which was not uncommon among images of control liposome-treated samples. Typically, AreaPipe processed 30 jpeg images in 3 min using a standard laptop, which in our experience was at least 20-times faster than the manual processing in ImageJ and avoided the excessive eye strain associated with the manual method. The only difference in the output is that the manual ImageJ method records a fraction of the fluorescent pixel area captured relative to the entire image area, while AreaPipe reports the actual number of fluorescent pixels captured from an image out of the total pixel area in images. In order to allow these data to be plotted on a log scale, when zero pixels were recorded, we substituted a value of 5 pixels, and with the manual method, when zero area was recorded, 0.0001 was substituted for the area, which was close to the lowest values recorded experimentally.

Quantitative inhibition and killing studies

Up to four types of assays were used in attempts to quantify DectiSome inhibition, killing, and/or survival after treatment with liposomal AmB. (1) Cell density was recorded at A_{610} nanometers in 96-well microtiter plates (BioTeK Synergy HT microplate reader). (2) Colony-forming units (CFUs) of *C. neoformans* were counted after plating dilutions of cells on YPD and incubating at 30°C. (3) Propidium iodide staining of dead cells followed our previous published protocol (Ambati, Ellis, et al., 2019). (4) CellTiter-Blue reagent (CTB, resazurin,

Promega Cat#G8081) was used to measure the reduction in live cell metabolic redox activity, with 20 μL of reagent being added to 100 μL of cells in 96-well microtiter plates. After CTB was added, *C. albicans, R. delemar*, and *C. neoformans* were respectively incubated for approximately 1 h at 37°C, 2 h at 37°C, and 18 to 24 h at 30°C before the fluorescent product resorufin was measured at Ex485/Em590 (BioTek Synergy HT). We have not seen fluorescent CTB assays of *C. neoformans* reported previously, but an XTT colorimetric redox assay had been used previously (Martinez & Casadevall, 2007). Fluorescent CTB assays have a much larger dynamic range than colorimetric XTT assays. Long incubation times (e.g., 24 h) with CTB's resazurin dye are commonly used to measure the viability of *Mycobacterium* spp. following drug treatments (Amin et al., 2009; Franzblau et al., 1998).

Data management

Data were recorded and managed in Excel (v. 16.69). The CellProfiler AreaPipe output data were in the .csv file format, which is compatible with Excel. Scatter bar plots were prepared, and standard errors from the mean were estimated in GraphPad Prism 9 (v. 9.5.0). Most of the data were normally distributed, so the Student's two-tailed *t*-test was used to estimate *p* values (T.TEST in Excel). In cases where the data for at least one sample in a comparison appeared to be non-parametric in their distribution, *p* values were estimated using the Mann–Whitney U test (Mann & Whitney, 1947) in Prism 9 and were indicated as P_{MW} values.

Author Contributions

Richard B. Meagher: Conceptualization; investigation; funding acquisition; writing – original draft; methodology; validation; writing – review and editing; visualization; project

administration; formal analysis; data curation; supervision; resources. **Quanita J. Choudhury:** Conceptualization; investigation; writing – original draft; methodology; validation; writing – review and editing; visualization; data curation; formal analysis. **Suresh Ambati:** Conceptualization; investigation; methodology; visualization; validation; writing – review and editing; formal analysis; data curation. **Collin D. Link:** Investigation; methodology; validation; writing – review and editing; software; visualization. **Xiaorong Lin:** Conceptualization; funding acquisition; writing – review and editing; project administration; resources. **Zachary A. Lewis:** Conceptualization; funding acquisition; writing – review and editing; software; methodology; resources; supervision; project administration; validation.

Acknowledgements

We would like to thank the technical team from the University of Georgia Franklin College of Arts and Science Office of Information Technology for helping us maintain the computer hardware and software used to obtain, manage, process, and publish various data. We wish to thank Matthew Whittaker and Professor Eileen Kennedy of UGA's Pharmaceutical and Biomedical Sciences Department for supplying the HEK293T cells for staining and Annalee Picket in UGA's Center for Applied Isotope Studies' Glass Blowing Shop for preparing the glass microscope slide chambers. The work was funded by the University of Georgia Research Foundation, Inc. (UGARF to S.A. and R.B.M.) and the National Institute of Allergy and Infectious Diseases (R21AI144498 and R21AI148890 to R.B.M. and Z.A.L., and R01AI162989 to R.B.M., S.A., Z.A.L., and X.L.). The funders had no role in study design, data collection, interpretation, or the decision to submit the work for publication and are not responsible for the content of this article.

Conflict of Interest Statement

UGARF has submitted patents to the United States Patent and Trademark Office. UGARF had no role in the design, execution, interpretation, or writing of this study. The authors declare that they have no conflicts of interest related to this study.

Data Availability Statement

All new data that were presented and/or discussed within this publication and its supplemental data section are included herein, and any previously published data that were discussed were appropriately cited. The AreaPipe pipeline for fluorescent area analysis will be uploaded at the Broad Institute's site for CellProfiler programs and made public once this study is accepted for publication as per the Broad Institute's suggestion for the time of release.

References

Albuquerque, P.C., Fonseca, F.L., Dutra, F.F., Bozza, M.T., Frases, S., Casadevall, A. et al. (2014) *Cryptococcus neoformans* glucuronoxylomannan fractions of different molecular masses are functionally distinct. *Future Microbiology*, 9, 147–161.

Ambati, S., Ellis, E.C., Lin, J., Lin, X., Lewis, Z.A. & Meagher, R.B. (2019) Dectin-2-targeted antifungal liposomes exhibit enhanced efficacy. *mSphere*, 4, 1–16.

Ambati, S., Ellis, E.C., Pham, T., Lewis, Z.A., Lin, X. & Meagher, R.B. (2021) Antifungal liposomes directed by Dectin-2 offer a promising therapeutic option for pulmonary aspergillosis. *mBio*, 12, 1–8.

Ambati, S., Ferarro, A.R., Kang, S.E., Lin, J., Lin, X., Momany, M. et al. (2019) Dectin-1-targeted antifungal liposomes exhibit enhanced efficacy. *mSphere*, 4, 1–15.

Ambati, S., Pham, T., Lewis, Z.A., Lin, X. & Meagher, R.B. (2021) DC-SIGN targets amphotericin B-loaded liposomes to diverse pathogenic fungi. *Fungal Biology and Biotechnology*, 8, 22.

Ambati, S., Pham, T., Lewis, Z.A., Lin, X. & Meagher, R.B. (2022) DectiSomes: glycan targeting of liposomal amphotericin B improves the treatment of disseminated candidiasis. *Antimicrobial Agents and Chemotherapy*, 66, 1–13.

Amin, A.G., Angala, S.K., Chatterjee, D. & Crick, D.C. (2009) Rapid screening of inhibitors of *Mycobacterium tuberculosis* growth using tetrazolium salts. *Methods in Molecular Biology (Clifton, N.J.)*, 465, 187–201.

Andrianaki, A.M., Kyrmizi, I., Thanopoulou, K., Baldin, C., Drakos, E., Soliman, S.S.M. et al. (2018) Iron restriction inside macrophages regulates pulmonary host defense against *Rhizopus* species. *Nature Communications*, 9, 3333.

Ariizumi, K., Shen, G.L., Shikano, S., Ritter, R., 3rd, Zukas, P., Edelbaum, D. et al. (2000) Cloning of a second dendritic cell-associated C-type lectin (dectin-2) and its alternatively spliced isoforms. *The Journal of Biological Chemistry*, 275, 11957–11963.

Banerjee, S., Denning, D.W. & Chakrabarti, A. (2021) One health aspects & priority roadmap for fungal diseases: a mini-review. *The Indian Journal of Medical Research*, 153, 311–319.

Blankson, V., Lobato-Pascual, A., Saether, P.C., Fossum, S., Dissen, E. & Daws, M.R. (2022) Human macrophage C-type lectin forms a heteromeric receptor complex with Mincle but not Dectin-2. *Scandinavian Journal of Immunology*, 95, e13149.

Bongomin, F., Gago, S., Oladele, R.O. & Denning, D.W. (2017) Global and multi-national prevalence of fungal diseases-estimate precision. *Journal of Fungi (Basel)*, 3, 1–29.

Briard, B., Fontaine, T., Kanneganti, T.D., Gow, N.A.R. & Papon, N. (2021) Fungal cell wall components modulate our immune system. *Cell Surface*, 7, 100067.

Brown, G.D., Denning, D.W., Gow, N.A., Levitz, S.M., Netea, M.G. & White, T.C. (2012) Hidden killers: human fungal infections. *Science Translational Medicine*, 4, 165rv13.

Carpenter, A.E., Jones, T.R., Lamprecht, M.R., Clarke, C., Kang, I.H., Friman, O. et al. (2006) CellProfiler: image analysis software for identifying and quantifying cell phenotypes. *Genome Biology*, 7, R100.

Choudhury, Q.J., Ambati, S., Lewis, Z.A. & Meagher, R.B. (2022) Targeted delivery of antifungal liposomes to *Rhizopus delemar*. *Journal of Fungi (Basel)*, 8, 1–14.

Cummings, R.D. & McEver, R.P. (2022) Chapter 31. C-type lectins. In: *Essentials of Glycobiology*, 4th edition. Cold Spring Harbor, NY: Cold Spring Harbor Laboratory Press.

Decote-Ricardo, D., LaRocque-de-Freitas, I.F., Rocha, J.D.B., Nascimento, D.O., Nunes, M.P., Morrot, A. et al. (2019) Immunomodulatory role of capsular polysaccharides constituents of *Cryptococcus neoformans*. *Frontiers in Medicine*, 6, 129.

Drickamer, K. & Taylor, M.E. (2015) Recent insights into structures and functions of C-type lectins in the immune system. *Current Opinion in Structural Biology*, 34, 26–34.

Flornes, L.M., Bryceson, Y.T., Spurkland, A., Lorentzen, J.C., Dissen, E. & Fossum, S. (2004) Identification of lectin-like receptors expressed by antigen presenting cells and neutrophils and their mapping to a novel gene complex. *Immunogenetics*, 56, 506–517.

Fokker, A.D. (1914) Die mittlere Energie rotierender elektrischer Dipole im Strahlungsfeld. *Annalen der Physik*, 348, 810–820.

Fonseca, F.L., Nimrichter, L., Cordero, R.J., Frases, S., Rodrigues, J., Goldman, D.L. et al. (2009) Role for chitin and chitooligomers in the capsular architecture of *Cryptococcus neoformans*. *Eukaryotic Cell*, 8, 1543–1553.

Franzblau, S.G., Witzig, R.S., McLaughlin, J.C., Torres, P., Madico, G., Hernandez, A. et al. (1998) Rapid, low-technology MIC determination with clinical *Mycobacterium tuberculosis* isolates by using the microplate Alamar blue assay. *Journal of Clinical Microbiology*, 36, 362–366.

Garcia-Rubio, R., de Oliveira, H.C., Rivera, J. & Trevijano-Contador, N. (2020) The fungal cell wall: *Candida, Cryptococcus*, and *Aspergillus* species. *Frontiers in Microbiology*, 10, 2993.

Gillum, A.M., Tsay, E.Y. & Kirsch, D.R. (1984) Isolation of the *Candida albicans* gene for orotidine-5′-phosphate decarboxylase by complementation of *S. cerevisiae* ura3 and *E. coli* pyrF mutations. *Molecular & General Genetics*, 198, 179–182.

Gow, N.A.R., Latge, J.P. & Munro, C.A. (2017) The fungal cell wall: structure, biosynthesis, and function. *Microbiology Spectrum*, 5, 1-25.

Goyal, S., Castrillon-Betancur, J.C., Klaile, E. & Slevogt, H. (2018) The interaction of human pathogenic fungi with C-type lectin receptors. *Frontiers in Immunology*, 9, 1261–1285.

Hole, C.R., Leopold Wager, C.M., Mendiola, A.S., Wozniak, K.L., Campuzano, A., Lin, X. et al. (2016) Antifungal activity of plasmacytoid dendritic cells against *Cryptococcus neoformans* In vitro requires expression of Dectin-3 (CLEC4D) and reactive oxygen species. *Infection and Immunity*, 84, 2493–2504.

Huang, H.R., Li, F., Han, H., Xu, X., Li, N., Wang, S. et al. (2018) Dectin-3 recognizes glucuronoxylomannan of *Cryptococcus neoformans* serotype AD and *Cryptococcus gattii* serotype B to initiate host defense against cryptococcosis. *Frontiers in Immunology*, 9, 1781.

Ibrahim, A.S., Spellberg, B., Avanessian, V., Fu, Y. & Edwards, J.E., Jr. (2005) *Rhizopus oryzae* adheres to, is phagocytosed by, and damages endothelial cells in vitro. *Infection and Immunity*, 73, 778–783.

Kitai, Y., Sato, K., Tanno, D., Yuan, X., Umeki, A., Kasamatsu, J. et al. (2021) Role of Dectin-2 in the phagocytosis of *Cryptococcus neoformans* by dendritic cells. *Infection and Immunity*, 89, e0033021.

Kottom, T.J., Hebrink, D.M., Monteiro, J.T., Lepenies, B., Carmona, E.M., Wuethrich, M. et al. (2019) Myeloid C-type lectin receptors that recognize fungal mannans interact with *Pneumocystis* organisms and major surface glycoprotein. *Journal of Medical Microbiology*, 68, 1649–1654.

Kuramae, E.E., Robert, V., Snel, B., Weiss, M. & Boekhout, T. (2006) Phylogenomics reveal a robust fungal tree of life. *FEMS Yeast Research*, 6, 1213–1220.

LaMastro, V., Campbell, K.M., Gonzalez, P., Meng-Saccoccio, T. & Shukla, A. (2023) Antifungal liposomes: lipid saturation and cholesterol concentration impact interaction with fungal and mammalian cells. *Journal of Biomedical Materials Research. Part A*, 111, 644–659.

Lecointe, K., Cornu, M., Leroy, J., Coulon, P. & Sendid, B. (2019) Polysaccharides cell wall architecture of Mucorales. *Frontiers in Microbiology*, 10, 469.

Low, C.Y. & Rotstein, C. (2011) Emerging fungal infections in immunocompromised patients. *F1000 Medicine Reports*, 3, 14.

Mann, H. & Whitney, D. (1947) On a test of whether one of two random variables is stochastically larger than the other. *The Annals of Mathematical Statistics*, 18, 50–60.

Marr, K.A., Balajee, S.A., McLaughlin, L., Tabouret, M., Bentsen, C. & Walsh, T.J. (2004) Detection of galactomannan antigenemia by enzyme immunoassay for the diagnosis of invasive aspergillosis: variables that affect performance. *The Journal of Infectious Diseases*, 190, 641–649.

Martinez, L.R. & Casadevall, A. (2007) *Cryptococcus neoformans* biofilm formation depends on surface support and carbon source and reduces fungal cell susceptibility to heat, cold, and UV light. *Applied and Environmental Microbiology*, 73, 4592–4601.

Meagher, R., Lewis, Z., Ambati, S. & Lin, X. (2021) Aiming for a bull's-eye: targeting antifungals to fungi with dectin-decorated liposomes. *PLoS Pathogens*, 17, 1–7.

Meagher, R., Lewis, Z., Ambati, S. & Lin, X. (2023) DectiSomes: C-type lectin receptor-targeted liposomes as Pan-antifungal drugs. *Advanced Drug Delivery Reviews*, 196, 1–20.

Montone, K.T. (2009) Regulating the T-cell immune response toward the H99 strain of *Cryptococcus neoformans*. *The American Journal of Pathology*, 175, 2255–2256.

Mori, D., Shibata, K. & Yamasaki, S. (2017) C-type lectin receptor Dectin-2 binds to an endogenous protein beta-glucuronidase on dendritic cells. *PLoS One*, 12, e0169562.

Planck, M. (1917) Über einen Satz der statistischen Dynamik und seine Erweiterung in der Quantentheorie. *Sitzungsberichte der Preussischen Akademie der Wissenschaften zu Berlin*, 24, 324–341.

Preite, N.W., Feriotti, C., Souza de Lima, D., da Silva, B.B., Condino-Neto, A., Pontillo, A. et al. (2018) The Syk-Coupled C-type lectin receptors Dectin-2 and Dectin-3 are involved in *Paracoccidioides brasiliensis* recognition by human plasmacytoid dendritic cells. *Frontiers in Immunology*, 9, 464.

Saijo, S. & Iwakura, Y. (2011) Dectin-1 and Dectin-2 in innate immunity against fungi. *International Immunology*, 23, 467–472.

Schiavone, M., Vax, A., Formosa, C., Martin-Yken, H., Dague, E. & Francois, J.M. (2014) A combined chemical and enzymatic method to determine quantitatively the polysaccharide components in the cell wall of yeasts. *FEMS Yeast Research*, 14, 933–947.

Spatafora, J.W., Aime, M.C., Grigoriev, I.V., Martin, F., Stajich, J.E. & Blackwell, M. (2017) The fungal tree of life: from molecular systematics to genome-scale phylogenies. *Microbiology Spectrum*, 5, 1-32.

Sun, H., Xu, X.Y., Shao, H.T., Su, X., Wu, X.D., Wang, Q. et al. (2013) Dectin-2 is predominately macrophage restricted and exhibits conspicuous expression during *Aspergillus fumigatus* invasion in human lung. *Cellular Immunology*, 284, 60–67.

Taylor, J.W. & Berbee, M.L. (2006) Dating divergences in the fungal tree of life: review and new analyses. *Mycologia*, 98, 838–849.

U.S. Food and Drug Administration. (1997) *Ambisome (amphotericin B)*. Silver Spring, MD: U.S. Food and Drug Administration, 050740.

Varshney, A., Scott, L.J., Welch, R.P., Erdos, M.R., Chines, P.S., Narisu, N. et al. (2017) Genetic regulatory signatures underlying islet gene expression and type 2 diabetes. *Proceedings of the National Academy of Sciences of the United States of America*, 114, 2301–2306.

Walker, L., Sood, P., Lenardon, M.D., Milne, G., Olson, J., Jensen, G. et al. (2018) The viscoelastic properties of the fungal cell wall allow traffic of AmBisome as intact liposome vesicles. *mBio*, 9, 1–15.

Wang, T., Pan, D., Zhou, Z., You, Y., Jiang, C., Zhao, X. et al. (2016) Dectin-3 deficiency promotes colitis development due to impaired antifungal innate immune responses in the gut. *PLoS Pathogens*, 12, e1005662.

Wilson, G.J., Marakalala, M.J., Hoving, J.C., van Laarhoven, A., Drummond, R.A., Kerscher, B. et al. (2015) The C-type lectin receptor CLECSF8/CLEC4D is a key component of anti-mycobacterial immunity. *Cell Host & Microbe*, 17, 252–259.

Yoshikawa, M., Yamada, S., Sugamata, M., Kanauchi, O. & Morita, Y. (2021) Dectin-2 mediates phagocytosis of *Lactobacillus paracasei* KW3110 and IL-10 production by macrophages. *Scientific Reports*, 11, 17737.

Zhu, L.L., Zhao, X.Q., Jiang, C., You, Y., Chen, X.P., Jiang, Y.Y. et al. (2013) C-type lectin receptors Dectin-3 and Dectin-2 form a heterodimeric pattern-recognition receptor for host defense against fungal infection. *Immunity*, 39, 324–334.

Figures

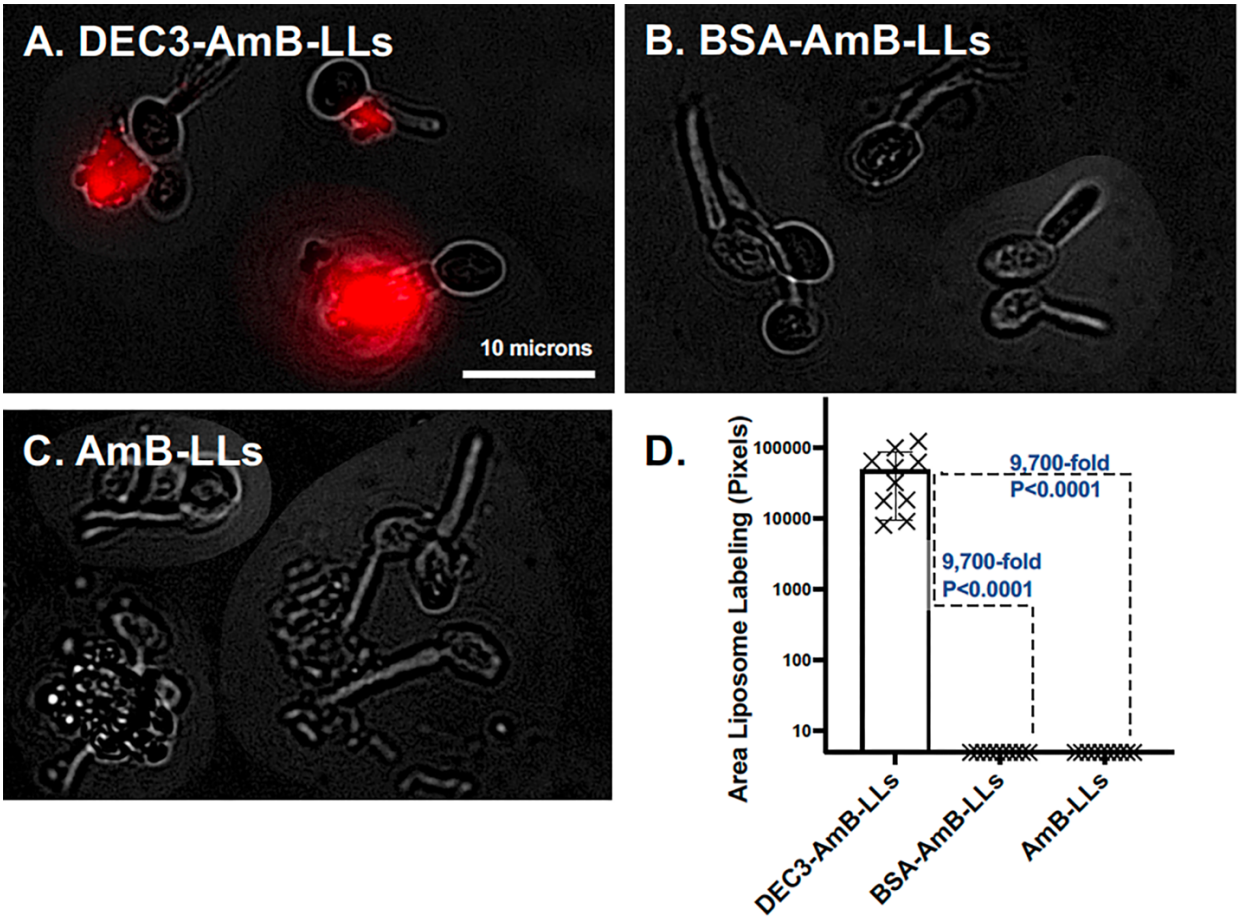

Figure 3.1. DEC3-AmB-LLs bound efficiently to *Candida albicans* during the yeast–hyphal transition stage of development. (**a–c**) respectively, show representative photographic images of red fluorescent DEC3-AmB-LLs, BSA-AmB-LLs, and AmB-LLs binding to *C. albicans* in the yeast–hyphal transition stage. After plating in media that stimulated hyphal development, yeast cells were grown for 1.5 h to reach this stage. The scale bar corresponds to 10 μm. Images were acquired at 60× magnification and equivalently cropped to enlarge cells for presentation. Composite images were prepared because the cells were widely dispersed in each 60× field. (**d**) The relative area of red fluorescent liposome binding ($\log_{10}$) was quantified using AreaPipe and is shown in scatter bar plots. $N = 10$ for each bar. Standard errors from the mean and p values are indicated.

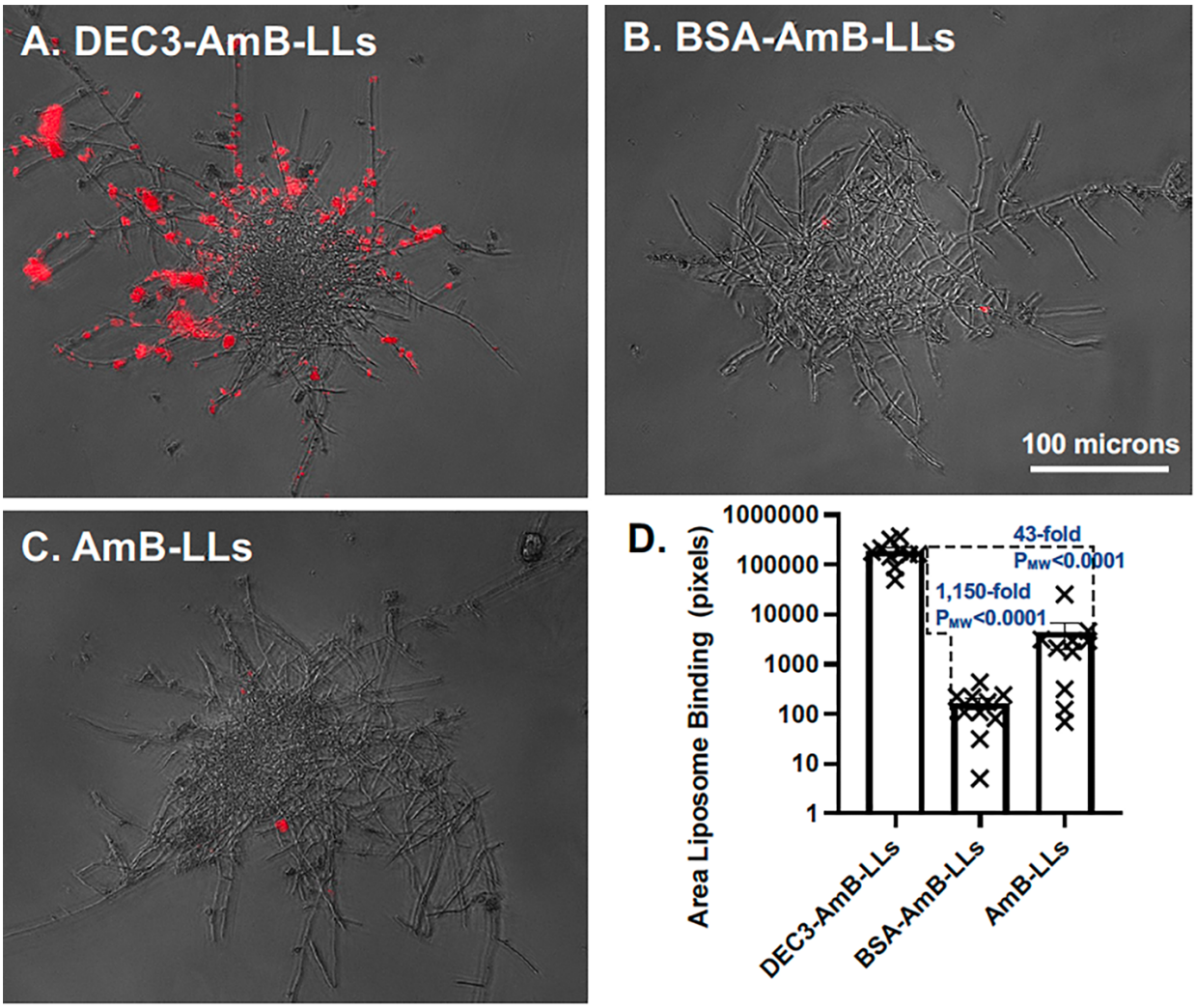

Figure 3.2. DEC3-AmB-LLs bound efficiently to *Candida albicans* hyphae. (**a–c**) respectively, show representative photographic images of red fluorescent DEC3-AmB-LLs, BSA-AmB-LLs, and AmB-LLs binding to 15-hr-old hyphal colonies. The scale bar indicates the size of the hyphae photographed at 20× magnification. (**d**) The relative area of red fluorescent liposome binding (log_{10}) was quantified using AreaPipe and is shown in a scatter bar plot. $N = 10$ for each bar. Standard errors from the mean and P_{MW} values are indicated.

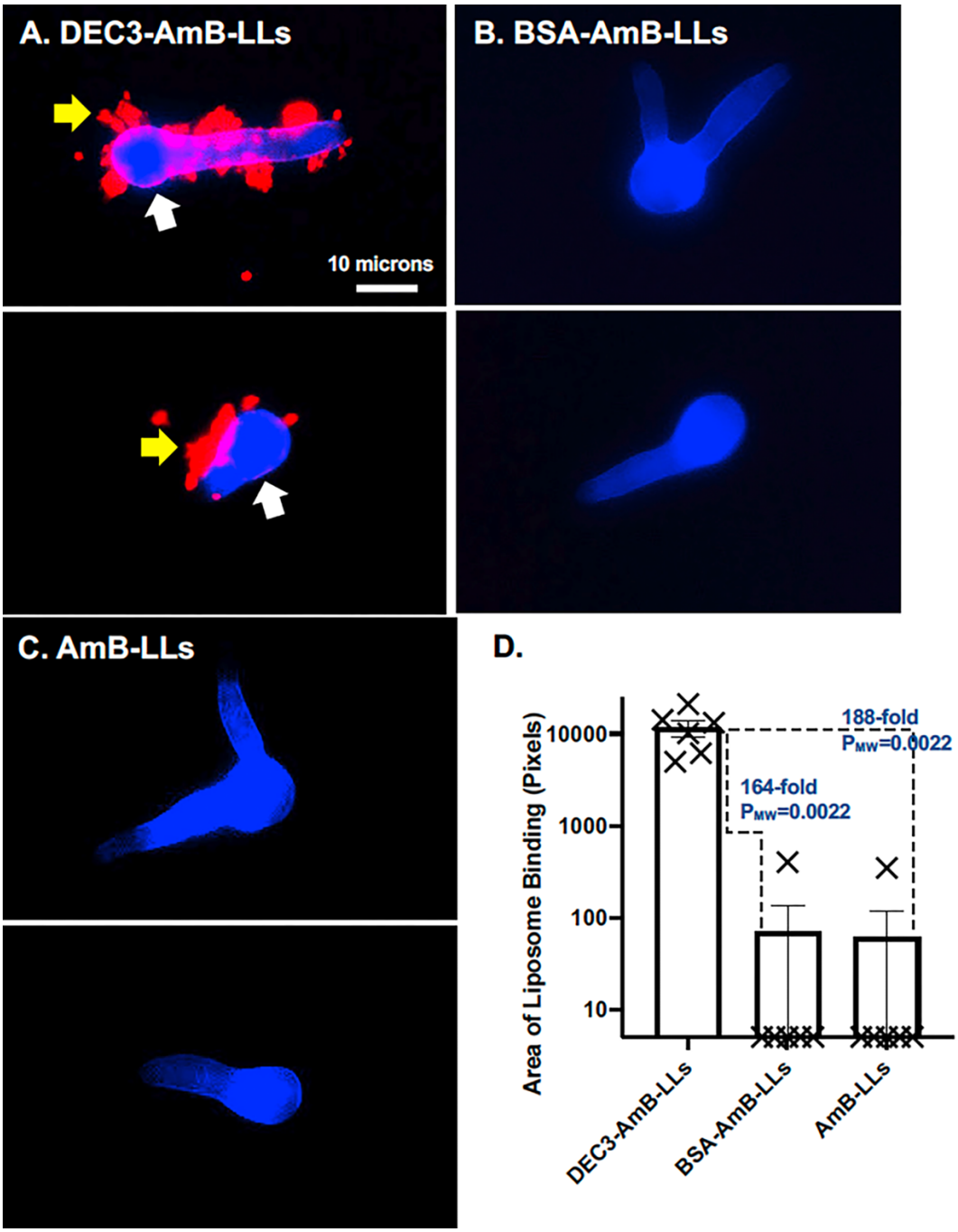

Figure 3.3. DEC3-AmB-LLs bound efficiently to *Rhizopus delemar* germlings. (**a–c**), respectively, show representative photographic images of red fluorescent DEC3-AmB-LLs, BSA-AmB-LLs, and AmB-LLs binding to CW-stained germinating sporangiospores and germling germ tubes. Sporangiospores were germinated on an agar surface for 6 h. The scale bar indicates the size of the germlings photographed at 20× magnification. The images were cropped to show enlarged germlings. (**d**) The relative area of red fluorescent liposome binding (log_{10}) was quantified using AreaPipe and is shown in a scatter bar plot. $N = 6$ for each bar. Standard errors from the mean and P_{MW} values are indicated.

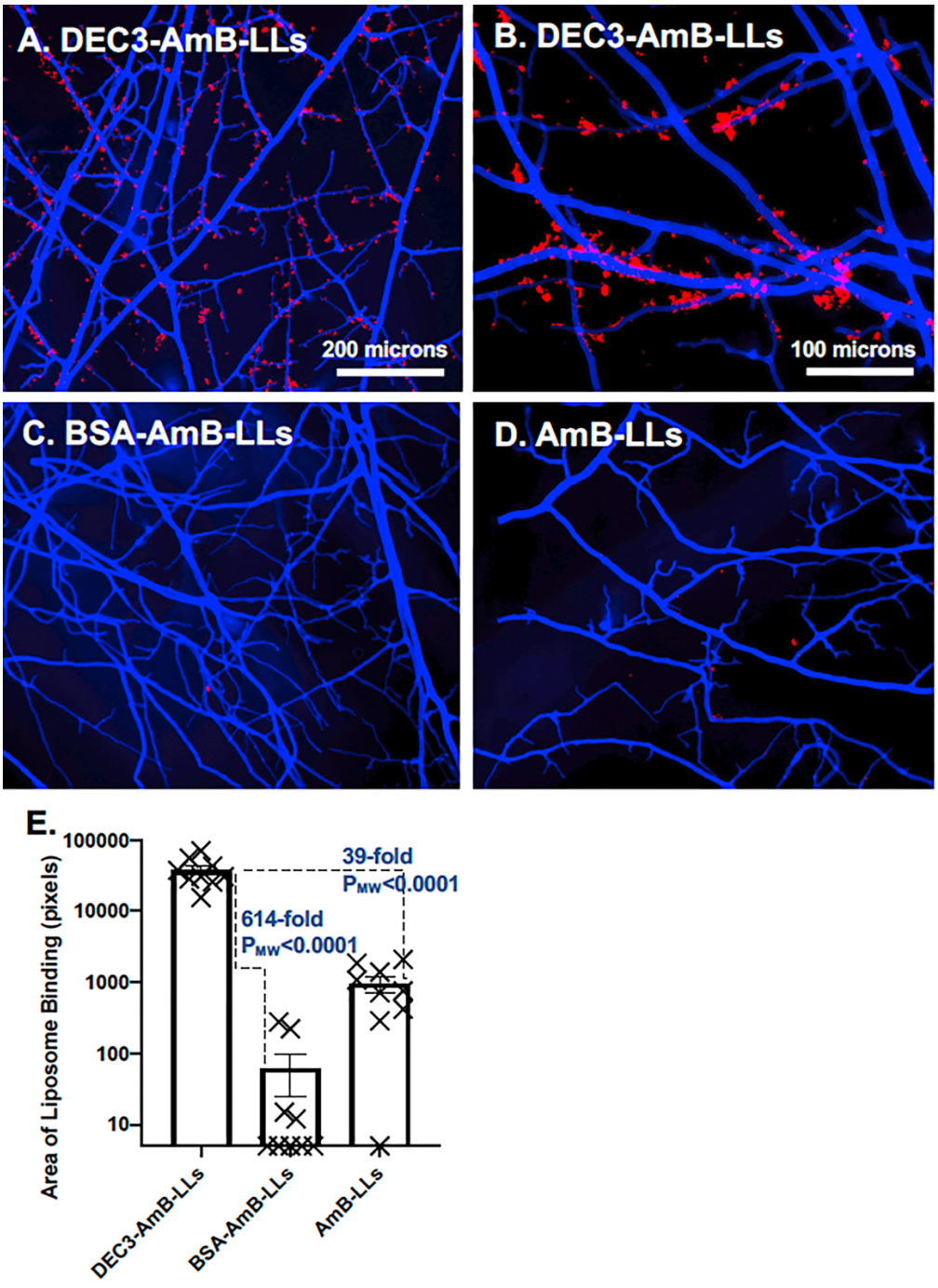

Figure 3.4. DEC3-AmB-LLs bound efficiently to fixed *Rhizopus delemar* hyphae. (**a–d**) respectively, show representative photographic images of red fluorescent DEC3-AmB-LLs, BSA-AmB-LLs, and AmB-LLs binding to CW-stained 15-hr-old hyphae grown on an agar surface photographed at 10×, and (**b**) shows DEC3-AmB-LLs photographed at 20× magnification. The scale bars indicate the size of the hyphae photographed at 10× (**a**, **c, and d**) or 20× magnification (**b**). (**d**) The relative area of red fluorescent liposome binding at 10X ($\log_{10}$) was quantified using AreaPipe and is shown in a scatter bar plot. $N = 9$ for each bar. Standard errors from the mean and P_{MW} values are indicated.

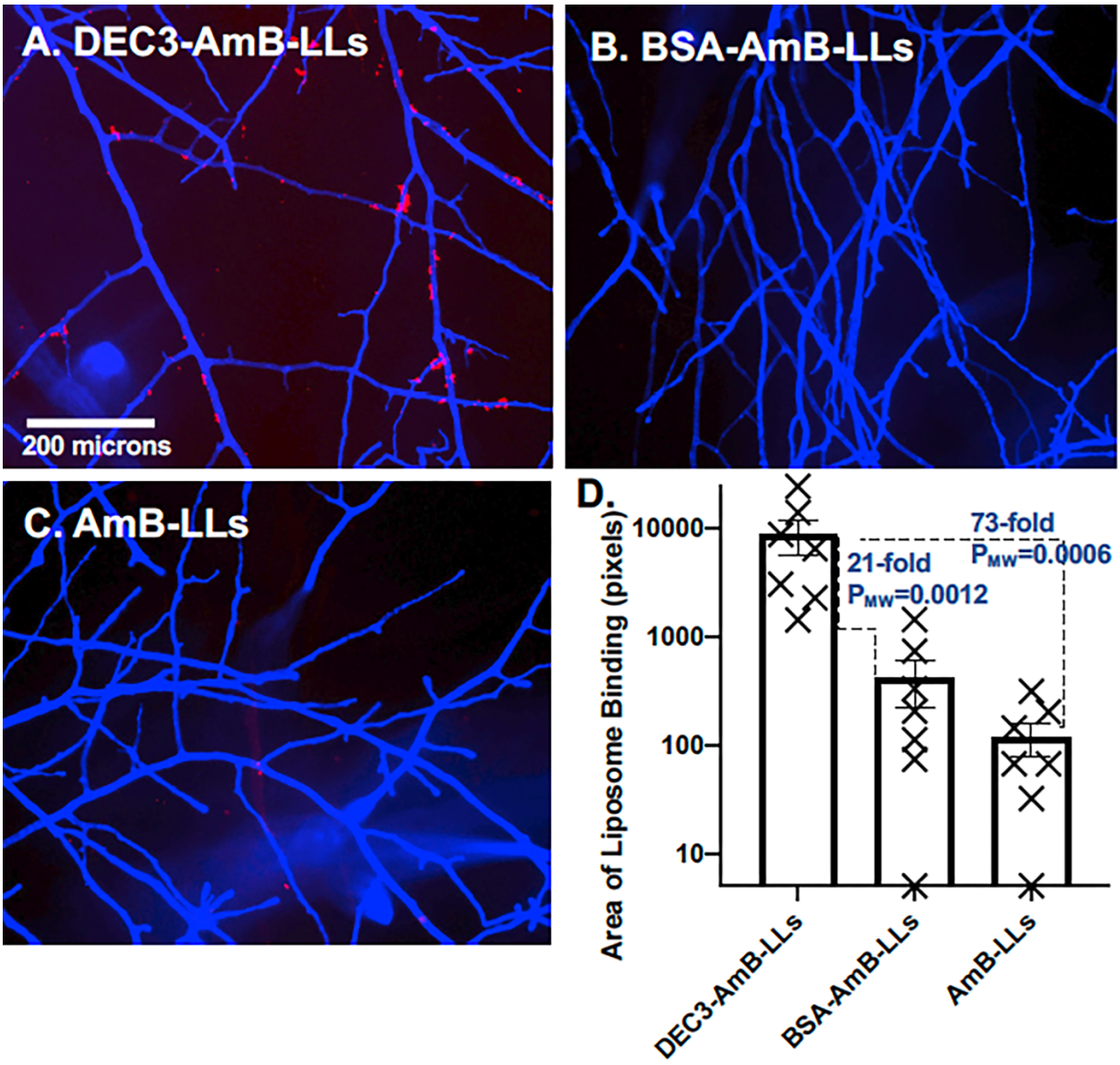

Figure 3.5. DEC3-AmB-LLs bound efficiently to live *Rhizopus delemar* hyphae. (**a–c**) respectively, show representative photographic images of red fluorescent DEC3-AmB-LLs, BSA-AmB-LLs, and AmB-LLs binding to live CW-stained hyphae. The scale bar indicates the size of the hyphae, which were photographed at 10× magnification. (**d**) The relative area of red fluorescent liposome binding ($\log_{10}$) was quantified using AreaPipe and is shown in a scatter bar plot. $N = 7$ for each bar. Standard errors from the mean and P_{MW} values are indicated.

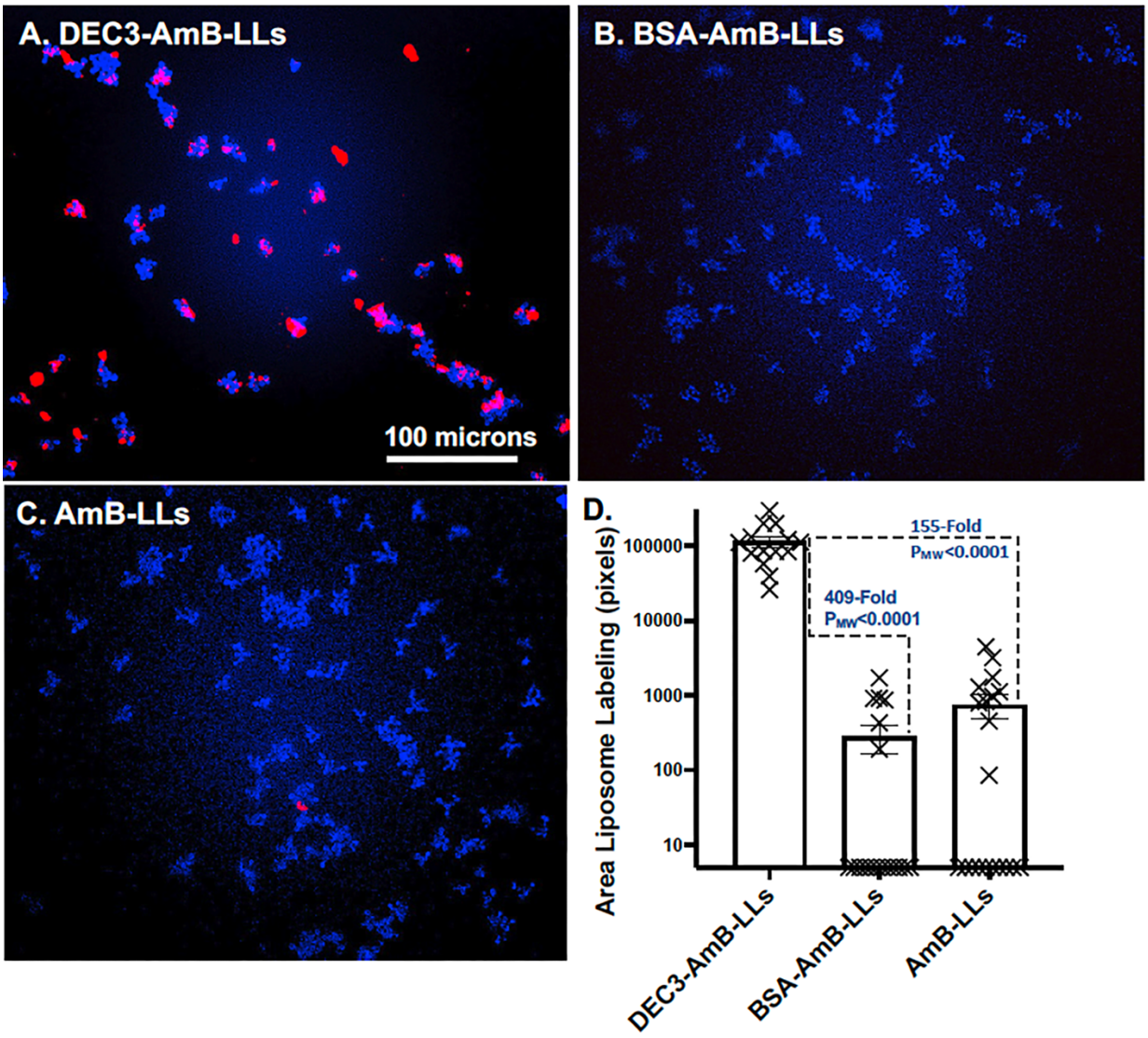

Figure 3.6. DEC3-AmB-LLs bound efficiently to the EPS matrices of small *Cryptococcus neoformans* colonies. (**a–c**) respectively, show representative photographic images of red fluorescent DEC3-AmB-LLs, BSA-AmB-LLs, and AmB-LLs binding to CW-stained 6-hr-old colonies of *C. neoformans* grown on an agar surface. The scale bar indicates the size of the colonies photographed at 20× magnification. (**d**) The relative area of red fluorescent liposome binding ($\log_{10}$) was quantified using AreaPipe and is shown in a scatter bar plot. $N = 14$ for each bar. Standard errors from the mean and P_{MW} values are indicated.

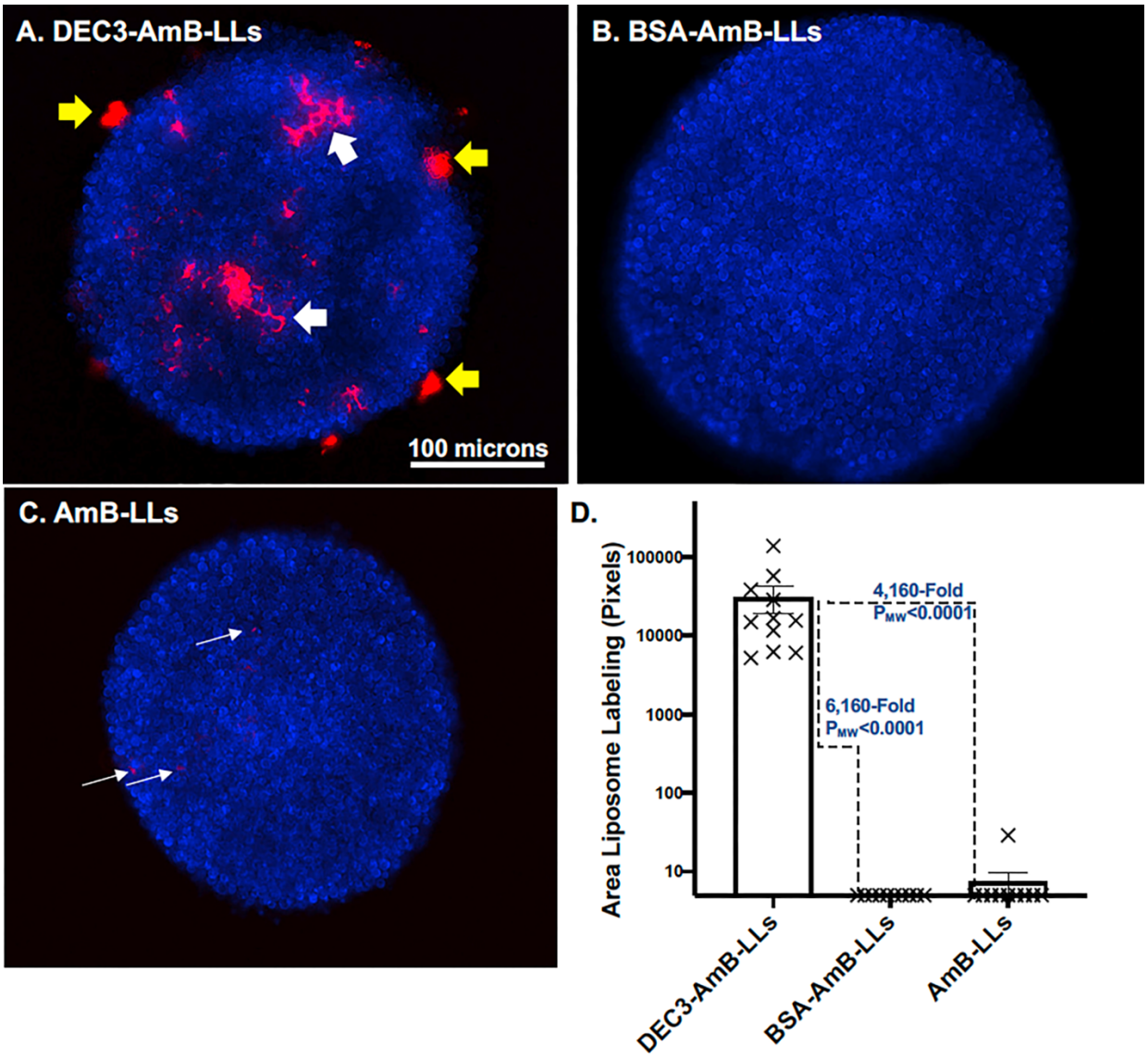

Figure 3.7. DEC3-AmB-LLs bound efficiently to large *Cryptococcus neoformans* colonies. (**a–c**) respectively, show representative photographic images of red fluorescent DEC3-AmB-LLs, BSA-AmB-LLs, and AmB-LLs binding to CW-stained 18-hr-old colonies of *C. neoformans* grown on an agar surface. Yellow arrows indicate DEC3-AmB-LL binding to EPS deposits, and large white arrows indicate binding that surrounds spherical yeast cells within the colonies. The scale bar indicates the size of the colonies photographed at 20× magnification. The uncommon red fluorescence of control liposome binding (white thin arrows in **c**) had to be greatly enhanced relative to that for DEC3-AmB-LLs to make it visible for presentation. (**d**) The relative area of red fluorescent liposome binding ($\log_{10}$) was quantified using AreaPipe and is shown in a scatter bar plot. $N = 11$ for each bar. Standard errors from the mean and P_{MW} values are indicated.

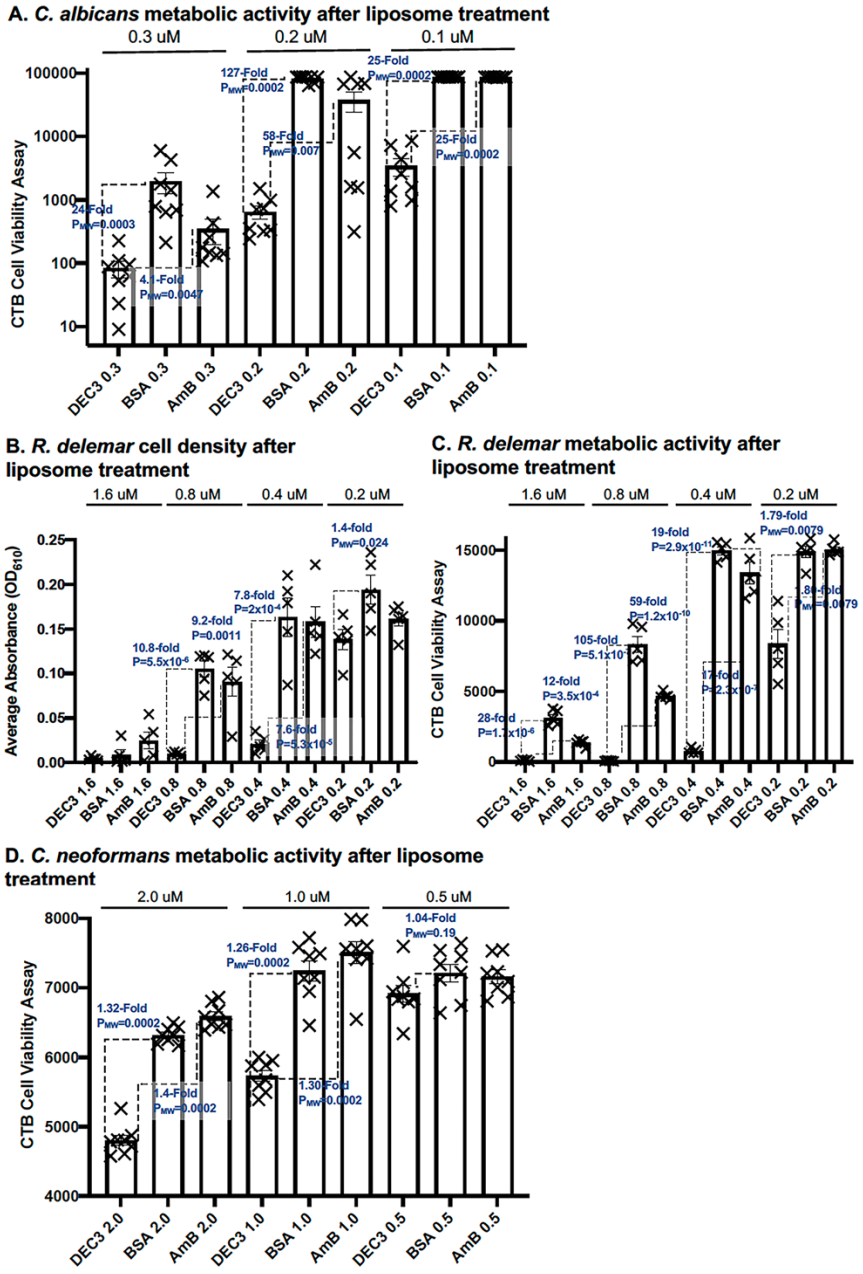

Figure 3.8. DEC3-AmB-LLs were efficient at inhibiting and/or killing two of the three fungal pathogens examined. *Candida albicans*, *Rhizopus delemar*, and *Cryptococcus neoformans* were grown in 96-well microtiter plates and treated with DEC3-AmB-LLs, AmB-LLs, and BSA-AmB-LLs, delivering the indicated micromolar concentrations of AmB. Growth inhibition and/or killing were assayed as reductions in cell density measured at A_{610} or reductions in viable cell metabolic activity by measuring the electrochemical reduction of the redox dye resazurin in CellTiter-Blue reagent to fluorescent resorufin after liposome treatment. (**a**) Residual metabolic activity of *C. albicans*. (**b**) Cell density of *R. delemar*. (**c**) Residual metabolic activity of *R. delemar*. (**d**) Residual metabolic activity of *C. neoformans*. Cell density and metabolic activity are shown in scatter bar plots. $N = 5$ to 8 for each bar. Standard errors from the mean and p or P_{MW} values are indicated.

SF1A. Native mouse Dectin-3
>NP_034949.3 Mouse (*Mus musculus*)C-type lectin domain family 4 member D isoform 1. Full length mouse Dectin-3. 219 a.a. residues. 25,619.07 kDa. Very hydrophobic (Tyr 4 residues, Trp 11, Phe 15, Val 19, Leu 14, Ile 7). With Cys reduced 2.594 O.D. or oxidized 2.6 O.D./mg/mL A280. Aliphatic index 65.3, Hydropathicity GRAVE= -0.361. Instability index 37.6. Yellow highlighted amino acid residues 1 to 43 encode the N-terminal signaling and transmembrane domains that were omitted in our construct. Green highlighted amino acid residues 44 to 219 encode stalk domain and C-terminal carbohydrate recognition domain (CRD) included in our construct called DEC3.

MWLEESQMKSKGTRHPQLIPCVFAVVSISFLSACFISTCLVTHYFLRWTRGSVVKLSDYHTRVTCIREE
PQPGATGGTWTCCPVSWRAFQSNCYFPLNDNQTWHESERNCSGMSSHLVTINTEAEQNFVTQLLDKRFSY
FLGLADENVEGQWQWVDKTPFNPHTVFWEKGESNDFMEEDCVVLVHVHEKWVWNDFPCHFEVRRICKLPG
ITFNWKPSK

SF1B. *HK-DEC3 (a.k.a. DEC3)* His-Lys-modified murine Dectin-3 coding sequence. DNA sequence encoding the truncated version of mouse DEC3 with codons optimized for expression in *E. coli* that was synthesized by GenScript for subcloning into the expression vector pET-45b+. The following sequence was ordered from GenScript. The synthetic sequences (AAA, AAG) encoding the lysine residues for coupling to NHS-Rhodamine or NHS-PEG-DHPE and the synthetic sequences(**GGT TCA GGG TCT GGC**) encoding the gly,ser,gly,ser,gly flexible spacer are highlighted in yellow. The *E. coli* codon-optimized DNA sequence for the mouse Dectin-3 stalk and CRD regions are highlighted in green. GenScript trimmed off the flanking underlined *Kpn*I (GGTACC) and *Pac*I (TTAATTAA)(subcloning sites bold black font) shown here from the order because they are part of the vector pE45b+ into which GenScript subcloned the sequence. The reading frame is indicated at the beginning and end of the sequence by separating some individual codons. An alanine codon GCT was added at the C-terminal end to accommodate an in-frame *Pac*I sequence.

ATG GCA CAT CAC CAC CAC CAT CAC GTG GGT ACC
GGA AGT GGA *AAA* GGC *AAG* GGT TCA GGG TCT GGC
CACTATTTCCTCCGCTGGACGAGAGGCTCTGTGGTGAAGCTTTCAGACTACCACACAAGA
GTTACCTGCATAAGGGAAGAGCCTCAGCCCGGTGCCACTGGTGGCACCTGGACATGCTGT
CCTGTCTCCTGGCGGGCCTTTCAGAGCAATTGCTACTTTCCTCTCAATGACAACCAGACG
TGGCATGAATCAGAAAGGAACTGTAGTGGGATGTCTAGCCACCTGGTCACCATCAACACA

GAGGCTGAGCAGAACTTTGTGACTCAACTGCTGGATAAACGTTTCTCCTATTTTCTAGGC
TTGGCAGATGAAAATGTGGAGGGGCAATGGCAGTGGGTAGATAAGACACCGTTTAATCCA
CATACTGTCTTCTGGGAGAAAGGAGAAAGTAACGATTTCATGGAGGAGGACTGTGTGGTT
TTAGTTCACGTGCATGAGAAGTGGGTGTGGAATGACTTCCCCTGTCACTTTGAAGTACGG
CGAATTTGCAAGCTGCCAGGAATCACCTTCAACTGGAAGCCAAGCAAAGC**T TAA TTA A**

SF1C. The modified MmsDectin-3 (HK-DEC3, DEC3) protein made from pET-45B+ in *E. coli* has the following sequence. The his tag, lysine residues, and gly,ser flexible spacer are shown in yellow. The mouse Dectin-3 CRD and stalk regions are shown in green. 199 a.a. residues. Mol Wgt. 23,024. PkI 6.52. Abs A280 2.6 OD/mg/mL. Aliphatic index: 53.77 indicating the protein has a large volume of hydrophobic side chains and is likely to be unstable in aqueous buffers. Grand average of hydropathicity (GRAVY): -0.638 indicating the opposite, that it may be soluble. We expect that the six added recombinant histidine residues dramatically influenced these conflicting values.
MAHHHHHHVGTGSGKGKGSGSGHYFLRWTRGSVVKLSDYHTRVTCIREEPQPGATGGTWTCCPVSWRAFQ
SNCYFPLNDNQTWHESERNCSGMSSHLVTINTEAEQNFVTQLLDKRFSYFLGLADENVEGQWQWVDKTPF
NPHTVFWEKGESNDFMEEDCVVLVHVHEKWVWNDFPCHFEVRRICKLPGITFNWKPSKA*

Supplemental Figure SF3.1. Annotated Dectin-3-related sequences. SF3.1A. The amino acid (a.a.) sequence of the full-length native *Mus musculus* Dectin-3 (MCL, *CLEC4D*, NP_034949.3, 219 a.a.). **SF3.1B.** Annotated DNA sequence of the *E. coli* codon-optimized recombinant truncated DEC3-encoding sequence expressed herein to make DEC3 protein. **SF3.1C.** Annotated a.a. sequence of the recombinant truncated isoform DEC3 polypeptide (199 a.a. residues) expressed in *E. coli* and employed herein in DEC3-AmB-LLs and DEC3-Rhod reagents.

SF2A. SDS PAGE analysis of modified Dectin-3 polypeptide (HK-DEC3)

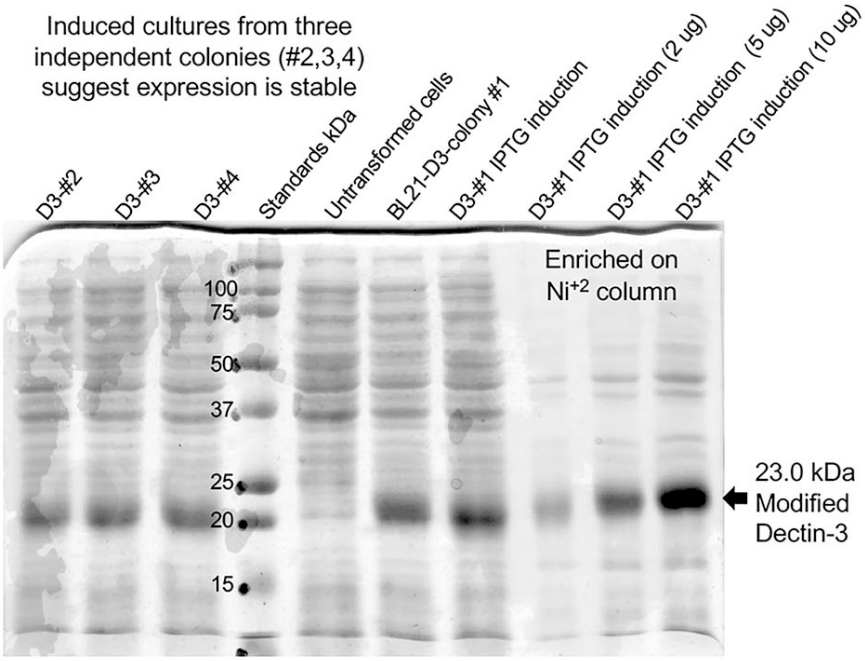

SF2B. Histogram of purified Dectin-3 (HK-DEC3) from SDS-PAGE gel, 5 ug sample from SF2A.

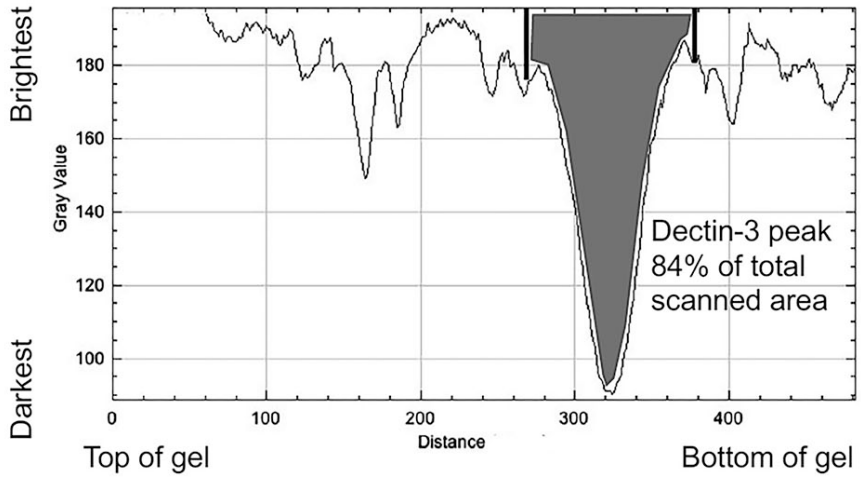

Supplemental Figure SF3.2. SDS-PAGE analysis of the affinity purification of the truncated isoform of Dectin-3 containing its CRD and stalk regions (DEC3). SF3.2A. Sodium dodecyl sulfate polyacrylamide gel electrophoretic analysis of various protein fractions containing recombinant DEC3 and control BL21 cells not expressing DEC3. On the left are crude protein fractions from 3 randomly selected colonies (#2, #3, #4) expressing DEC3 (D3). On the right are protein fractions from colony #1 grown to 1L in Luria broth, and from IPTG-induced cells, and the affinity purified protein from Ni(II) column loaded on the gel at three total protein concentrations (2, 5, 10 ug) to resolve the remaining contaminants. This is a 15% acrylamide gel with 5% bis-acrylamide crosslinker. **SF3.2B.** A density scan of the 5 ug sample estimating the purity of the protein.

SF3A. Comparison of manual to CellProfiler AreaPipe image analysis of red fluorescent DectiSome stained area

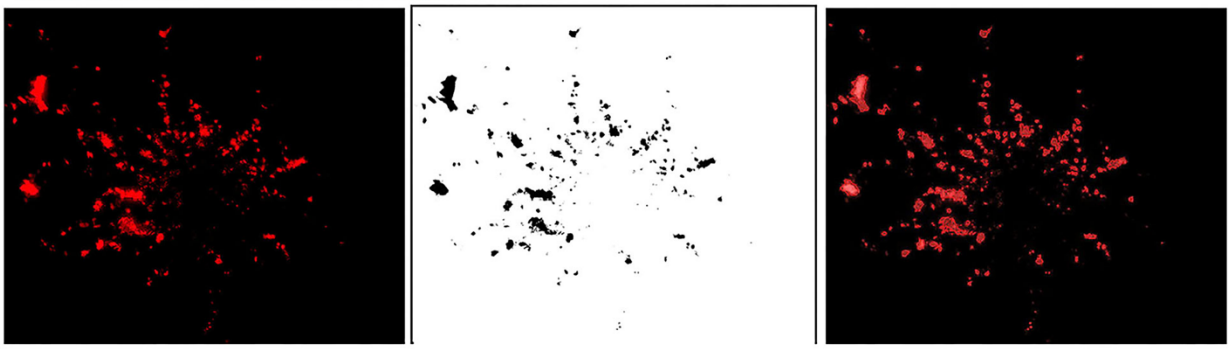

SF3A1. Original red fluorescent TRITC jpg image. The entire image is composed of ~5x10^6 pixels.

SF3A2. Manual capture of fluorescent area in ImageJ. Threshold setting 30/255. Reported as % of pixel area captured.

SF3A3. AreaPipe automated capture of red fluorescent area. Reported as numbers of pixels captured out of ~5x10^6 pixels.

Supplemental Figure SF3.3. AreaPipe automated analysis of fluorescent area data for liposome binding. Examples of the processing of fluorescent images that compare the output of the manual ImageJ to CellProfiler AreaPipe methods of capturing fluorescent area data. **SF3.3A1.** An original red fluorescent jpg image of rhodamine B-tagged DEC3-AmB-LLs binding to a *C. albicans* colony used to estimate the area of red fluorescence. **SF3.3A2.** The fluorescent area captured using manual image processing in ImageJ using a Threshold setting of 30/255. **SF3.3A3.** The output image from the CellProfiler AreaPipe automated analysis of this same image. Close inspection of this image shows that the areas captured by AreaPipe are outlined in red.

SF4A. Replicate of binding to *C. albicans* yeast-hyphal transition stage

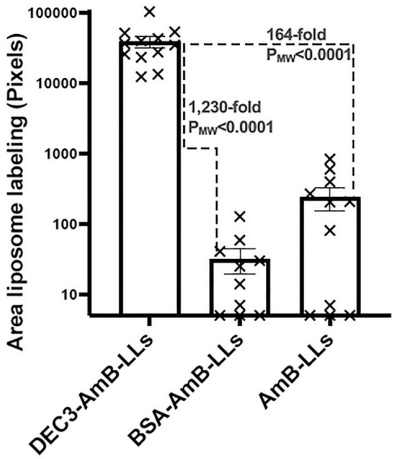

SF4B. Replicate of binding to mature *C. albicans* hyphal colonies

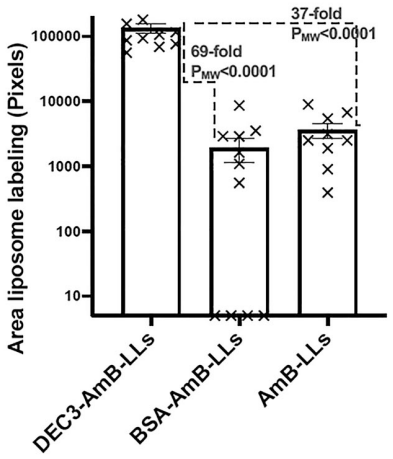

SF4C. Replicate of binding to *R. delemar* germlings

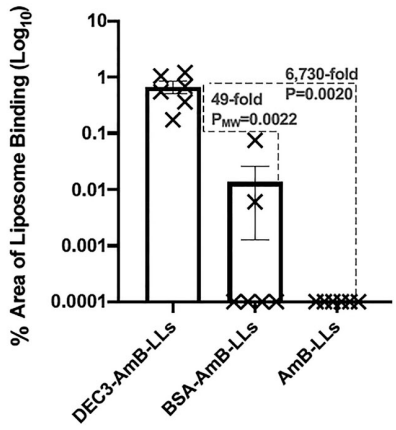

SF4D. Replicate of binding to fixed *R. delemar* hyphae

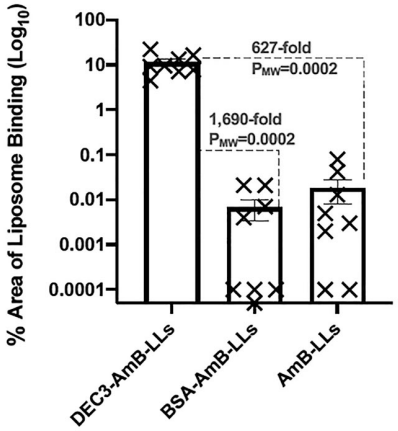

SF4E. Replicate of binding to live *R. delemar* hyphae

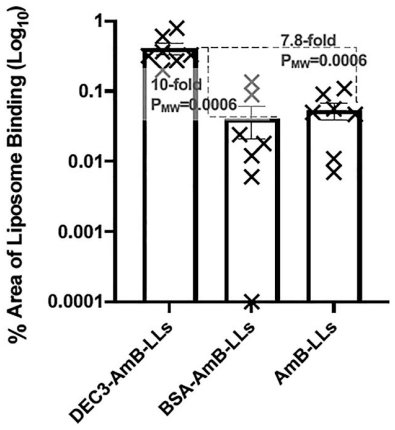

SF4F. Liposome binding to 6-hr old *C. neoformans* colonies

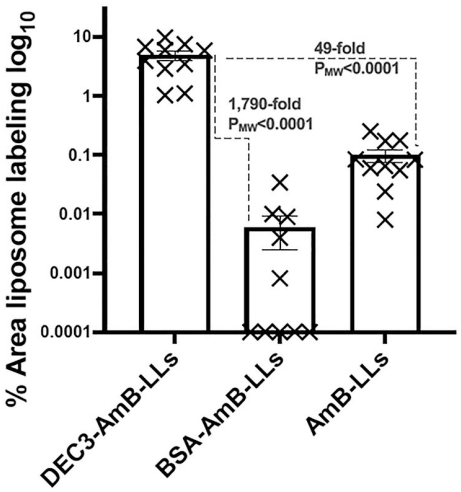

SF4G. Liposome binding to 18-hr old *C. neoformans* colonies

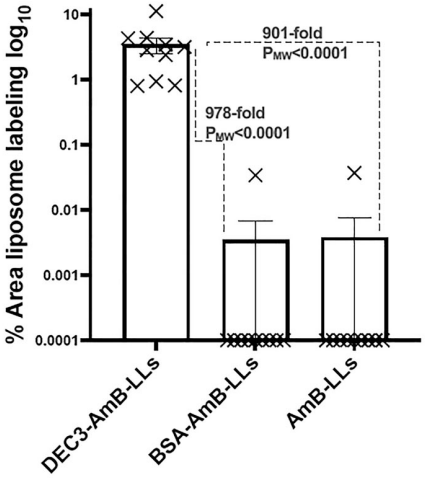

Supplemental Figure SF3.4. Biological replicates of quantitative liposome binding experiments. Liposomes targeted by DEC3, DEC3-AmB-LLs, bound more efficiently to the EPS matrices associated with three fungal pathogens than untargeted control liposomes BSA-AmB-LLs or AmB-LLs. Biological replicates of quantified fluorescent binding data are presented. **A.** *C. albicans* in the early developmental transition from yeast cell to hyphal cell morphology (replicate of experiment shown in **Fig. 3.1**). **B.** Mature *C. albicans* hyphal colonies (replicate of experiment shown in **Fig. 3.2**). We attribute the high background values in this figure to our having included CW during the original liposome staining, which causes some aggregation and precipitation of liposomes, instead of adding it in a separate step as normally done. **C.** *R. delemar* germlings (replicate of experiment shown in **Fig. 3.3**). **D.** *R. delemar* formalin-fixed hyphae (biological replicate of experiment shown in **Fig. 3.4**). **E.** *R. delemar* live hyphae (replicate of experiment shown in **Fig. 3.5**). **F.** *C. neoformans* very early-stage colonies with only a few to a few dozen cells per colony (replicate of experiment shown in **Fig. 3.6**). **G.** *C. neoformans* large colonies that are a few hundred microns in diameter (replicate of experiment shown in **Fig. 3.7**). The relative area of red fluorescent liposome binding data were quantified and are shown in scatter bar plots. N=6 to 12 images for each bar. Standard errors from the mean and P_{MW} or P values are indicated. Areas of liposome binding were quantified in ImageJ using either the manual method that calculated the percent of the pixel area or the CellProfiler AreaPipe automated pipeline that calculated the number of fluorescent pixels.

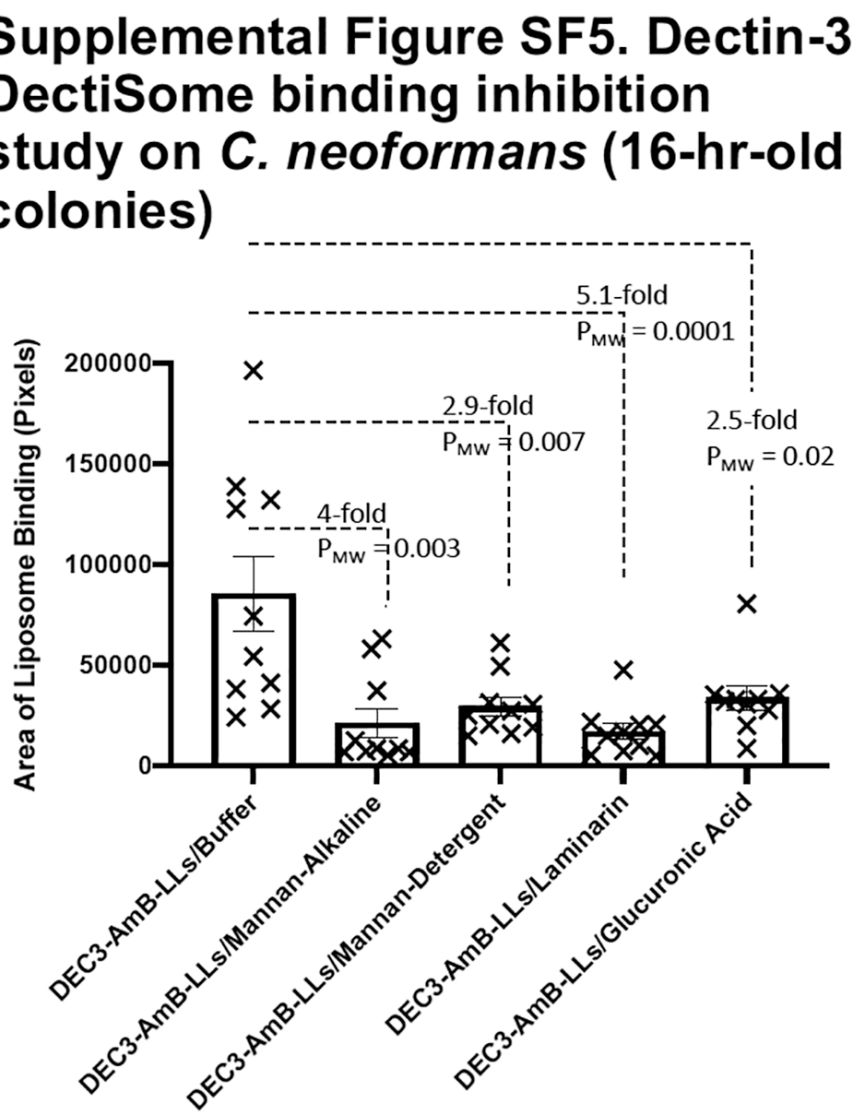

Supplemental Figure SF3.5. Inhibition of DEC3-AmB-LL binding to *C. neoformans* by various glycans. DEC3-AmB-LLs were preincubated in PBS buffer alone or buffer containing the various glycans indicated and then these samples of DEC3-AmB-LLs were incubated with sixteen hr old fixed colonies of *C. neoformans* grown on agar, similar to the treatments shown in **Fig. 3.7**. Colonies were photographed top down at 10X magnification (N=10 images for each treatment). A scatter bar plot compares the area of fluorescent liposome binding for each glycan treatment to the buffer treated control samples. Standard errors from the mean and P_{MW} values are indicated.

Supplemental Fig. SF6. Neither Dectin-3-coated DEC3-AmB-LLs nor control liposomes bound efficiently to the artificially immortalized human line HEK293T

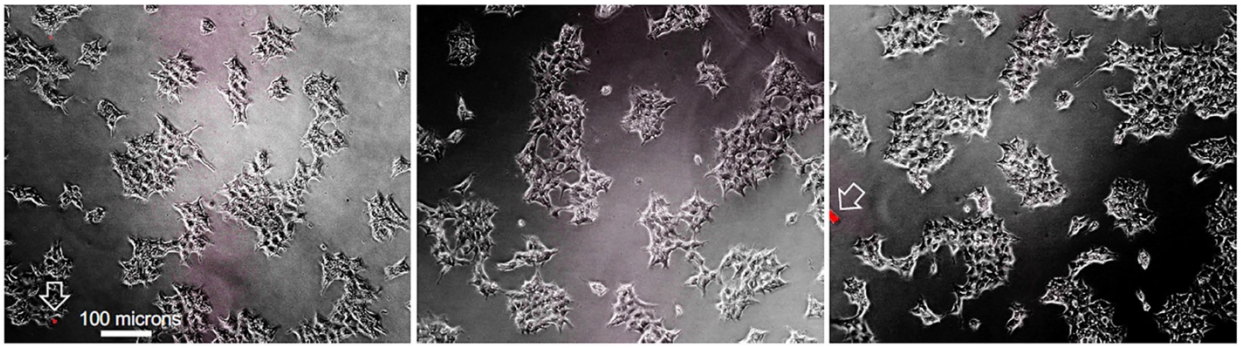

Supplemental Figure SF3.6. Neither DEC3-AmB-LLs, BSA-AmB-LLs, nor AmB-LLs have measurable affinities for human HEK293T cells. Fixed HEK293T cells were incubated with rhodamine labeled liposomes and washed similar to the treatments of fungal cells shown in **Fig. 3.1 through 3.7**. Cells were photographed bottom up at 10X magnification (see scale bar) combining visible and red fluorescent channels. Only an occasional red dot of background binding was observed for any of the three LNPs (see arrows in left-most and right most panels).

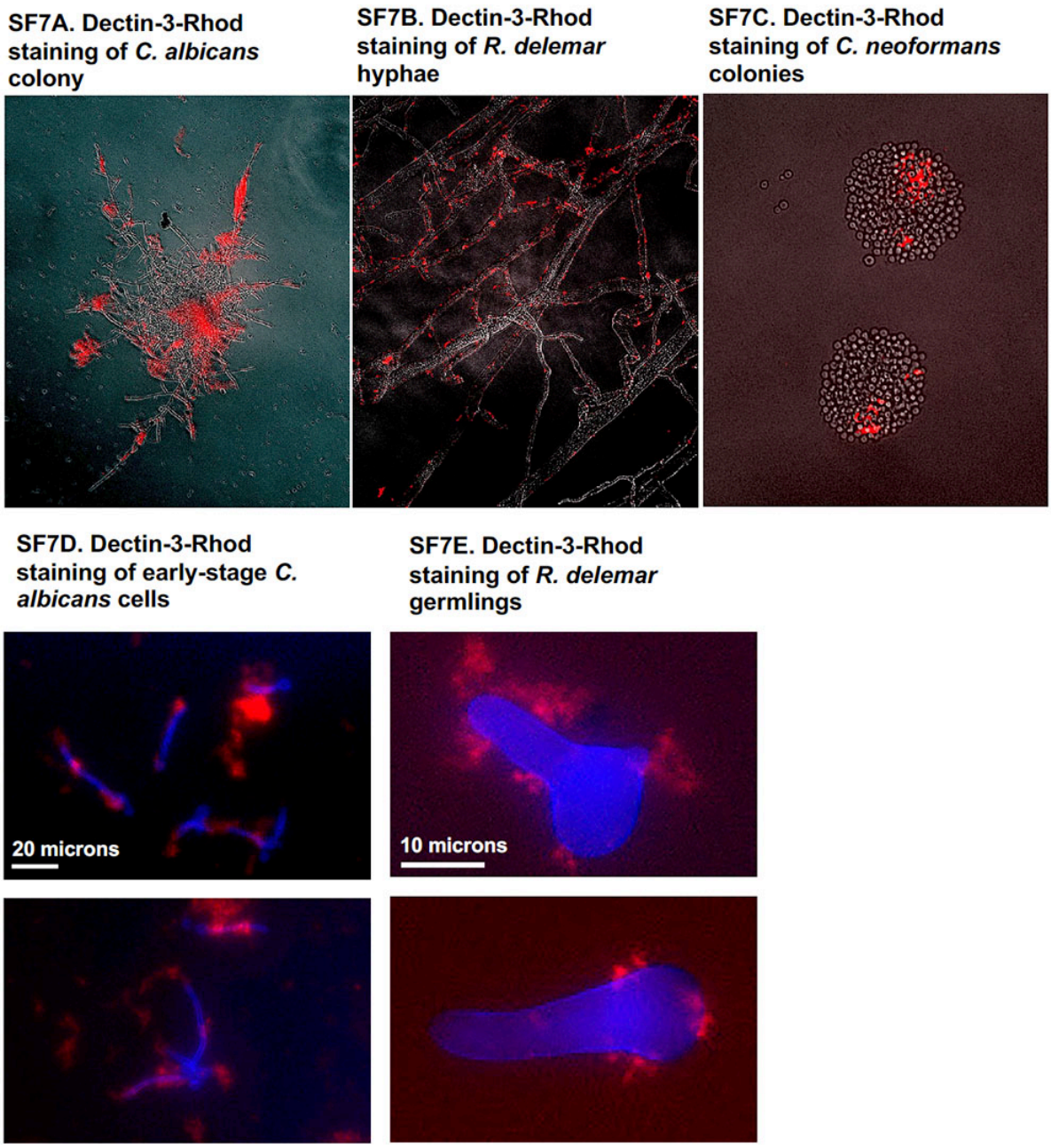

Supplemental Figure SF3.7. *C. albicans, R. delemar,* and *C. neoformans* stained with Dectin-3 protein conjugated to rhodamine B, DEC3-Rhod. Images are of fixed cells stained with DEC3-Rhod protein. **A.** *C. albicans* hyphal colony grown on a polystyrene plate. **B.** *R. delemar* hyphal colony grown on agar. **C.** *C. neoformans* colony grown on agar. **D.** *C. albicans* early-stage cells grown on polystyrene plate. **E.** *R. delemar* germlings grown on agar. Phase contrast images of cells and epi-fluorescence of DEC3-Rhod staining was photographed bottom-up (**A, D**) or top-down (**B, C, E**). These results should be compared to the staining by the liposomal reagent DEC3-AmB-LL shown in **Figs. 3.1 through 3.7**.

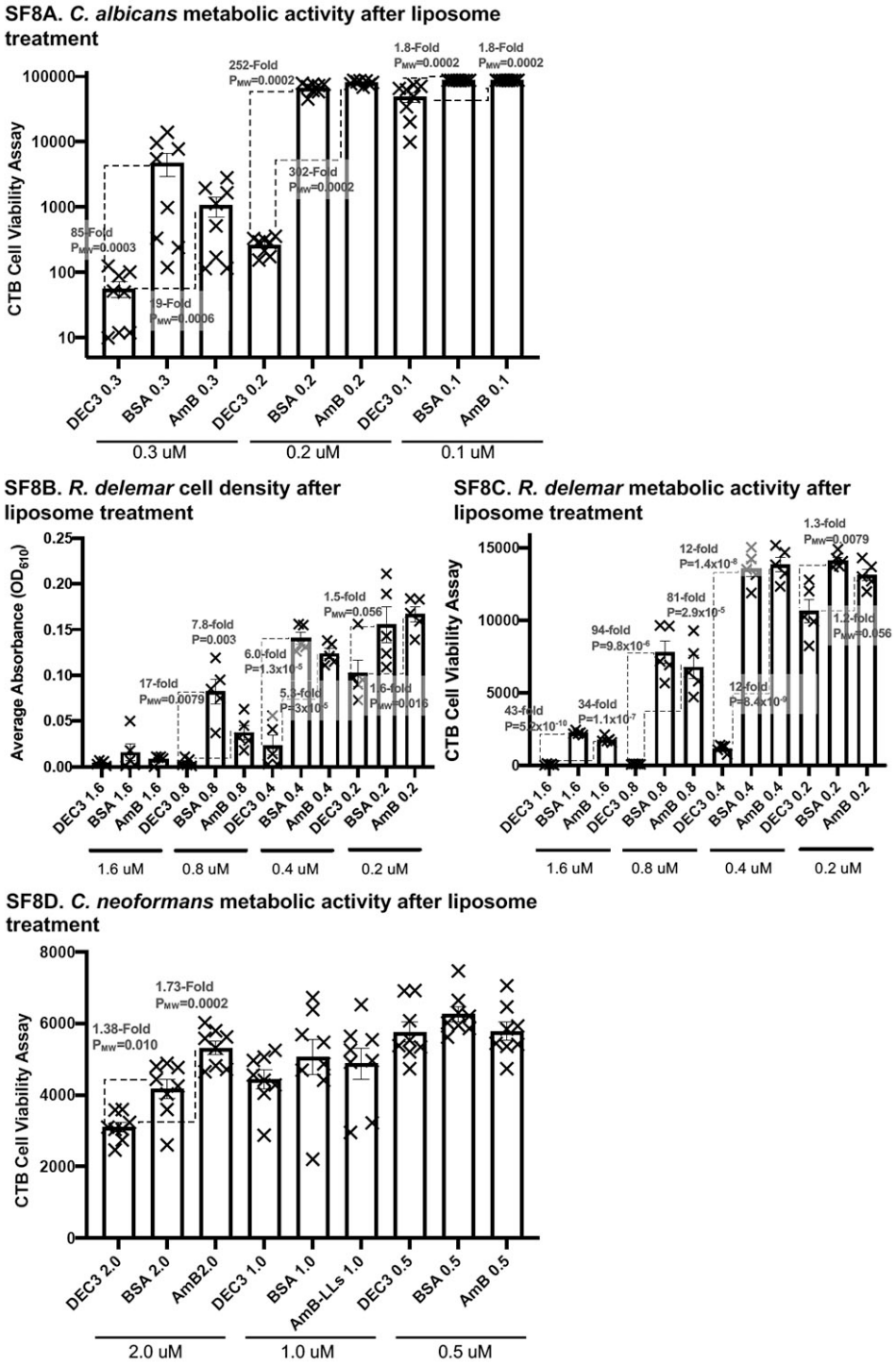

Supplemental Figure SF3.8. Biological replicates of quantitative liposome inhibition and/or killing experiments. *C. albicans*, *R. delemar*, and *C. neoformans* were grown in 96-well microtiter plates and treated with DEC3-AmB-LLs, AmB-LLs, and BSA-AmB-LLs delivering the indicated micromolar concentrations of AmB. **A.** Residual metabolic activity of *C. albicans.* **B.** Cell density of *R. delemar.* **C.** Residual metabolic activity of *R. delemar*. **D.** Residual metabolic activity of *C. neoformans*. Cell density and metabolic activity are shown in scatter bar plots. N=5 to 8 for each bar. Standard errors from the mean and P or P_{MW} values are indicated.

SF9. Reusable glass chambers for cell growth on microscope slides

SF9A. Glass chambers. Left (fire polished side up). Right (ground glass side up).

- 22mm Outer Diameter
- 17mm Inner Diameter
- 2.5mm Wall thickness
- 11mm Tall

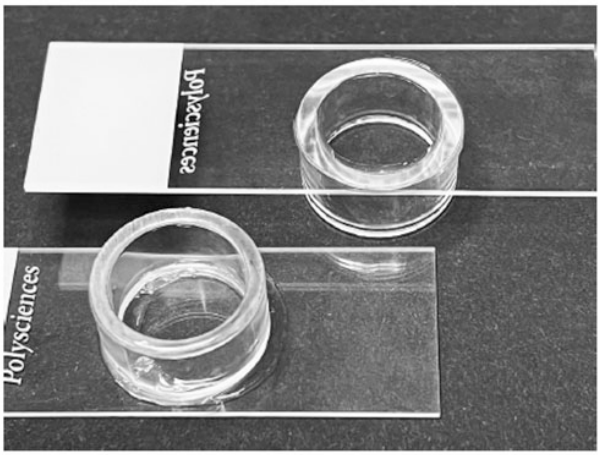

SF9B. Chamber slides. Left (fire polished side up). Right (ground glass side up) shows the continuous silicone greased contact to the slide with no air bubbles. The chamber is removed and replaced with a coverslip for microscopy.

Supplemental Figure SF3.9. Reusable glass chambers for cell growth on glass microscope slides. A. Cylindrical glass chambers 11 mm in height were cut from glass tubing with an outer diameter of 21 mm and inner diameter of 17 mm (i.e., 2 mm thick wall). One side was fire polished smooth (left) and the other side was rough polished (right) on a water-cooled sanding wheel. **B.** Silicone grease was smeared evenly to the rough side. The chamber was applied to a poly-L-lysine-coated microscope slide (Polysciences, Inc. Cat#22247) by pressing down with a clockwise and counterclockwise rotational motion to exclude any air pockets in the grease at the area of contact. The slide was turned over for inspection to ensure that the silicone grease seal did not contain large air pockets. The chamber slides were autoclaved using a dry cycle before use. The cells were grown in 1 mL of media within a chamber and then fixed, stained, and washed. The glass cylinder was removed by rotating it and pulling upwards and replaced with a glass cover slip, pressing down slowly to expel any excess silicone grease and media. The aqueous chamber within the circular ring of silicone grease contained approximately 5 to 8 uL of buffer once the coverslip was applied.

CHAPTER 4

DECTISOMES AS POTENTIAL BIOLOGICAL PROBES

Introduction

The development of affinity chromatography over the last century has greatly expanded both our ability to rapidly and efficiently purify biomolecules and cells and our understanding of molecular interactions within a variety of biological systems. The range of options within this methodology - from small-scale vs. large-scale studies to the types of immobilization ligands and affinity resins - make this a versatile technique for basic and clinical research. The development and diverse applications of this technology have been previously discussed in-depth (Hage and Matsuda, 2015). One example of an affinity chromatography technique is the pull-down assay. Within the context of traditional protein-protein interaction studies, a bait protein is tagged with a known affinity tag, such as a series of histidine residues, and immobilized to a corresponding affinity resin in a column. A solution of interest (perhaps containing a mixture of proteins) is added to the column, and potential partners bind to the immobilized bait protein. The bait protein is then released from the resin, and the newly-bound protein complexes can be further studied.

Given its broad applicability, affinity chromatography can be further divided into subcategories. One example is lectin affinity chromatography (LAC), where non-immune system lectins, such as concanavalin A (ConA) or wheat germ agglutinin (WGA), are used to characterize various glycoproteins (Hage and Matsuda, 2015). Lectins can also be used to differentiate between cell types via cell surface protein interactions (Rodriguez et al., 2020). Common sources for LAC lectins include a variety of plants and vegetable seeds; however,

many of these lectins are cost-prohibitive and have a very narrow range of known ligands (Freeze, 2001).

DectiSomes were designed as a novel antifungal liposomal treatment with a unique specificity for fungal pathogens. The addition of Dectins – C-type lectins that recognize fungal cell wall carbohydrates – to the liposomal surface led to significant increases in binding activity against several fungi compared to untargeted liposomes (Ambati et al., 2019a; Ambati et al., 2019b; Choudhury et al., 2022; Choudhury et al., 2023). Some of the known ligands for Dectin-1, Dectin-2, and Dectin-3 have been previously summarized (Meagher et al., 2023). However, the complexity of these ligands cannot be overstated. For example, differences between linkage patterns (α vs. β, 1,3- vs. 1,6-, N-linked vs. O-linked, etc.) have an effect on binding affinity. This information is typically ascertained through a combination of techniques such as the use of artificial ligands (Brown and Gordon, 2001), the construction of certain types of fungal mutants (Esteban et al., 2011), or the manipulation of immune cell lines (Taylor et al., 2006). These techniques, while informative, can inherently limit the range of ligands that can be studied to a specific subset.

Given the crucial role of Dectins in the immune response, characterizing their broad range of ligands has biological relevance. Since the Dectins in DectiSomes are conjugated to the surface of the liposome, they should be able to mimic the behavior of Dectins found on the surface of various immune cells; therefore, the binding activity of DectiSomes should be indicative of genuine biological affinity rather than an artificial anomaly. The streamlined production pipeline of DectiSomes has also been discussed at length (Meagher et al., 2023).

We wondered if DectiSomes could be utilized as an experimental tool to further characterize Dectin-ligand interactions. DectiSomes have a big advantage over purified protein

reagents because they are typically coated with more than a thousand Dectin proteins. Hence, avidity should greatly enhance the binding and stability of probe-ligand complexes. For an example specific to this discussion, given DectiSomes' increased affinity for fungal cells, we suspected that they could be adapted into a pull-down tool by incorporating biotin onto the surface of the liposome. Biotin has an extremely high affinity for streptavidin (e.g., Kd = 10^{-14} M (mol/L)), thus making this interaction an ideal choice for pull-down assays. Dectins have ligand affinities in the 10^{-4} to 10^{-7} M range. Hence, there is the potential to release cognate ligands from these Dectin-ligand complexes and not break the link between DectiSome and resin. This could enable effective isolation of fungal cells from more complex sources. In addition, we evaluated whether DectiSomes could be utilized as a microbial array tool for simultaneous analyses of different types of Dectin-ligand interactions. This could further our understanding on topics ranging from the functions of Dectins in the immune response to the identification of potential ligands in various fungi.

Materials and Methods

Fungal cultures and growth conditions

Rhizopus delemar 99-880 is a clinical isolate that was generously provided by Dr. Xiaorong Lin. Long-term (-80°C storage) and short-term (4°C storage) sporangiospore stocks were prepared as recently described (Choudhury et al., 2022). Sporangiospores were grown in liquid RPMI + 0.165M MOPS containing kanamycin and ampicillin at 37°C for subsequent experiments.

Cryptococcus neoformans H99 is a clinical isolate that was generously provided by Dr. Xiaorong Lin. Long-term (-80°C storage) stocks were stored in 15% glycerol. For short-term

storage, the strain was plated on YPD plates containing kanamycin and ampicillin and incubated at 30°C for up to two days. The plates were then stored at 4°C for future experiments. Cells were picked with sterile sticks and inoculated in liquid YPD containing kanamycin and ampicillin at 30°C with 200 rpm shaking overnight for subsequent experiments.

Constructing biotinylated liposomes and binding liposomes to streptavidin beads

The carbohydrate recognition domain and partial stalk domain of Dectin-1 was purified and modified with DSPE-PEG as previously described (Ambati et al., 2019b). DSPE-PEG-Biotin (BroadPharm, Cat# BP-22723) was dissolved in a 1:5 ratio of dimethyl sulfoxide (DMSO) and sterile water with a 5 minute heat treatment at 60°C. Rhodamine B-DHPE (ThermoFisher, Cat# L1392) was dissolved in DMSO. The biotin, the rhodamine B, and the modified Dectin-1 protein were incubated with pegylated liposomes (FormuMax, Cat# F20203A) at final mol% of 0.5 mol%, 0.5 mol%, and 1 mol%, respectively, relative to moles of lipid. Untargeted liposomes contain only biotin and rhodamine B at equivalent mol%. Both batches of liposomes were covered and incubated for 1 hr at 60°C to facilitate integration into the liposome bilayer. Previous studies have shown that these lipid complexes are quantitively inserted into liposomes during this incubation. The liposome batches were stored in RN#5 buffer (0.1M NaH_2PO_4, 10 mM triethanolamine pH 8.0, 1M L-arginine, 100 mM NaCl, 5 mM EDTA, and 5 mM 2-mercaptoethanol [BME]) at 4°C and periodically reduced with 1 mM BME in order to maintain the protein's structural integrity.

The liposomes were bound to streptavidin beads (ThermoFisher, Cat# 11205D) immediately before the pull-down experiments according to the manufacturer's protocol. Briefly, 5 uL of beads per treatment (i.e., DEC-Bio-LLs, Bio-LLs, beads control, etc.) were washed by

suspending them in an equal volume (5 uL per treatment) of PBS (pH 7.4) and placing them on a magnetic rack for 1 minute, after which the beads were noticeably bound to the magnet. The buffer was removed, fresh PBS was added to the original volume (5 uL per treatment), and the beads were resuspended. 5 uL of the respective liposomes (or 5 uL of PBS for the beads control) were mixed with 5 uL of beads in 500 uL of PBS and incubated on a rotating platform for 30 mins at room temperature in the dark. The liposome-bead complexes were then washed five times with 500 uL PBS + 0.1% BSA (pH 7.4) and finally resuspended in 10 uL of PBS. They were stored at 4°C until they were used.

Pull-down experiments with Rhizopus delemar and biotinylated liposomes

R. delemar sporangiospores were diluted to 150,000 spores/mL in a 24-well plate containing RPMI + 0.165M MOPS and incubated at 37°C until they showed early signs of germination (~5-6 hours). The germlings were fixed with 3.7% formalin (diluted in PBS from a 37% formalin stock; J.T. Baker, Cat# 2106-01) for 30 mins at room temperature with gentle shaking, followed by three PBS washes (5 mins per wash). The germlings were blocked with PBS + 5% bovine serum albumin (BSA) (Sigma-Aldrich, Cat# A7906-500G) + 1 mM BME for 1 hr at room temperature with gentle shaking. The germlings were then stained with a 1:1000 dilution of a 25 mM calcofluor white stock (Bayer Corp., Blankophor BBH, Cat# 4193-55-9) for 30 mins at room temperature in the dark with gentle shaking. Aggressive pipetting was used to detach the germlings from the wells and transfer them to low-binding centrifuge tubes (Sarstedt, Cat# 72.695.700). It is worth noting that more consistent and reproducible *Rhizopus* growth was observed when grown on a flat surface vs. grown in tubes. However, the pull-down experiments

can only be done in centrifuge tubes due to the design of our magnetic rack; hence, the transfer step was incorporated here.

The prebound liposome-bead complexes were added to the respective centrifuge tubes and incubated on a rotator for 1 hr at room temperature in the dark. The tubes were then placed on a magnetic rack for 5 mins to ensure that any bound cells would have sufficient time to gravitate towards the magnet. The buffer was removed and saved for subsequent imaging ("unbound fraction"). 500 uL of PBS + 0.1% BSA was added to the liposome-bead-cell complexes, which were then placed on a rotator for 5 mins at room temperature in the dark. The tubes were placed on a magnetic rack for 5 mins, and the buffer was saved ("wash fraction"). The liposome-bead-cell complexes were then resuspended in a final volume of 30 uL of PBS ("bound fraction") and saved for imaging. All images were taken with an ECHO Revolve microscope (model# RVSF1000/Revolve R4).

Membrane array experiments with Cryptococcus neoformans

For this series of experiments, liposomes that only contain the respective Dectin protein and rhodamine B-DHPE (i.e., Dectin-1-LLs, Dectin-2-LLs, and Dectin-3-LLs) were constructed (i.e., they lacked biotin). Approximately 1 mol% of the respective Dectin protein and 0.5 mol% of rhodamine B-DHPE were loaded onto liposomes as previously described. Controls include an uncoated Rhodamine B-labeled liposome (Plain-LLs) and a BSA-coated, rhodamine-B-labeled liposome (BSA-LLs).

C. neoformans cultures were grown overnight in 1 mL YPD containing kanamycin and ampicillin at 30°C with 200 rpm shaking. The cultures were diluted to a starting concentration of 5,000,000 cells/mL in centrifuge tubes. Cells were blocked with PBS + 5% BSA + 1 mM BME

(blocking buffer) for 30 mins at room temperature with gentle shaking. After two minutes of centrifugation at 1500 rcf to pellet the cells, the buffer was removed and the cells were treated with a 1:200 dilution of the light-sensitive RNA dye Ribogreen (Invitrogen, Cat# R11490) for 30 mins at room temperature with gentle shaking. After two minutes of centrifugation at 1500 rcf to pellet the cells, the dye was removed, and the cells were resuspended in blocking buffer. They were subsequently divided into 400 uL aliquots containing approximately 2,000,000 cells each. The liposomes were added to their respective aliquots at a 1:100 dilution and incubated for 1 hr at room temperature with gentle shaking in the dark.

A nitrocellulose membrane (Bio-Rad, Cat# 162-0115) was cut to size and soaked in PBS for approximately 5 minutes. This membrane was then transferred to a 96-well vacuum manifold (Schleicher and Schuell Minifold I, SRC-96) to dry. The liposome-treated cells were gently resuspended and spotted in 100 uL aliquots onto the membrane for a final total of approximately 500,000 cells/spot. The vacuum manifold was run for approximately two minutes. The membrane was removed and gently washed by soaking in a petri dish containing sterile diH_2O for two minutes. The membrane was transferred to a separate petri dish to dry before scanning with an Amersham Typhoon 5 imager (Cytiva, Product# 29187191) using preset Cy2, Cy3, and/or Cy5 filters. Individual images were merged together using the manufacturer's ImageQuant software.

Results

Constructing biotinylated liposome-bead complexes

Briefly, liposomes were incubated with (1) rhodamine B, (2) the respective Dectin protein, and (3) biotin altogether at 60°C for 1 hr. All three components contain lipid moieties

that enable integration into the liposomal membrane at high temperatures. **Figure 4.1** is a model of the final biotinylated Dectin-coated liposome bound to a magnetic streptavidin bead.

First, to determine if biotinylated liposomes bind to streptavidin beads, we incubated the respective liposomes with the beads for 30 mins, washed the complexes several times, and imaged them. **Figure 4.2** is a series of images of streptavidin beads alone (**Fig. 4.2A**), biotinylated uncoated liposomes (Bio-LLs) bound to the beads (**Fig. 4.2B**), and biotinylated Dectin-1-coated liposomes (DEC1-Bio-LLs) bound to the beads (**Fig. 4.2C**). Although minor autofluorescence is visible with just the streptavidin beads alone, there are substantially higher levels of fluorescence when the beads are bound to either set of rhodamine B-tagged biotinylated liposomes. Unbound streptavidin beads are also visible in **Fig. 4.2B** (indicated with orange arrows). The majority of the liposome-bead complexes in **Figs. 4.2B** and **4.2C** appear to be aggregates, but we were unable to obtain images at higher magnification to confirm this because the autofluorescence levels of the beads alone increased dramatically. The low level of BSA in the wash buffer may not have been sufficient to prevent aggregation.

Evaluating pull-down efficacy of biotinylated liposome-bead complexes with Rhizopus delemar germlings

Given a Dectin-1 DectiSome's ability to bind to *R. delemar* germlings (Choudhury et al., 2022), we wanted to see if our DEC1-Bio-LLs effectively isolated *R. delemar* germlings from a liquid culture compared to the untargeted Bio-LLs. Briefly, fixed *R. delemar* germlings were blocked to prevent non-specific binding. The cells were stained and incubated with the prebound liposome-bead complexes for 1 hr. The liposome-bead-cell complexes were washed, and the respective fractions were saved for imaging. **Figure 4.3** is a series of images of the final fractions

of a pull-down experiment using the three different experimental conditions (Beads + Cells [**Fig. 4.3A**], Bio-LLs + Beads + Cells [**Fig. 4.3B**], and DEC1-Bio-LLs + Beads + Cells [**Fig. 4.3C-4.3D**]). An occasional *R. delemar* cell was spotted in the final fraction (bound fraction) of the Bio-LL treatment (**Fig. 4.3B**). However, a substantial number of cells were spotted in the final fraction (bound fraction) of the DEC1-Bio-LL treatment (**Figs. 4.3C** and **4.3D**). The DEC1-Bio-LLs appear to preferentially bind to presumed exopolysaccharide deposits instead of the germlings themselves (**Figure 4.4**), which corresponds with previous observations (Choudhury et al., 2022). Images of 10 uL aliquots of the bound fractions on a hemocytometer also indicate that the DEC1-Bio-LLs pull down more *R. delemar* germlings compared to the controls (**Figure 4.5**).

Evaluating DectiSome potential as an array tool

In an attempt to expand the analytical applicability of DectiSomes, we evaluated their potential as an array tool. **Figure 4.6** is a model of a multi-strain array treated with DectiSomes. Briefly, a range of strains (different types of mutants, different sources of isolation, divergent species, etc.) can be plated on an array. A single type of fluorescent DectiSome can be added across the array. After washing out unbound DectiSomes, the array can be scanned, and information regarding Dectin interactions with these strains can potentially be ascertained. Alternatively, a single strain can be plated on an array, and several types of DectiSomes can be added across the array to evaluate different Dectin interactions simultaneously.

Cryptococcus neoformans was chosen as the initial test species due to its streamlined growth conditions and DectiSomes' known ability to bind to it in vitro (Ambati et al., 2019a; Ambati et al., 2019b; Choudhury et al., 2023). The biotin was unnecessary for this particular

experimental design and therefore omitted, but all of the experimental liposomes still contained rhodamine B. **Figure 4.7** is a picture of a *C. neoformans* array that had been treated with DectiSomes and gently washed. Red spots were visible where the DectiSomes were used, whereas no red spots were visible where the control liposomes were used. Therefore, we were cautiously optimistic that the subsequent membrane scan would validate these observations. However, the scan shown in **Figure 4.8** indicated that nothing was bound to the Ribogreen-stained cells. A series of trial-and-error attempts with a variety of modifications yielded no discernible results. Examples of modifications that were tested include different cell stains (calcofluor white vs. Ribogreen), different membrane surfaces (nitrocellulose vs. polyvinylidene fluoride [PVDF]), different blocking agents (bovine serum albumin [BSA] vs. linear acrylamide), and different scanning settings on the Typhoon.

Discussion

DectiSomes were originally designed as a novel antifungal treatment against several clinically relevant fungal pathogens (Ambati et al., 2019a; Ambati et al., 2019b; Choudhury et al., 2022; Choudhury et al., 2023). DectiSomes have improved fungal specificity over untargeted liposomes due to the addition of a Dectin coating on the liposome's surface, and Dectins recognize certain types of carbohydrates that are primarily present in the fungal cell wall. However, given the structural complexity of these carbohydrates and the inherent limitations of the techniques used to evaluate Dectin-ligand interactions, the true range of potential Dectin ligands is still being elucidated. We wanted to see whether DectiSomes could potentially address this question by repurposing them as potential biochemical and cell biological probes.

The preliminary data indicate that DectiSomes can be modified into a biotinylated version that can be used with magnetic streptavidin beads to isolate *Rhizopus delemar* germlings from a liquid culture. We chose to work with Dectin-1 biotinylated liposomes (DEC1-Bio-LLs) because Dectin-1 has significant binding efficacy against *R. delemar* (Choudhury et al., 2022). As previously shown for DEC1-AmB-LLs, DEC1-Bio-LLs preferentially bound to presumed exopolysaccharide (EPS) deposits around the germlings rather than the cell wall. This could be indicative of a higher proportion of ligands in the EPS or greater levels of ligand accessibility in the EPS vs. the cell wall. Alternatively, since the biotinylated liposomes are complexed to streptavidin beads prior to incubation with the fixed germlings, the beads' size could be a limiting factor for ligand accessibility in a rigid fungal cell wall. It is also possible that the high affinity ligands for Dectin-1 are not present in sufficient quantities in the cell wall for our reagent to adhere to them. We have not evaluated pull-down efficacy of a Dectin-2 or Dectin-3 biotinylated liposome, and we have not evaluated pull-down efficacy against other fungal species, but we expect similar levels of improvement over the controls based on our previous DectiSome studies.

Although there appears to be qualitative improvements in pull-down efficacy, we have not evaluated our results quantitatively. **Figure 4.5** is a semi-quantitative evaluation; however, individual cells in the fractions are difficult to count due to the occasional clumps of germlings that are visible. Evaluating pull-down efficacy with yeast cells or using an automatic cell counter could help address those issues. Fungal DNA extractions from the final (bound) fractions led to low yields with poor quality, possibly due to the relatively low amount of starting material or contamination with the streptavidin beads. The biotin-streptavidin bond is notoriously difficult to break, and the harsh conditions that can break this bond could compromise the integrity of the

cells themselves. A brief heat treatment after the final wash step is a potential option to break this bond (Holmberg et al., 2005). Anti-biotin magnetic beads and corresponding separation columns could be an alternative modification (Hersch et al., 2015), but the large size of fungal cells could be a limiting factor.

Potential applications of a biotinylated DectiSome include improved fungal isolation from tissue or environmental samples. DectiSomes bind at fungal infection centers of murine models of various diseases (Ambati et al., 2021; Ambati et al., 2022; Pham et al., 2024). However, we have not attempted to isolate fungal cells (or fragments) from tissue samples. A substantial amount of biotinylated DectiSomes may be required in order to isolate a sufficient amount of fungal cells from more complex samples. Dectins are also involved in the immune response against some bacteria (Deerhake and Shinohara, 2021), which could be an additional complication. A different application could be to affinity-purify potential Dectin ligands from complex EPS deposits. Fungal EPS production and extraction can be optimized for maximum yield, although a variety of growth conditions must be examined in the process (Hamidi et al., 2022). Biotinylated DectiSomes are able to bind to minuscule quantities of EPS. Mass spectrometry analyses of affinity-purified EPS could further contribute to our understanding of both Dectin-ligand interactions and EPS compositions from various fungi. However, ensuring that DectiSomes bind to a sufficient amount of EPS for such analyses could be a limiting factor.

We also evaluated the potential of DectiSomes as an array tool. A variety of protocol modifications were incorporated, but there was no discernible difference in DectiSome binding in any membrane scan. Since the background fluorescence in the nitrocellulose membrane in **Figure 4.8** is so high, it's possible that that membrane isn't ideal for fluorescence scanning with the Typhoon. Switching to a polyvinylidene fluoride (PVDF) membrane generally reduced

background fluorescence, but cell adherence was inconsistent between attempts, and there was no improvement in DectiSome binding. An attempt with glass slides as the membrane substrate yielded high levels of background, but this was likely due to residual buffer drying down on the slides. Silicon and polydimethylsiloxane are substrates that have been used in prokaryotic cell arrays (Elad et al., 2008). Nitrocellulose film slides (rather than membranes) are also an alternative option (Wu et al., 2023). Although the excitation/emission spectra for the Typhoon filters cannot be adjusted, it's possible that adjusting other parameters (such as the photomultiplier tube voltage, the pixel size, etc.) would lead to more consistent scans. Alternatively, using a different array scanner with more flexible settings could be more promising. But, in short, we do not yet understand the reasons that we failed to show that highly fluorescent DectiSomes were a sound probe for fungal arrays.

Preprinted glycan arrays, such as those offered by the National Center for Functional Glycomics, could be used in conjunction with our existing DectiSomes to further characterize Dectin-ligand interactions. An extensive variety of defined glycans are included on the array (National Center for Functional Glycomics, Microarrays), established protocols exist (National Center for Functional Glycomics, Protocols), and scanners specifically designed for microarray analyses are utilized (National Center for Functional Glycomics, Equipment). However, the approval process for using these arrays significantly lengthens the expected timeline for a single experiment. Glycan arrays from other manufacturers exist, but cost may be a limiting factor since, for example, the amount of DectiSomes required for such an experiment has not been fully elucidated.

In conclusion, we have generated a biotinylated version of DectiSomes that can pull down *Rhizopus delemar* germlings from a liquid culture. This indicates that DectiSomes have

potential as a biological probe. Future studies would need to evaluate pull down efficacy against other fungal species in pure and more complex sources, and quantitative methods are needed to validate these qualitative observations. Attempts to evaluate the utility of DectiSomes as an array tool have been unsuccessful but show potential. Future studies would need to focus on tweaking the parameters of the experimental design, tweaking the scanning parameters of the Typhoon, or utilizing other types of array-specific scanners altogether.

References

Ambati, S., Ellis, E.C., Lin, J., Lin, X., Lewis, Z.A., and Meagher, R.B. (2019a). Dectin-2-Targeted Antifungal Liposomes Exhibit Enhanced Efficacy. *mSphere*, 4 (5).

Ambati, S., Ellis, E.C., Pham, T., Lewis, Z.A., Lin, X., and Meagher, R.B. (2021). Antifungal Liposomes Directed by Dectin-2 Offer a Promising Therapeutic Option for Pulmonary Aspergillosis. *mBio*, 12 (1).

Ambati, S., Ferraro, A.R., Kang, S.E., Lin, J., Lin, X., Momany, M., Lewis, Z.A., and Meagher, R.B. (2019b). Dectin-1-Targeted Antifungal Liposomes Exhibit Enhanced Efficacy. *mSphere*, 4 (2).

Ambati, S., Pham, T., Lewis, Z.A., Lin, X., and Meagher, R.B. (2022). DectiSomes: Glycan Targeting of Liposomal Drugs Improves the Treatment of Disseminated Candidiasis. *Antimicrobial Agents and Chemotherapy*, 66 (1).

Brown, G.D., and Gordon, S. (2001). A new receptor for β-glucans. *Nature*, 413.

Choudhury, Q.J., Ambati, S., Lewis, Z.A., and Meagher, R.B. (2022). Targeted Delivery of Antifungal Liposomes to *Rhizopus delemar*. *Journal of Fungi*, 8 (4).

Choudhury, Q.J., Ambati, S., Link, C.D., Lin, X., Lewis, Z.A., and Meagher, R.B. (2023). Dectin-3-targeted antifungal liposomes efficiently bind and kill diverse fungal pathogens. *Molecular Microbiology*, 120 (5).

Deerhake, M.E., and Shinohara, M.L. (2021). Emerging roles of Dectin-1 in noninfectious settings and in the CNS. *Trends in Immunology*, 42 (10).

Elad, T., Lee, J.H., Belkin, S., and Gu, M.B. (2008). Microbial whole-cell arrays. *Microbiology Biotechnology*, 1 (2).

Esteban, A., Popp, M.W., Vyas, V.K., Strijbis, K., Ploegh, H.L., and Fink, G.R. (2011). Fungal recognition is mediated by the association of dectin-1 and galectin-3 in macrophages. *Proceedings of the National Academy of Sciences of the United States of America*, 108 (34).

Freeze, H.H. (2001). Lectin Affinity Chromatography. *Current Protocols in Protein Science*, 9

Hage, D.S., and Matsuda, R. (2015). Affinity Chromatography: A Historical Perspective. In: Reichelt, S. (eds) *Affinity Chromatography*. *Methods in Molecular Biology*, *vol 1286.* Humana Press, New York, NY.

Hamidi, M., Okoro, O.V., Milan, P.B., Khalili, M.R., Samadian, H., Nie, L., and Shavandi, A. (2022). Fungal exopolysaccharides: Properties, sources, modifications, and biomedical applications. *Carbohydrate Polymers*, 284.

Hersch, N., Wolters, B., Ungvari, Z., Gautam, T., Deshpande, D., Merkel, R., Csiszar, A., Hoffmann, B., and Csiszár, A. (2015). Biotin-conjugated fusogenic liposomes for high-quality cell purification. *Journal of Biomaterials Applications*, 30 (6).

Holmerg, A., Blomstergren, A., Nord, O., Lukacs, M., Lundeberg, J., and Uhlén, M. (2005). The biotin-streptavidin interaction can be reversibly broken using water at elevated temperatures. *Electrophoresis*, 26 (3).

Meagher, R.B., Lewis, Z.A., Ambati, S., and Lin, X. (2023). DectiSomes: C-type lectin receptor-targeted liposomes as pan-antifungal drugs. *Advanced Drug Delivery Reviews*, 196.

National Center for Functional Glycomics. Equipment. Accessible at: https://research.bidmc.org/ncfg/equipment.

National Center for Functional Glycomics. Microarrays. Accessible at: https://research.bidmc.org/ncfg/microarrays.

National Center for Functional Glycomics. Protocols. Accessible at: https://research.bidmc.org/ncfg/protocols.

Pham, T., Shi, R., Ambati, S., Meagher, R., and Lin, X. (2024). All hands on Dec: Treating cryptococcosis with dectin decorated liposomes loaded with antifungals. *iScience*, 27 (7).

Rodriguez, E.L., Poddar, S., Iftekhar, S., Suh, K., Woolfork, A.G., Ovbude, S., Pekarek, A., Walters, M., Lott, S., and Hage, D.S. (2020). Affinity Chromatography: A Review of Trends and Developments over the Past 50 Years. *Journal of Chromatography B*, 1157.

Taylor, P.R., Tsoni, S.V., Willment, J.A., Dennehy, K.M., Rosas, M., Findon, H., Haynes, K., Steele, C., Botto, M., Gordon, S., and Brown, G.D. (2006). Dectin-1 is required for β-glucan recognition and control of fungal infection. *Nature Immunology*, 8.

Wu., S-C., Jan, H-M., Vallecillo-Zúniga, M.L., Rathgeber, M.F., Stowell, C.S., Murdock, K.L., Patel, K.R., Nakahara, H., Stowell, C.J., Nahm, M.H., Arthur, C.M., Cummings, R.D., and Stowell, S.R. (2023). Whole microbe arrays accurately predict interactions and overall antimicrobial activity of galectin-8 toward distinct strains of *Streptococcus pneumoniae*. *Scientific Reports*, 13.

Figures

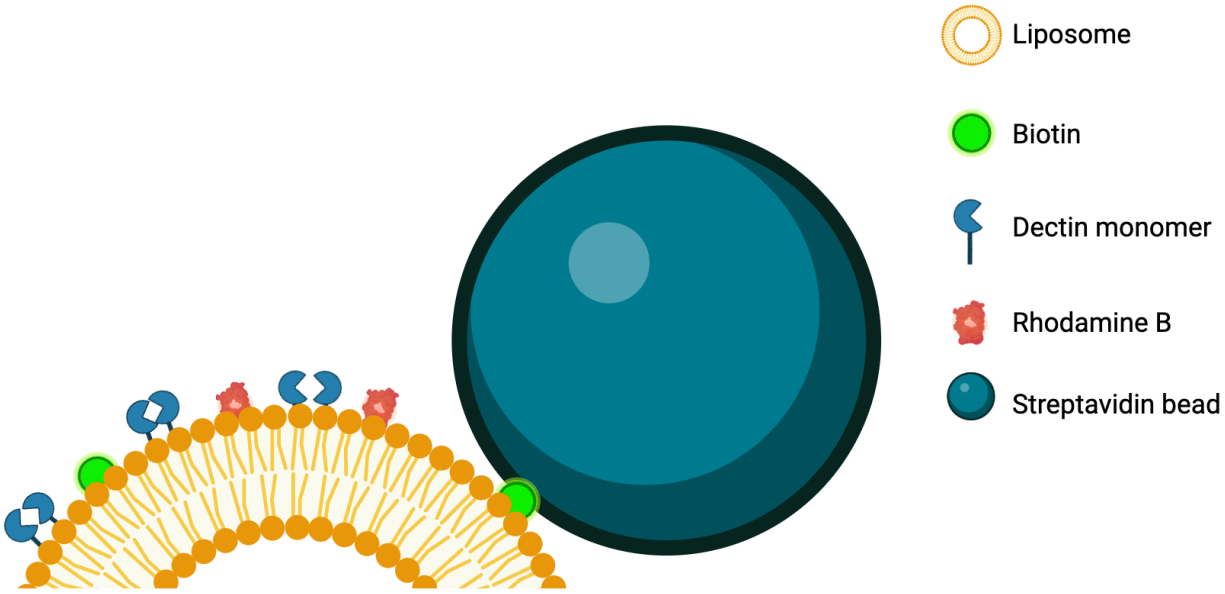

Figure 4.1. A model of a biotinylated Dectin-coated liposome bound to a magnetic streptavidin bead. The surface of the liposome contains three components: 1) Dectin monomers, which facilitate binding to fungal carbohydrates, 2) Rhodamine B for fluorescence microscopy purposes, and 3.) Biotin, which facilitates binding to the magnetic streptavidin bead. The biotinylated Dectin-coated liposome-streptavidin bead complex can facilitate the isolation of fungal cells from cultures. Figure (not to scale) made in BioRender.

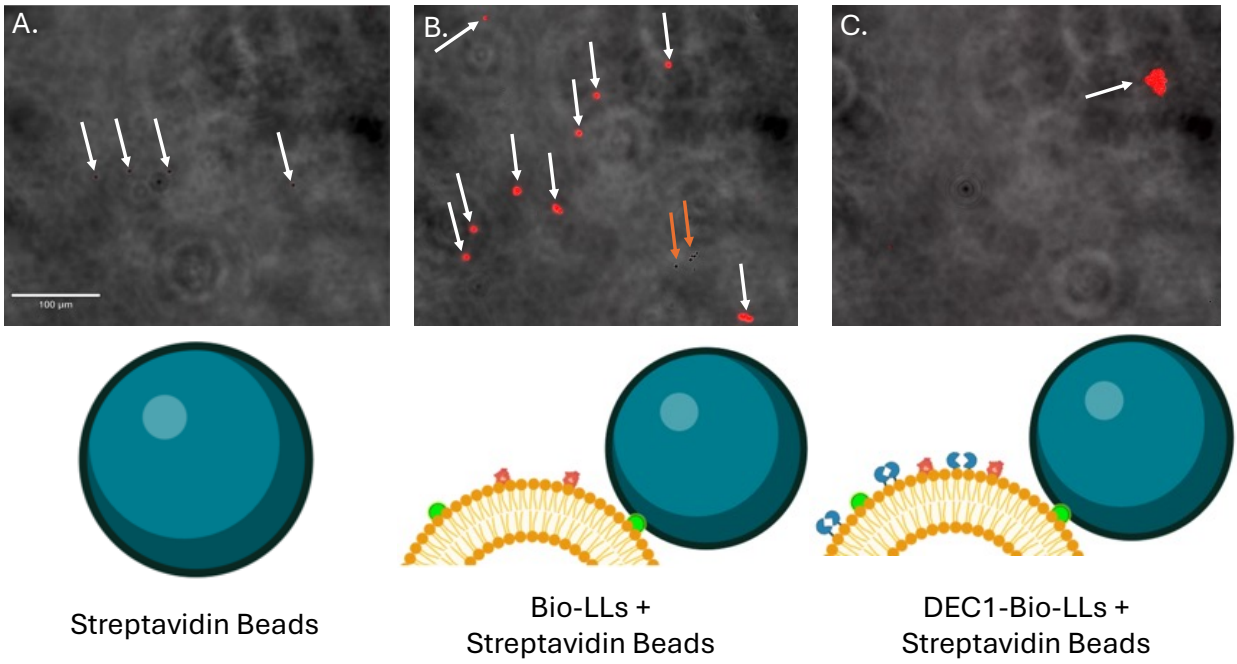

Figure 4.2. Biotinylated liposomes bind to streptavidin beads. (**A**) Streptavidin beads (white arrows) have minimal levels of autofluorescence. (**B**) Fluorescent, untargeted biotinylated liposomes (Bio-LLs) bind to streptavidin beads (white arrows). Beads alone are also visible (orange arrows). (**C**) Fluorescent, biotinylated Dectin-1-coated liposomes (DEC1-Bio-LLs) bind to streptavidin beads (white arrow) in small clusters. Models (not to scale) made in BioRender.

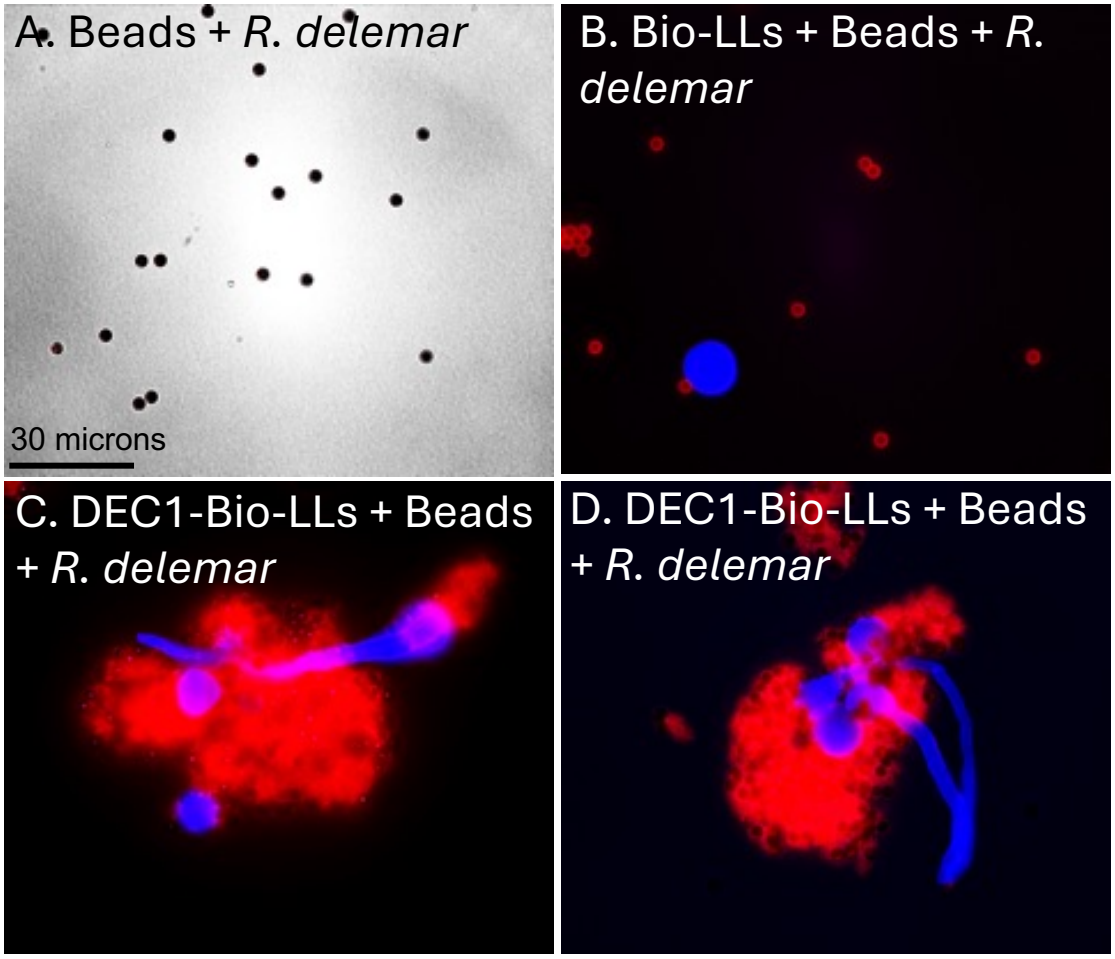

Figure 4.3. DEC1-Bio-LLs complexed to streptavidin beads bind to *Rhizopus delemar* germlings. (**A**) Streptavidin beads do not bind to cells. (**B**) Bio-LLs complexed to streptavidin beads (red) can pull down an occasional *R. delemar* cell (blue) but are primarily isolated. (**C**) and (**D**) DEC1-Bio-LLs complexed to streptavidin beads (red) pull down *R. delemar* germlings (blue) of varying sizes.

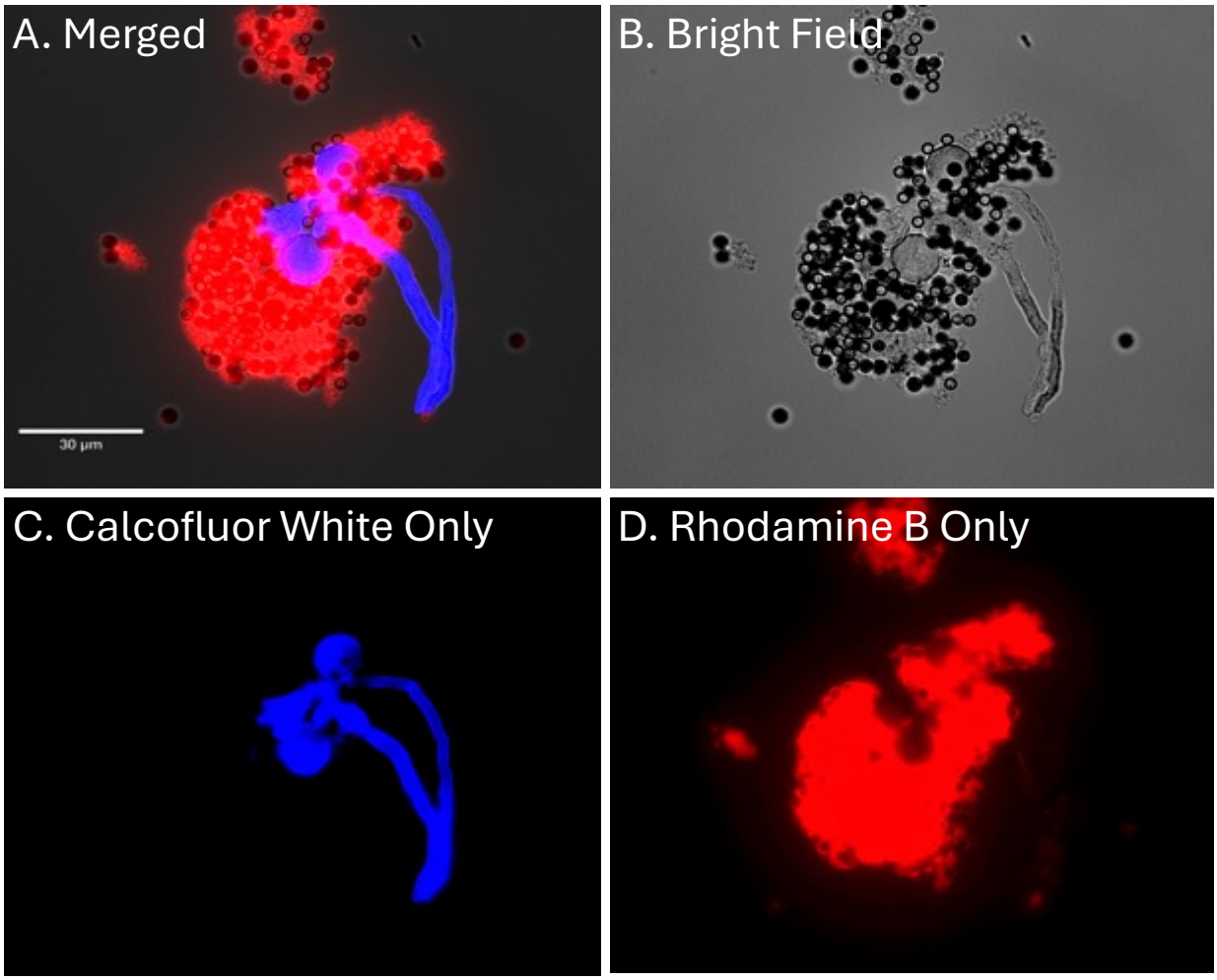

Figure 4.4. DEC1-Bio-LLs bind to presumed *Rhizopus delemar* exopolysaccharide deposits. (**A**) Merged image. (**B**) Bright field channel only. (**C**) DAPI channel only, which enables visualization of the chitin stain calcofluor white. (**D**). Texas Red channel only, which enables visualization of the fluorescent liposome component Rhodamine B.

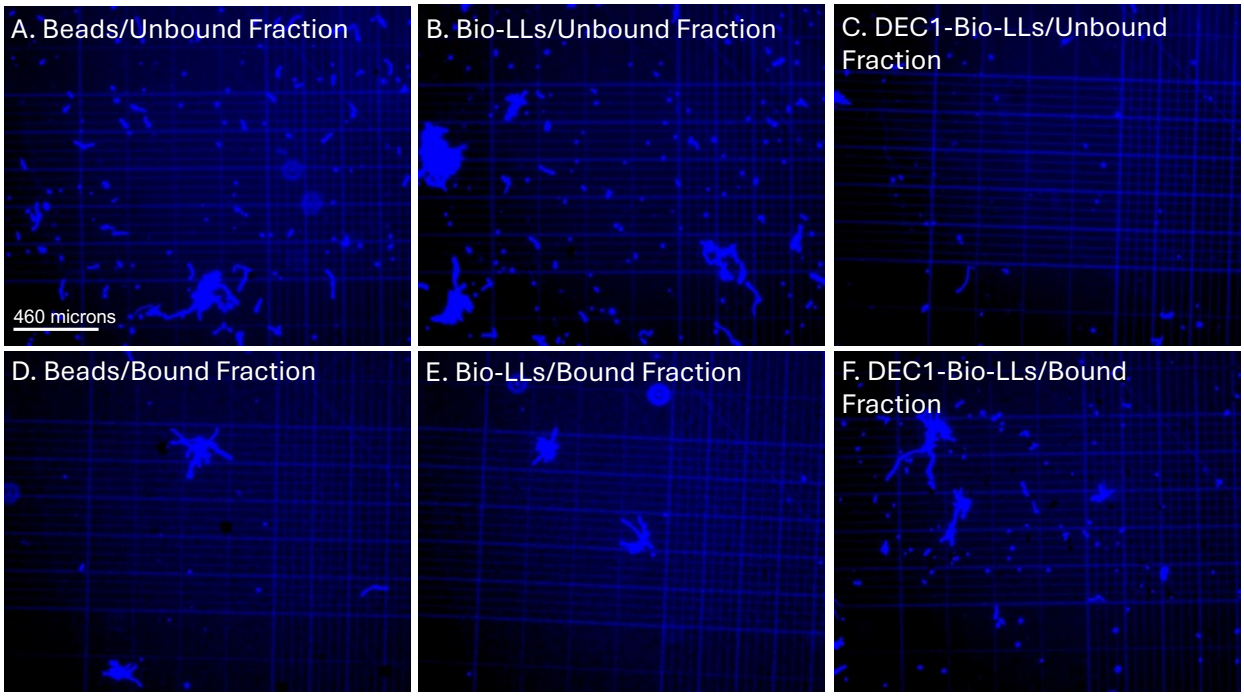

Figure 4.5. DEC1-Bio-LLs complexed to streptavidin beads pull down *Rhizopus delemar* germlings. The unbound fraction is the supernatant that was removed after the liposome-bead-cell complexes were placed on the magnetic rack. The bound fraction is the final resuspension of the germlings that had been isolated by the respective complexes. Cells (blue) were stained with the chitin stain calcofluor white. (**A**) Unbound fraction of *R. delemar* germlings that had been incubated with streptavidin beads. (**B**) Unbound fraction of *R. delemar* germlings that had been incubated with Bio-LLs complexed to streptavidin beads. (**C**) Unbound fraction of *R. delemar* germlings that had been incubated with DEC1-Bio-LLs complexed to streptavidin beads. (**D**) Bound fraction of *R. delemar* germlings that had been incubated with streptavidin beads. (**E**) Bound fraction of *R. delemar* germlings that had been incubated with Bio-LLs complexed to streptavidin beads. (**F**) Bound fraction of *R. delemar* germlings that had been incubated with DEC1-Bio-LLs complexed to streptavidin beads.

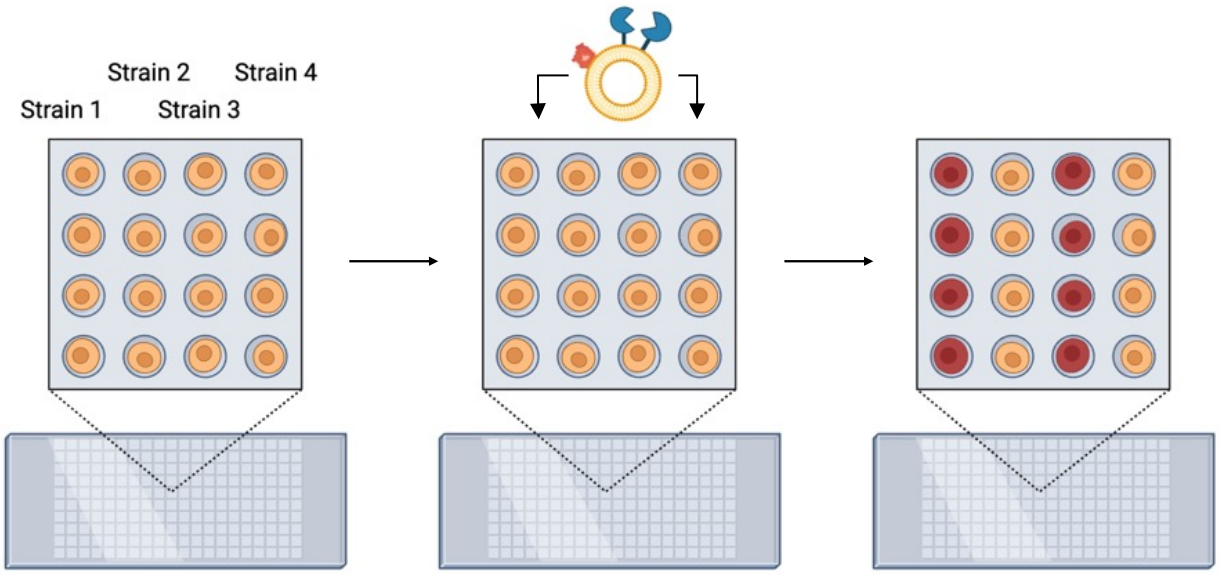

Figure 4.6. Proposed model of utilizing DectiSomes as an array tool. Multiple fungal strains can be plated across a single array. Fluorescent DectiSomes can then be added to the array. The array can be washed to remove unbound DectiSomes, and potential binding interactions can be simultaneously assessed. Figure made in BioRender.

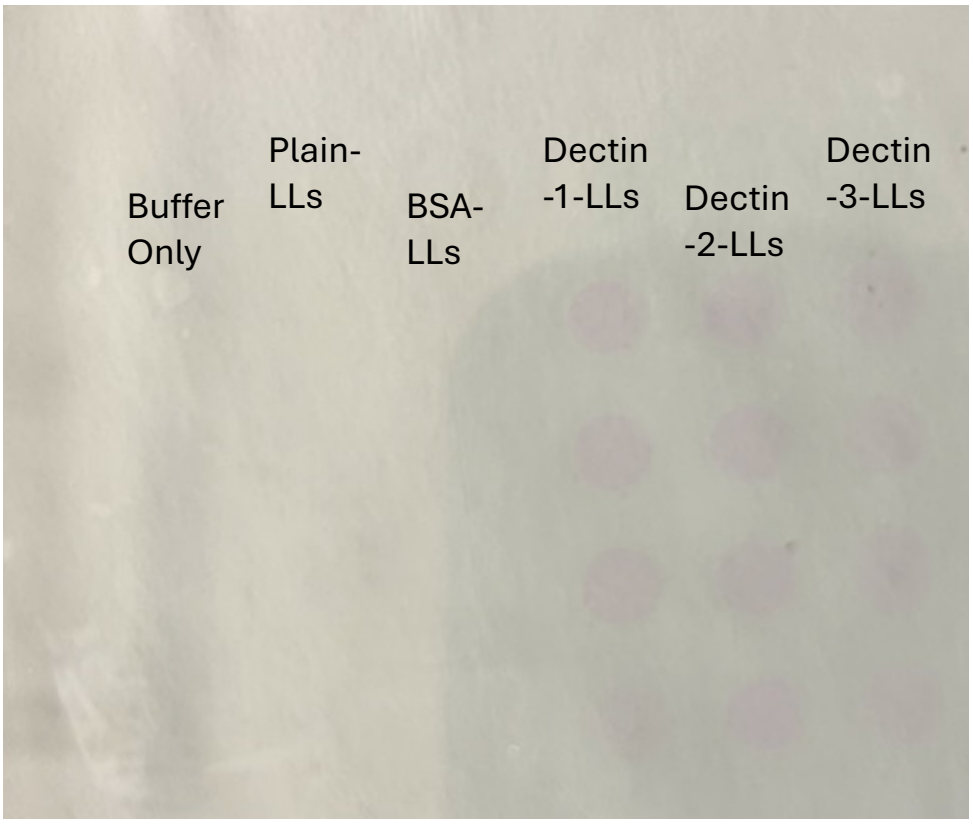

Figure 4.7. *Cryptococcus neoformans* array treated with DEC-LLs prior to scanning. *C. neoformans* cells that had been treated with the respective liposomes had been spotted onto a nitrocellulose membrane. A vacuum manifold was used to ensure adherence to the membrane. The membrane was washed once prior to scanning. Red spots appear to indicate bound DEC-LLs.

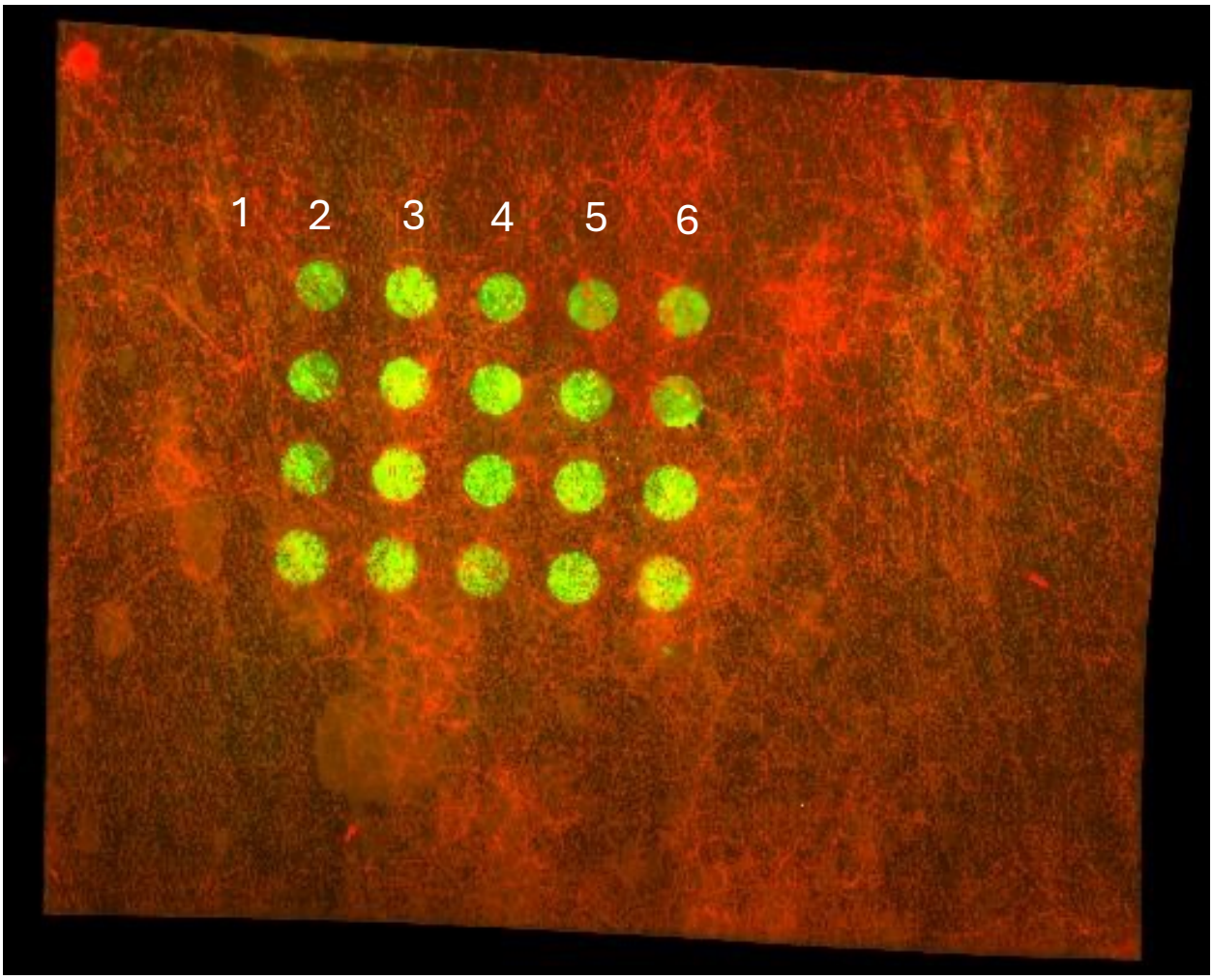

Figure 4.8. Fluorescence scan of *C. neoformans*/DEC-LL array introduced in Figure 4.7. The Amersham Typhoon was used for scanning, and the merged image was generated using the manufacturer's ImageQuant software. Green spots are *C. neoformans* cells stained with the RNA dye Ribogreen prior to addition on the membrane. (1) Buffer Only. (2) Cells + Plain-LLs. (3) Cells + BSA-LLs. (4) Cells + DEC1-LLs. (5) Cells + DEC2-LLs. (6) Cells + DEC3-LLs.

CHAPTER 5

DISCUSSION

Prior to this dissertation project, our research group had designed two types of DectiSomes (targeted antifungal liposomes) and evaluated their efficacy in vitro against three clinically relevant fungal pathogens. The goal of this dissertation was to expand upon the potential uses of DectiSomes in multiple directions. We have shown that a Dectin-1-targeted liposome loaded with amphotericin B (Dectin-1 DectiSome) significantly binds to *Rhizopus delemar*, a common causative agent of mucormycosis, at multiple stages of fungal development and effectively inhibits and/or kills *R. delemar* in vitro compared to untargeted antifungal liposomes. We have also constructed a novel Dectin-3 DectiSome that effectively binds to and inhibits the divergent human fungal pathogens *Candida albicans*, *Cryptococcus neoformans*, and *R. delemar* in vitro. We have also constructed a biotinylated targeted liposome that can pull down *R. delemar* germlings from a liquid culture, thus indicating that DectiSomes can have potential uses outside of an antifungal treatment.

Targeted Delivery of Antifungal Liposomes to *Rhizopus delemar*

Mucormycosis is a severe opportunistic infection that is characterized by symptoms such as angioinvasion and tissue necrosis. It is primarily acquired via the inhalation of spores from causative agents such as *Rhizopus delemar*. Treatment usually requires a combination of antifungals and surgery to remove infected tissue. Mucormycosis has a baseline mortality rate of approximately 50% (Centers for Disease Control and Prevention, 2024) which indicates that

existing antifungal treatments are ineffective. Given the predicted rise of immunocompromising conditions that further facilitate the development of mucormycosis, more effective treatments are urgently needed.

Our research group's ultimate goal is to develop DectiSomes into an effective pan-fungal treatment. Dectin-1 and Dectin-2 DectiSomes have improved targeting efficacy against multiple human fungal pathogens within the Dikarya subkingdom (Ambati et al., 2019a; Ambati et al., 2019b), and we needed to expand beyond that in order to assess pan-fungal activity. Based on these criteria, *R. delemar* was a logical choice for testing DectiSome efficacy. We chose to focus on Dectin-1 DectiSomes because Dectin-1 had previously been reported to be involved in the immune response against *Rhizopus* species (Chamilos et al., 2010).

We showed that Dectin-1 DectiSomes had significantly higher levels of binding activity against fixed *R. delemar* cells at multiple stages of fungal development compared to untargeted controls. The binding activity was mediated by the Dectin-1 protein rather than the liposome or amphotericin B, as evidenced by the binding levels of a Dectin-1-Rhodamine B fusion protein. Additionally, there were high levels of binding observed against "live" hyphae compared to the untargeted controls, indicating that fixation was not a significant contributing factor for binding activity. Dectin-1 binding specificity appeared to be primarily towards glucans, as evidenced by a decrease in binding activity when the DectiSomes were preincubated with laminarin compared to yeast mannans.

We also showed that Dectin-1 DectiSomes have improved inhibition efficacy in vitro against *R. delemar*. A single dose of Dectin-1 DectiSomes inhibited fungal germination after 24 hours of treatment at much lower amphotericin B concentrations than our controls, as evidenced by microscopy images; this difference was even more pronounced after 48 hours of treatment.

Cell density and metabolic activity measurements taken after 24 hours of treatment further validated this observation. Taken together, these results indicate that Dectin-1 DectiSomes are a promising treatment against *R. delemar* and have additional potential as a pan-fungal treatment.

There are several directions to pursue for future studies. Evaluating Dectin-1 DectiSome efficacy in a mouse model of mucormycosis is a necessary step. Other directions include evaluating efficacy of other types of DectiSomes against *R. delemar* and evaluating DectiSome efficacy against other causative agents of mucormycosis. Additionally, given that the *Rhizopus* cell wall structure is not precisely defined compared to other clinically relevant fungal pathogens, the binding activity and specificity of DectiSomes could serve as a tool to further our understanding of both cell wall and exopolysaccharide carbohydrates that may be present.

Dectin-3-Targeted Antifungal Liposomes Efficiently Bind and Kill Diverse Fungal Pathogens

There are three known Dectin receptors, appropriately named Dectin-1, Dectin-2, and Dectin-3 (also known as macrophage C-type lectin or MCL). Prior to this dissertation project, our research group had already constructed Dectin-1 and Dectin-2 DectiSomes. Dectin-1 and Dectin-2 are known to recognize several fungal species (Goyal et al., 2018). In contrast, Dectin-3 interactions with different fungal species, such as *Candida* and *Cryptococcus* spp., have only been minimally reported (Zhu et al., 2013; Huang et al., 2018; Wang et al., 2016; Preite et al., 2018; Kottom et al., 2019). This is potentially a reflection of the minimal body of knowledge regarding Dectin-3 (compared to Dectin-1 and Dectin-2) rather than an indicator of poor biological relevance. Dectin-3 is known to recognize fungal mannans, including glucuroxylomannan, a significant component of the *Cryptococcus* capsule (Huang et al., 2018).

Although there had been no reported interactions between Dectin-3 and *Rhizopus* spp., we had already optimized our in vitro protocols for DectiSome efficacy against *Rhizopus* (Choudhury et al., 2022). Given this information and our previously stated goal of developing DectiSomes as a pan-fungal treatment, we wanted to construct and evaluate the potential of Dectin-3 DectiSomes as an additional treatment option. This represented an opportunity to evaluate efficacy of a novel DectiSome with a minimally-characterized receptor against several clinically relevant fungal pathogens.

We showed that Dectin-3 DectiSomes have improved binding efficacy in vitro against all three fungal pathogens at multiple stages of fungal development. Binding against *R. delemar* and *C. neoformans* appeared to be on the cell or colony surface as well as to adjacent exopolysaccharide deposits. In contrast, binding against *C. albicans* appeared to be localized to the periphery of the colony. This may be indicative of higher levels of ligand exposure at hyphae that are actively developing vs. "older" hyphae that may be less accessible at the center of a colony. The binding levels observed for all three species was specifically due to the Dectin-3 protein rather than the liposome or amphotericin B.

Dectin-3 DectiSomes led to significant reductions in metabolic activity across all three species at low amphotericin B concentrations. However, a higher drug dose was required against *Cryptococcus* (compared to *Candida* and *Rhizopus*) in order to observe this effect. This result was perplexing given the high binding levels that were observed compared to our controls. Nonetheless, the results collectively indicate that Dectin-3 is an effective addition to the list of DectiSome receptors. The results contribute to existing knowledge regarding Dectin-3 interactions with *Candida* and *Cryptococcus*. This is also the first report regarding interactions between Dectin-3 and *Rhizopus*.

Future directions include evaluating Dectin-3 DectiSome efficacy against other clinically relevant fungal species or against mouse models of candidiasis, cryptococcosis, and mucormycosis, respectively. Additionally, Dectin-3 is known to recognize trehalose 6,6-dimycolate, a cell wall carbohydrate found in *Mycobacterium tuberculosis* (Zhao et al., 2014); future studies could evaluate the efficacy of Dectin-3 DectiSomes (loaded with the appropriate drugs used to treat tuberculosis) against *M. tuberculosis*. This would further highlight the versatility of DectiSomes by exploring efficacy outside of the fungal kingdom.

An additional direction to consider would be the construction of heterodimeric DectiSomes. Dectin-2 and Dectin-3 from mice can form a heterodimer that is able to recognize mannans from *Candida albicans* (Zhu et al., 2013); they also appear to function as a complex in response to metastasis of liver cancer (Kimura et al., 2016). Additionally, human Dectin-3 and Mincle - another C-type lectin that recognizes similar ligands - can form a functional complex (Lobato-Pascual et al., 2013). However, human Dectin-2 and Dectin-3 do not form a functional complex for reasons that are currently unknown (Blankson et al., 2022). This could be reflective of structural differences between the receptors in mice and humans, and this would be an important consideration when constructing heterodimeric DectiSomes for clinical purposes.

DectiSomes as Potential Biological Probes

Our research group's primary focus has been to evaluate the efficacy of DectiSomes as an antifungal treatment. Although this is an important use of this novel technology, we also wanted to see if we could repurpose DectiSomes as experimental tools outside of a clinical context. This serves two primary purposes: 1.) It highlights the versatile nature of DectiSomes, and 2.) it can further contribute to our understanding of Dectin-ligand interactions.

We have successfully designed a biotinylated version of a DectiSome that can be used with magnetic streptavidin beads to pull down fungal cells. Pilot experiments indicate that biotinylated Dectin-1 DectiSomes qualitatively pull down *Rhizopus delemar* germlings more effectively than biotinylated untargeted liposomes. However, quantitative studies that evaluate the efficacy of other types of biotinylated DectiSomes against other fungal species would be necessary to further validate this adaptation as a versatile tool. Another important step is to evaluate pull-down efficacy from more complex sources, such as mixed microbial cultures, tissue samples, or environmental samples.

Attempts to repurpose DectiSomes as an array tool have so far been unsuccessful. Protocol modifications addressed some issues but simultaneously created new issues. Crucial details that need to be addressed include choosing the appropriate membrane substrate, determining the appropriate amount of DectiSomes needed for such an experiment, and optimizing the scanning settings (or using a different scanner altogether). A different approach could involve the use of defined microbial glycan arrays (rather than a whole cell array) to identify more specific Dectin ligands.

Since our DectiSomes have been used exclusively as drug delivery vehicles, another direction to pursue would be whether other types of cargo could be delivered via DectiSomes. For example, can DectiSomes be used as a transformation tool? Liposome-mediated transformation in fungi has been previously studied (Chai et al., 2013). Additionally, we have established that DectiSomes sufficiently deliver amphotericin B to inhibit and/or kill various fungi. Liposomes can be analogous to the extracellular vesicles that fungi naturally produce to carry a variety of cargo (Liu and Hu, 2023), and both vehicles have been reviewed as potential drug delivery vesicles (van der Koog, Gandek, and Nagelkerke, 2021). Therefore, given the right

combination of liposome composition and cargo, DectiSomes could potentially facilitate more effective fungal transformations.

References

Ambati, S., Ellis, E.C., Lin, J., Lin, X., Lewis, Z.A., and Meagher, R.B. (2019a). Dectin-2-Targeted Antifungal Liposomes Exhibit Enhanced Efficacy. *mSphere*, 4 (5).

Ambati, S., Ferraro, A.R., Kang, S.E., Lin, J., Lin, X., Momany, M., Lewis, Z.A., and Meagher, R.B. (2019b). Dectin-1-Targeted Antifungal Liposomes Exhibit Enhanced Efficacy. *mSphere*, 4 (2).

Blankson, V., Lobato-Pascual, A., Saether, P.C., Fossum, S., Dissen, E., and Daws, M.R. (2022). Human macrophage C-type lectin forms a heteromeric receptor complex with Mincle but not Dectin-2. *Scandinavian Journal of Immunology*, 95 (5).

Centers for Disease Control and Prevention. (2024). Clinical Overview of Mucormycosis. Accessible at: https://www.cdc.gov/murcomycosis/hcp/clinical-overview/index.html

Chai, R., Zhang, G., Sun, Q., Zhang, M., Zhao, S., and Qiu, L. (2013). Liposome-mediated mycelial transformation of filamentous fungi. *Fungal Biology*, 117 (9).

Chamilos, G., Ganguly, D., Lande, R., Gregorio, J., Meller, S., Goldman, W.E., Gilliet, M., and Kontoyiannis, D.P. (2010). Generation of IL-23 Producing Dendritic Cells (DCs) by Airborne Fungi Regulates Fungal Pathogenicity via the Induction of T_H-17 Responses. *PLoS ONE*, 5 (9).

Choudhury, Q.J., Ambati, S., Lewis, Z.A., and Meagher, R.B. (2022). Targeted Delivery of Antifungal Liposomes to *Rhizopus delemar*. *Journal of Fungi*, 8 (4).

Goyal, S., Castrillón-Betancur, J.C., Klaile, E., and Slevogt, H. (2018). The Interaction of Human Pathogenic Fungi with C-Type Lectin Receptors. *Frontiers in Immunology*, 9.

Huang, H-R., Li, F., Han, H., Xu, X., Li, N., Wang, S., Xu, J-F., and Jia, X-M. (2018). Dectin-3 Recognizes Glucuroxylomannan of *Cryptococcus neoformans* Serotype AD and *Cryptococcus gattii* Serotype B to Initiate Host Defense Against Cryptococcosis. *Frontiers in Immunology*, 9.

Kimura, Y., Inoue, A., Hangai, S., Saijo, S., Negishi, H., Nishio, J., Yamasaki, S., Iwakura, Y., Yanai, H., and Taniguchi, T. (2016). The innate immune receptor Dectin-2 mediates the phagocytosis of cancer cells by Kupffer cells for the suppression of liver metastasis. *Proceedings of the National Academy of Sciences of the United States of America*, 113 (49).

Kottom, T.J., Hebrink, D.M., Monteiro, J.T., Lepenies, B., Carmona, E.M., Wuethrich, M., Santo Dias, L.D., and Limper, A.H. (2019). Myeloid C-type lectin receptors that recognize fungal mannans interact with *Pneumocystis* organisms and major surface glycoprotein. *Journal of Medical Microbiology*, 68 (11).

Liu, J., and Hu, X. (2023). Fungal extracellular vesicle-mediated regulation: from virulence factor to clinical application. *Frontiers in Microbiology*, 14.

Lobato-Pascual, A., Saether, P.C., Fossum, S., Dissen, E., and Daws, M.R. (2013). Mincle, the receptor for mycobacterial cord factor, forms a functional receptor complex with MCL and FcεRI-γ. *European Journal of Immunology*, 43 (12).

Preite, N.W., Feriotti, C., Souza de Lima, D., da Silva, B.B., Condino-Neto, A., Pontillo, A., Calich, V.L.G., and Loures, F.V. (2018). The Syk-Coupled C-Type Lectin Receptors Dectin-2 and Dectin-3 Are Involved in *Paracoccidioides brasiliensis* Recognition by Human Plasmacytoid Dendritic Cells. *Frontiers in Immunology*, 9.

Van der Koog, L., Gandek, T.B., and Nagelkerke, A. (2021). Liposomes and Extracellular Vesicles as Drug Delivery Systems: A Comparison of Composition, Pharmacokinetics, and Functionalization. *Advanced Healthcare Materials*, 11 (5).

Wang, H., Li, M., Lerksuthirat, T., Klein, B., and Wüthrich, M. (2016). The C-Type Lectin Receptor MCL Mediates Vaccine-Induced Immunity against Infection with *Blastomyces dermatitidis*. *Infection and Immunity*, 84 (3).

Zhao, X-Q., Zhu, L-L., Chang, Q., Jiang, C., You, Y,. Luo, T., Jia, X-M., and Lin, X. (2014). C-type Lectin Receptor Dectin-3 Mediates Trehalose 6,6'-Dimycolate (TDM)-induced Mincle Expression through CARD9/Bcl10/MALT1-dependent Nuclear Factor (NF)-κB Activation. *Journal of Biological Chemistry*, 289 (43).

Zhu, L-L., Zhao, X-Q., Jiang, C., You, Y., Chen, X-P., Jiang, Y-Y., Jia, X-M., and Lin, X. (2013). C-Type Lectin Receptors Dectin-3 and Dectin-3 Form a Heterodimeric Pattern-Recognition Receptor for Host Defense against Fungal Infection. *Immunity*, 39 (2).